AGU ADVANCING EARTH AND SPACE SCIENCE

Tectonics

RESEARCH ARTICLE
10.1029/2019TC005865

Special Section:
Tectonic evolution of West-Central Tethysides

Key Points:
- Apatite (U-Th)/He thermochronometric data, growth strata, and balanced cross sections reveal chronology of deformation in the NW Zagros belt
- Forward modeled cross sections elucidate shift of tectonic style from thin-skinned to hybrid thin- and thick-skinned system during ~8–5 Ma
- NW Zagros orogenic growth is tied to mechanical stratigraphy, inherited basement discontinuities, and effects of deep Earth geodynamics

Supporting Information:
- Supporting Information S1

Correspondence to:
R. I. Koshnaw,
renas.i.koshnaw@gmail.com

Citation:
Koshnaw, R. I., Stockli, D. F., Horton, B. K., Teixell, A., Barber, D. E., & Kendall, J. J. (2020). Late Miocene deformation kinematics along the NW Zagros fold-thrust belt, Kurdistan region of Iraq: Constraints from apatite (U-Th)/He thermochronometry and balanced cross sections. *Tectonics*, *39*, e2019TC005865. https://doi.org/10.1029/2019TC005865

Received 4 SEP 2019
Accepted 15 NOV 2020
Accepted article online 20 NOV 2020

Late Miocene Deformation Kinematics Along the NW Zagros Fold-Thrust Belt, Kurdistan Region of Iraq: Constraints From Apatite (U-Th)/He Thermochronometry and Balanced Cross Sections

Renas I. Koshnaw[1,2], Daniel F. Stockli[1], Brian K. Horton[1,3], Antonio Teixell[4], Douglas E. Barber[1], and Jerome J. Kendall[5]

[1]Department of Geological Sciences, Jackson School of Geosciences, University of Texas at Austin, Austin, TX, USA, [2]Now at Department of Structural Geology and Geodynamics, Geoscience Center, University of Göttingen, Göttingen, Germany, [3]Institute for Geophysics, Jackson School of Geosciences, University of Texas at Austin, Austin, TX, USA, [4]Departament de Geologia, Universitat Autònoma de Barcelona, Bellaterra, Spain, [5]Department of Earth and Planetary Sciences, University of New Mexico, Albuquerque, NM, USA

Abstract Apatite (U-Th)/He (AHe) thermochronometric results are integrated with geologic cross sections, structural relationships, and stratigraphic data to reconstruct the growth of the NW Zagros orogenic belt in the Kurdistan region of Iraq. Prolonged exhumation is documented across the belt with deformation advances and retreats from ~14 Ma onward. After in-sequence propagation of deformation during middle to late Miocene times, preserved growth strata and AHe data show a deformation retreat by latest Miocene time (~5 Ma). In the NW Zagros, the Phanerozoic succession contains two principal décollements in Lower Triassic and middle Miocene units. The Triassic strata are interpreted as the main décollement for a thin-skinned system that was dominant during most of the Cenozoic. By ~8–5 Ma, the fold-thrust belt shifted to basement-involved deformation in association with growth of the mountain front flexure and reactivation of frontal structures. The shift from thin-skinned to a hybrid thin- and thick-skinned mode of shortening may reflect variations in the mechanical behavior of the upper crust and the presence of inherited basement discontinuities. On the basis of two NE-SW balanced cross sections spanning the NW Zagros, the estimated total minimum horizontal shortening is ~18.2 km (6%) in the central and ~16 km (7%) in the southern sectors of the Kurdistan region of Iraq. These findings suggest that the evolution of the NW Zagros orogenic belt was likely driven by the mechanical stratigraphy of the sedimentary cover, inherited basement discontinuities, and the dynamic and thermomechanical effects of potential slab breakoff and lithospheric mantle delamination events.

1. Introduction

The architectural evolution of contractional mountain belts in large part relates to temporal and spatial interplay between thin-skinned or thick-skinned style of deformation. Whereas thin-skinned shortening of sedimentary cover strata involves multiple fold-thrust structures detached above crystalline basement along a single or composite regional décollement, thick-skinned shortening is accommodated chiefly by displacement along deeply rooted, crustal-scale faults that penetrate crystalline basement (e.g., Chapple, 1978; Coward, 1983; Lacombe et al., 2016; Molinaro et al., 2005; Pfiffner, 2006, 2016, 2017). Previous studies showed that thin-skinned shortening generally involves large magnitude of tectonic transport accommodated through a series of faults with ramp-flat geometries and considerable duplexing in association with a forward breaking, in-sequence pattern of deformation. In contrast, thick-skinned belts are characterized by lower amounts of total shortening, duplexing with greater basement involvement, and a common association with either less systematic or out-of-sequence deformation (e.g., Butler et al., 2004; Kley, 1996; Lacombe & Bellahsen, 2016; Morley, 1988; Stuart et al., 2011). As contractional orogens grow, deformation commonly propagates from internal hinterland sectors toward the foreland often resulting in shortening within the sedimentary foreland basin, leading to systematic migration of depozones (DeCelles & Coogan, 2006; DeCelles & Giles, 1996). This deformation in the foreland could be achieved by purely thin-skinned structures restricted to the sedimentary cover or by combined thin- and thick-skinned deformation, also involving discrete basement structures (e.g., Fuentes et al., 2016; Lacombe & Mouthereau, 2002; Vergés, Goodarzi, et al., 2011). These contrasting tectonic styles often vary in time and space within individual orogenic systems, potentially leading to complex and contrasting deformational histories for sedimentary cover and crystalline basement (Madritsch et al., 2008). Natural examples show spatial variations in style both along and across strike, with irregular patterns and degrees of basement involvement (e.g., North American Cordillera, Andean orogenic belt; DeCelles, 2004; Dickinson, 2004; Horton, 2018a; Kley et al., 1999; Lacombe & Bellahsen, 2016; Lacombe & Mouthereau, 2002; Ramos et al., 2004; Yonkee & Weil, 2015). Furthermore, the timing and advances of foreland deformation also commonly show nonsystematic variations as illustrated in the Sierras Pampeanas of the Andean foreland, Jura Mountains of the western Alpine foreland, or the Dezful embayment of the central Zagros Mountains (e.g., Ahmadhadi et al., 2007, 2008; Horton, 2018b; Lacombe & Bellahsen, 2016; Lacombe & Mouthereau, 2002; Madritsch et al., 2008; Nemčok et al., 2013; Vergés et al., 2007; Vergés, Goodarzi, et al., 2011).

Accurately depicting the tectonic styles of contractional orogenic belts is essential for economic exploration and seismic hazard mitigation, particularly in regions known for prolific hydrocarbon reserves and active seismicity such as the Zagros fold-thrust belt (Butler et al., 2004; Lacombe & Bellahsen, 2016). Identification of the degree and timing of basement involvement helps elucidate the timing of hydrocarbon migration and the spatial distribution of petroleum systems in terms of their construction and destruction (Kendall et al., 2019). For instance, inaccurate considerations of stacked thrust sheets of sedimentary cover rocks via duplexing versus basement-involved deformation could lead to incorrect interpretations and predictions of petroleum plays (e.g., Cooper & Warren, 2010). Constraining the timing of individual structures and the overall temporal progression of the fold-thrust belt growth is critical for evaluating petroleum system processes, including the assessment of relative timing of structural traps formation and hydrocarbon generation and migration that could substantially reduce exploration risks (Butler et al., 2004; Mora et al., 2010). Moreover, constraining the subsurface architecture of a fold-thrust belt in terms of thin- or thick-skinned geometries can help with the identification of seismogenic fault zones. In the Zagros, faults within the basement appear to have been associated with large earthquakes, such as the 2017 *Mw*7.3 NW Zagros earthquake, and therefore to be more destructive than faults confined to the sedimentary cover (Barnhart et al., 2018; Berberian, 1995; Nissen et al., 2019; Talebian & Jackson, 2004; Tavani, Corradetti, et al., 2018).

The Zagros fold-thrust belt, with its topographically front delineated by the mountain front flexure (MFF), extends from southeastern Turkey through Iraq to southern Iran (Figure 1). It has been subdivided from NW to SE into the Kirkuk embayment, Lurestan salient, Dezful embayment, and Fars salient (Alavi, 1994; Berberian, 1995; Berberian & King, 1981; Emami et al., 2010; Falcon, 1961; Hessami et al., 2001; Koop & Stoneley, 1982). This study focuses on the NW segment of the Zagros fold-thrust belt, along the Kirkuk embayment in the Kurdistan region of Iraq (Figures 1 and 2). Fundamental questions persist concerning the dominant structural architecture, thin- versus thick-skinned geometries, and the timing and sequence of deformation. In the Zagros of Iran, a thin-skinned ramp-flat architecture has been suggested (McQuarrie, 2004) with a sequential forward (southwestward) advance of the deformation (Hessami et al., 2001). However, others invoke a hybrid thin- and thick-skinned style of shortening (Allen et al., 2013; Leturmy et al., 2010; Mouthereau et al., 2006; Mouthereau, Lacombe, et al., 2007; Mouthereau, Tensi, et al., 2007; Oveisi et al., 2009; Sherkati et al., 2006), involving either in-sequence (Saura et al., 2015; Vergés, Goodarzi, et al., 2011) or out-of-sequence deformation (Blanc et al., 2003; Molinaro, Leturmy, et al., 2005). In the Kurdistan region of Iraq, regional cross sections of the fold-thrust belt and adjacent foreland variably show thin-skinned (Hinsch & Bretis, 2015) or hybrid thin- and thick-skinned geometries (de Vera et al., 2009; Le Garzic et al., 2019; Tozer et al., 2019; Zebari et al., 2020). Whereas others solely focused on the uppermost sedimentary cover with no interpretation of structures below Jurassic strata (e.g., Frehner et al., 2012; Reif et al., 2011). For a cross section of the study area to be properly balanced, it has to honor all structural geometries and be retrodeformable and restorable to the unreformed state with preservation of bed length or cross sectional area (Dahlstrom, 1969; Woodward et al., 1989). Whereas these aforementioned cross sections provide insights on structural style and the difficulties in subsurface structural interpretations, they have some shortcomings, such as a lack of a Triassic shale décollement level and intraforeland structures; unidentified fold and fault kinematics (de Vera et al., 2009); impermissible

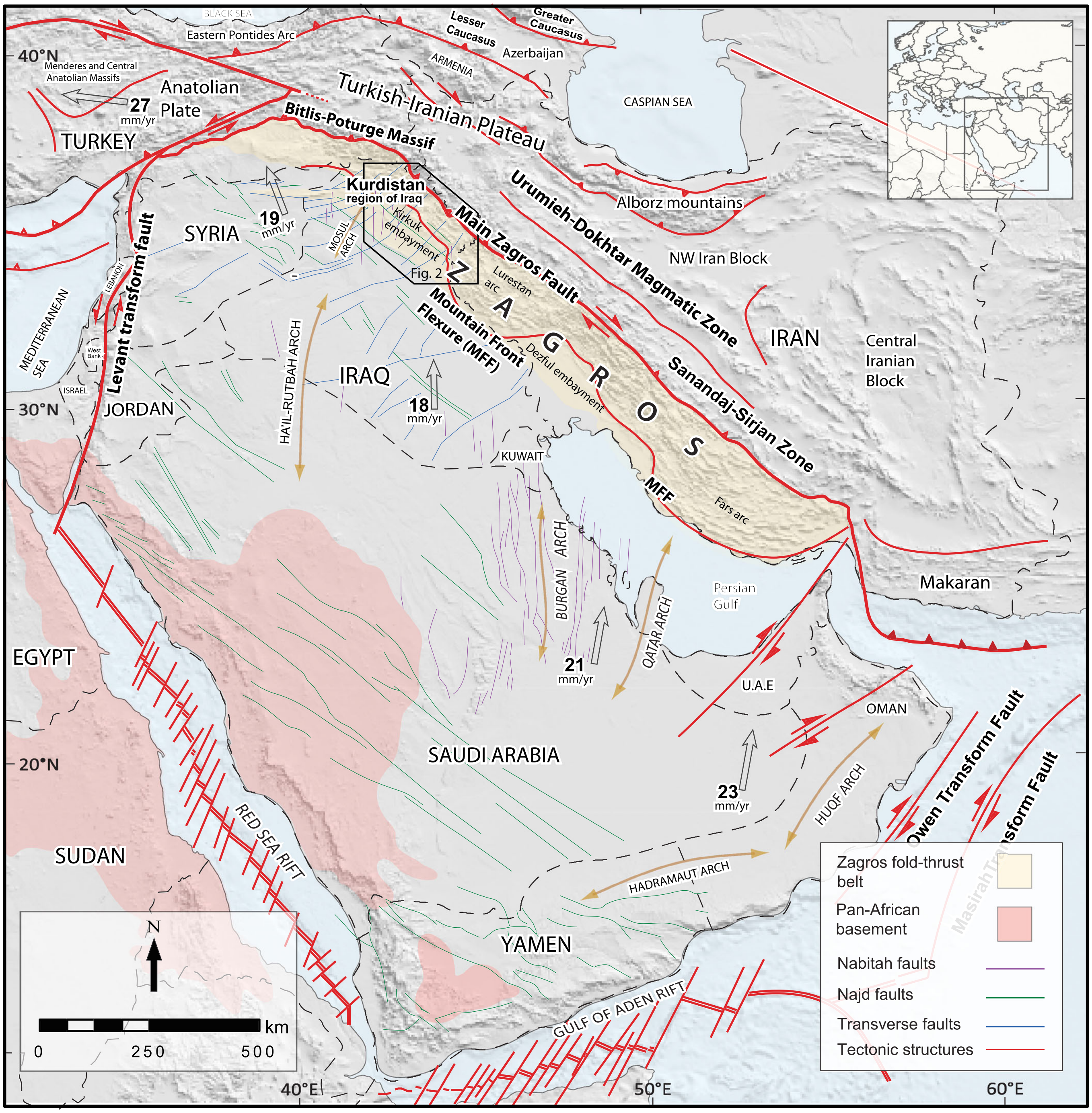

Figure 1. Regional tectonic map of the Middle East showing key tectonic elements and the Zagros orogenic belt, including the NW Zagros segment in the Kurdistan region of Iraq (Kirkuk embayment), basement-rooted faults of the Arabian plate, basement highs (arches), and the Pan-African basement exposure, plotted on a shaded relief map (ASTER Global Digital Elevation Map (GDEM) v.2, 2011). Tectonic features are compiled from: Ameen, 1992; Authemayou et al., 2006; Burberry, 2015; de Lamotte et al., 2011; English et al., 2015; Jassim & Buday, 2006; Konert et al., 2001; Vergés, Goodarzi, et al., 2011; Wrobel-Daveau et al., 2010; Ziegler, 2001. Arrow vectors represent GPS-derived plate motion velocities of the Arabia and Anatolia relative to Eurasia (Authemayou et al., 2006).

amounts of shortening in frontal structures (Hinsch & Bretis, 2015); mismatch between basement and cover shortening; or unclear accommodation of basement shortening in the sedimentary cover during late-stage deformation with apparently limited shortening in surface structures (Le Garzic et al., 2019, Figures 9e and 10d; Tozer et al., 2019). Further limitations include the assumption of continuous high-angle crustal-

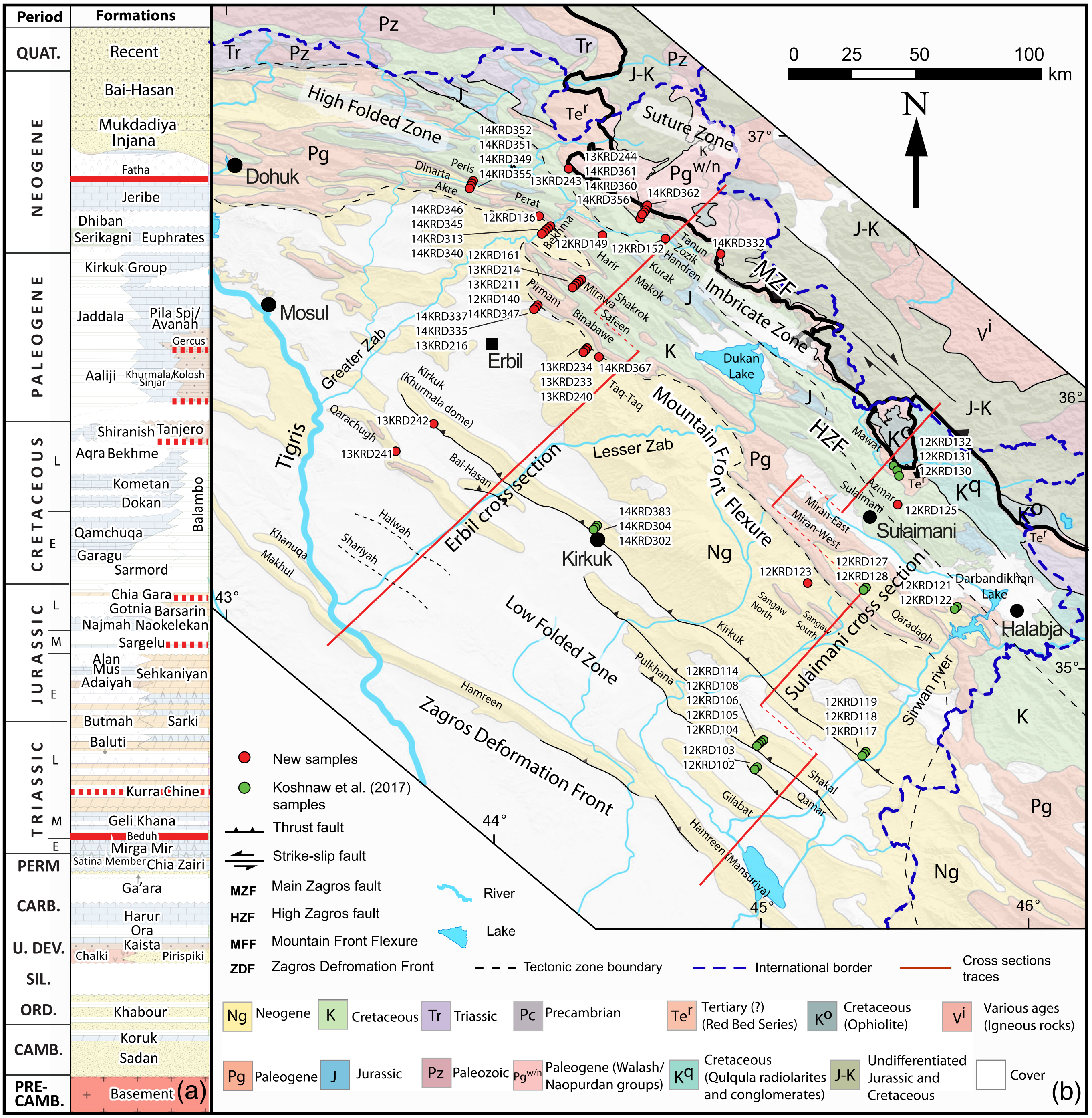

Figure 2. (a) Phanerozoic stratigraphic column showing the age, lithology, and nomenclature for the principal stratigraphic units (after English et al., 2015) for NW Zagros orogenic belt in the Kurdistan region of Iraq. Continuous red lines represent principal décollement levels, and the dashed red lines represent less influential décollement levels. (b) Regional geologic map for the NW Zagros orogenic belt in Iraq and adjacent territories of Iran and Turkey (modified from Alavi, 1991; Fouad, 2015; Gunay & Senel, 2002; Haghipour, 2009; Haghipour & Aghanabati, 1989; Ma'ala, 2008; Obaid & Allen, 2017; Sissakian, 1997, 2000) with location of samples and traces of balanced cross sections.

scale fault ramps beyond the seismogenic depth of brittle deformation (~25–30 km) (Abdulnaby et al., 2014; Engdahl et al., 2006; Karasözen et al., 2019; Nissen et al., 2019) to explain surface uplift (Tozer et al., 2019). Additionally, the mode of deformation advance has also been debated. Deformation propagation into the foreland has mainly been interpreted as an in-sequence process that advanced systematically from

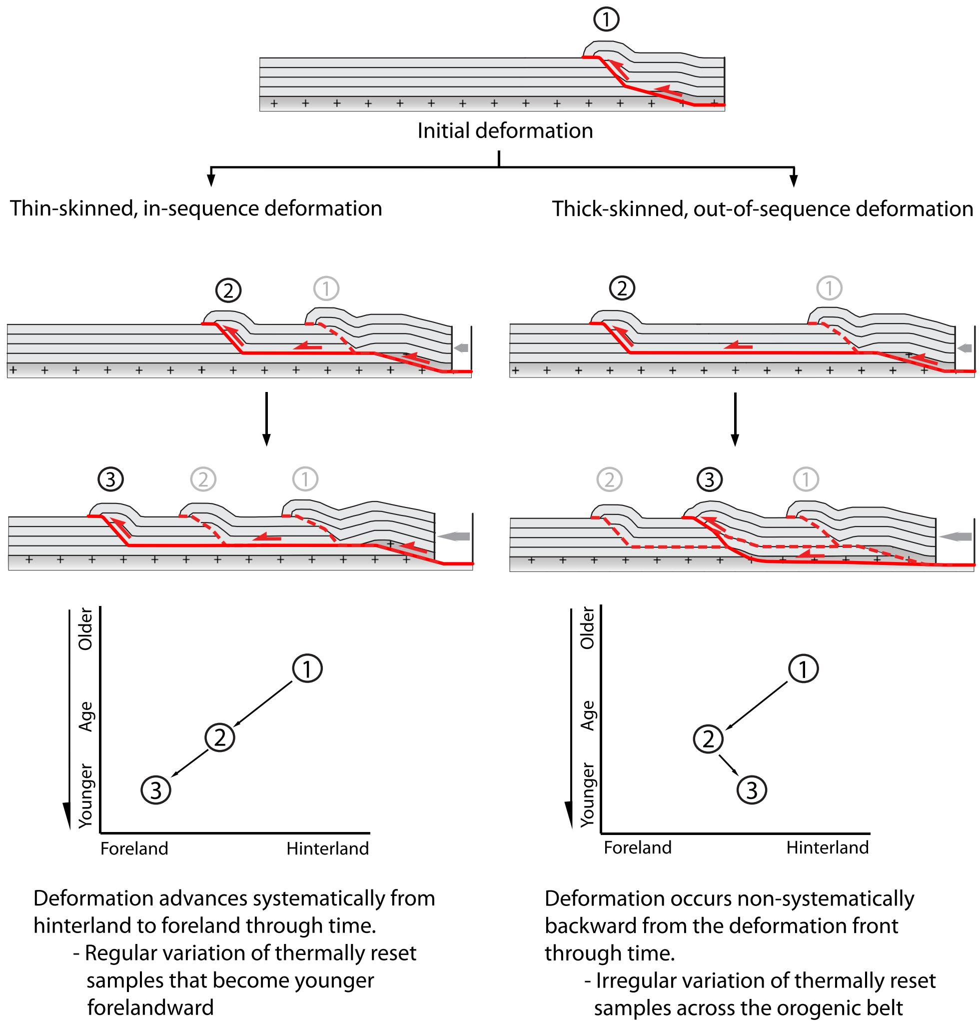

Figure 3. Conceptual diagram illustrating alternative models of deformation for the NW Zagros orogenic belt by thin-skinned, in-sequence deformation (left) and thick-skinned, out-of-sequence deformation (right), each model with its characteristic deformation in space and time.

internal to external portions of the fold-thrust belt on the basis of the spatial distribution of unconformities (Lawa et al., 2013) and 2-D restorations incorporating structural and burial/erosion constraints (Le Garzic et al., 2019). However, Koshnaw et al. (2017) proposed a temporally more complex kinematic evolution involving out-of-sequence basement-involvement on the basis of surface geologic constraints, provenance sigantures, and low-temperature thermochronometry.

In this paper, we build upon past understanding of the NW Zagros in the Kurdistan region of Iraq by exploring the temporal and spatial interplay between thin- and thick-skinned deformation. We seek to unravel the magnitude and timing of shortening, and evaluate how the fault systems evolved through time to accommodate shortening in the basement and the sedimentary cover. Figure 3 illustrates the timing differences between propagation as a thin-skinned in-sequence shortening versus thick-skinned out-of-sequence shortening in the NW Zagros. In order to document the temporal and spatial evolution of shortening deformation, we present new apatite (U-Th)/He low-temperature thermochronometry data from the principal fold and thrust structures, integrated with field observations and seismic reflection profiles, and two restored balanced cross sections across the central and southern segments of the NW Zagros in the Kurdistan region of Iraq. These new results provide new insights into the broader geodynamic processes and mechanisms of mountain building in collisional orogens such as the Zagros.

10.1029/2019TC005865

2. Background

2.1. Tectonostratigraphic Summary

The Zagros fold-thrust belt and foreland basin are the product of the Cenozoic Arabia-Eurasia collision (Beydoun, 1993; Dercourt et al., 1986; Stampfli et al., 2013; Stampfli & Borel, 2002). The Phanerozoic stratigraphic record in the Zagros (Figure 2a) reaches ~12 km in the Kirkuk and Dezful embayments (~6 km in Fars and Lurestan arcs) and covers crystalline Neoproterozoic juvenile crust and accreted Pan-African terranes of the Arabian basement that were accreted during the collision of East and West Gondwana in the East-African Orogeny (Alavi, 2007; Peterson & Wilson, 1986, in Alsharhan & Nairn, 1997; Konert et al., 2001; Stern & Johnson, 2010).

After cessation of East-African Orogeny (~580 Ma), the newly formed crystalline basement underwent strike-slip deformation (~550 Ma) followed by rifting of the Cimmerian terrane away from the NE margin of Gondwana during the late Permian to Early Triassic (~250 Ma), resulting in the opening of the Neotethys Ocean. The structural imprints of these events in the basement are evidenced by the N-S Nabitah, NW-SE Najid, and NE-SW transverse faults, respectively (Figure 1) (Alavi, 2007; Edgell, 1996; Jassim & Buday, 2006; Stern & Johnson, 2010; Talbot & Alavi, 1996). This inherited basement structural fabric substantially influenced later sedimentation, depositional facies, and stratigraphic thicknesses, such as the Eo-Cambrian Hormuz salt, as well as regional patterns of deformation and hydrocarbon accumulation (Ahmadhadi et al., 2007; Alavi, 2007; Ameen, 1991a; Ameen, 1992; Bahroudi & Talbot, 2003; Beydoun, 1993; Burberry, 2015; Edgell, 1996; Sepehr et al., 2006; Sepehr & Cosgrove, 2005; Stewart, 2018).

After Neotethys opening, the NE margin of Arabia developed into a Mesozoic passive margin characterized by deposition of shale, carbonate, and evaporite rocks upon the previously rifted margin (Aqrawi et al., 2010; English et al., 2015; Koop & Stoneley, 1982; Sharland et al., 2001; Stampfli & Borel, 2002; Ziegler, 2001). During the Mesozoic, Permo-Triassic rift-related troughs in northern Arabia experienced further extension and thermal subsidence, possibly due to slab pull associated with northward subduction of Neotethyan oceanic crust (Brew et al., 2001; Lovelock, 1984). These depressions were filled with marine deposits (Aqrawi et al., 2010; English et al., 2015; Fouad & Nasir, 2009) and by Maastrichtian-Paleocene time, were selectively inverted due to far-field stresses linked to relative plate motion changes of Africa, resulting in regional compression and inversion throughout North Africa and Arabia as well as ophiolite obduction (Bosworth et al., 1999, 2008; Brew et al., 2001, 2003; Chaimov et al., 1992; Fouad, 2007; Fouad & Nasir, 2009).

During the Maastrichtian, the intraoceanic convergent margin within the Neotethyan ocean reached the NE margin of the Arabian plate, leading to ophiolite obduction onto the Arabian continental margin, and initiation of the proto-Zagros foreland basin (Barber et al., 2018, 2019; Farahpour & Hessami, 2012; Homke et al., 2009; Lovelock, 1984; Saura et al., 2011). In response, a thick (locally >2 km) package of deep-marine clastic sediments (Tanjero Formation; equivalent to Amiran Formation in Iran) was deposited in a flexural basin, sourced from obducted ophiolites and older carbonate rocks to the NE (Ali & Mohmmad, 2018; Bellen et al., 1959; Çelik & Salih, 2018; Karim & Surdashy, 2005a; Koshnaw et al., 2017; Lawa, 2018). Flexural subsidence in proto-Zagros foreland basin continued into the Paleogene with deposition of the Kolosh and Gercus Formations and their equivalents in the Amiran basin of the Lurestan segment in Iran (Barber et al., 2018; Saura et al., 2011). In the Kurdistan region of Iraq, deposits of the proto-Zagros foreland basin were covered by Eocene lagoonal shallow-marine carbonate of the Pila-Spi Formation, followed by an Oligocene unconformity (Aqrawi et al., 2010; English et al., 2015). During the Neogene, mixed clastic-carbonate-evaporite deposits of the lower/middle Miocene Fatha Formation regionally overlay these older strata. Deposition of the Fatha Formation was succeeded by up to ~4–5 km late Miocene and younger disposition of the synorogenic clastic nonmarine fluvial succession of the Injana, Mukdadiya, and Bai-Hasan Formations, accompanying the accelerated Zagros shortening (Dunnington, 1958; Koshnaw et al., 2017, 2020).

2.2. Mechanical Stratigraphy

The thick Phanerozoic succession of the Arabian margin and platform involved in the Zagros contains several mechanically stiff (e.g., carbonate rocks) and weak (e.g., evaporites and shale) layers (Figure 2a). In Iran, the broad distribution of the ~0.5–2 km thick Eo-Cambrian Hormuz salt at the base of the Phanerozoic succession strongly influenced the style of shortening, largely decoupling basement from cover deformation (Alavi, 2007; Bahroudi & Koyi, 2004; Kent, 1979; McQuarrie, 2004). In the Lurestan segment, the Hormuz salt may be absent but an equivalent shale likely formed an important décollement (Alavi, 2007; Vergés, Goodarzi, et al., 2011). Similar to the Lurestan segment, in the study area of the NW Zagros in Iraq, the regional Hormuz salt appears to be absent, thus promoting stronger coupling between the basement and sedimentary cover rocks (Ameen, 1991a; Bahroudi & Koyi, 2003; Kent, 2010; Talbot & Alavi, 1996). The oldest exposed unit in Iraq is the Upper Ordovician Khabour Formation, although the Zap and Çukurca anticlines in southeastern Turkey contain Neoproterozoic (Sadan/Zabuk Formation), Cambrian (Koruk Formation), and Orodovician rocks (Seydişehir, Şort Tepe, and Bedinan Formations) (Al-Bassam, 2010; Bellen et al., 1959; Cater & Tunbridge, 1992; Ghienne et al., 2010; Janvier et al., 1984). Based on unit thicknesses in northern Iraq and southeastern Turkey, the Neoprotereozic through Paleozoic sections have an estimated composite thickness of 4–5 km. Based on gravity and magnetic data for western Iraq, estimations of the depth-to-basement require a comparable thickness of the Paleozoic and older rocks (Najar, 1999, in Al-Hadidy, 2007).

Within the Mesozoic passive-margin succession, other relatively mechanically weak formations include the Lower Triassic Mirga Mir (marly limestone and shale, 200 m) and Beduh (shale and marl, 65 m) Formations, the Upper Triassic Kurra Chine (limestone and shale, 834 m) and Baluti (shale and marl, 65 m) Formations, and the Jurassic Sargelu (limestone and shale, 115 m) and Chia Gara (limestone and shale, 200 m) Formations (Bellen et al., 1959). The Upper Cretaceous Tanjero Formation of the proto-Zagros basin varies from NE to SW, from a ~2,000 m thick succession of conglomerate, sandstone, and siltstone to a ~500 m section of shale, marl, and limestone (Abdel-Kireem, 1986; Ahmed et al., 2016; Bellen et al., 1959; Karim & Surdashy, 2005b; Lawa, 2018), followed by the Paleogene Kolosh (shale, fine sandstone, 780 m) and Gercus (shale, marl, mudstone, 840 m) Formations (Bellen et al., 1959). Up section, the Neogene Zagros foreland basin contains the incompetent Fatha (Lower Fras) Formation (mixed clastic-carbonate–evaporite, ~600 m) that is widely distributed in the NW Zagros (Aqrawi et al., 2010; Koshnaw et al., 2020; Shawkat & Tucker, 1978).

In brief, the stratigraphic record of the NW Zagros in the Kurdistan region of Iraq is characterized by multiple weak layers of differing lithologies, thicknesses, and lateral distributions. Importantly, however, lack of a weak decollement horizon at the Precambrian-Paleozoic transition suggests in principle a stronger coupling between the Paleozoic sedimentary cover and the basement compared to the Zagros of Iran. Such vertical and lateral variations in mechanical stratigraphy within the rock column are critical for the development of structures and the overall architecture of the fold-thrust belts (Bahroudi & Koyi, 2003; Butler & McCaffrey, 2004; Casciello et al., 2009; Cawood & Bond, 2018; Cotton & Koyi, 2000; Dunnington, 1968; Farzipour-Saein et al., 2009; Lee et al., 2018; O'Brien, 1957; Vergés, Saura, et al., 2011; Yamato et al., 2011).

2.3. Structural Framework

On the basis of deformation intensity, structural style, mechanical stratigraphy, and surface morphology, the study area is divided into five structural zones: the Zagros Suture zone, Imbricate zone, High Folded zone, Low Folded zone, and the Mesopotamian foredeep (Fouad, 2015) (Figures 1 and 2). These zones are separated by the Main Zagros fault (MZF), High Zagros fault (HZF), Mountain Front Flexure (MFF), and Zagros Deformation Front, respectively (Figure 2b). The Suture zone is characterized by intensely sheared allochthonous sheets of metamorphic and ophiolitic rocks. The Imbricate zone includes narrowly spaced anticlines and synclines cut by SW-vergence imbricate thrust faults (e.g., Tanun and Zozik anticlines; Figure 2b). The anticlines of the High Folded Zone are mostly large-amplitude box folds, accompanied by significant changes in structural level and topographic relief. The Low Folded zone contains more widely spaced structures and broad synclines. The Mesopotamian foredeep preserves the entire Phanerozoic stratigraphic succession of the Arabian platform and shows limited surface deformation, but buried structures have been inferred from reflection seismic and gravity data (Fouad, 2014, 2015; Mohammed, 2006). Generally, most shortening structures in the NW Zagros High Folded Zone are SW-verging, with fold wavelengths of 5–10 km (median = 7.4 km) and amplitudes <2.5 km, showing linear to curvilinear hinge lines generated by lateral fold propagation (Fouad, 2014; Le Garzic et al., 2019; Reif et al., 2012; Zebari & Burberry, 2015). In contrast, structures near Mosul and Duhok area of the northwestern-most Zagros, exhibit both SW and NE vergence (Numan and Al-Azzawi, 1993). Studies of High Folded Zone structures suggest that most folds are concentric, upright box folds that represent detachment-folds and minor/occasional fault-related folds (e.g., Awdal et al., 2013; Balaki & Omar, 2019; Fouad, 2014; László et al., 2012; Omar et al., 2015; Omar & Othman, 2018; Omar & Syan, 2016; Reif et al., 2012; Sapin et al., 2017; Zebari & Burberry, 2015).

3. Apatite (U-TH)/He Thermochronometry

This study employed structurally integrated low-temperature apatite (U-Th)/He (AHe) thermochronometry to constrain the timing of faulting and folding. AHe dating has been widely applied in structural and geomorphic studies to define the timing of faulting and erosional exhumation (e.g., Anderson et al., 2018; Ehlers & Farley, 2003; Fosdick et al., 2015; Gavillot et al., 2010; Levina et al., 2014; Lock & Willett, 2008; McQuarrie & Ehlers, 2017; Mackaman-Lofland et al., 2020; Stockli et al., 2000). The technique is based on radiogenic ingrowth of ^{4}He from the radioactive decay of ^{238}U, ^{235}U, ^{232}Th, and ^{147}Sm. Apatite is characterized by a low He closure temperature of ~70° ± 10°, making it sensitive to faulting and exhumation in the uppermost crust (Farley, 2000, 2002; Farley & Stockli, 2002; Stockli et al., 2000). Above ~80°, He is lost from apatite by thermally activated volume diffusion, as modulated by radiation damage, but He is completely retained below ~40°C—a temperature window known as the Partial Retention Zone (HePRZ) (Flowers et al., 2009; Reiners & Brandon, 2006; Shuster et al., 2006; Stockli et al., 2000; Wolf et al., 1996).

3.1. Analytical Method

For this study, apatite grains were separated from rock samples following standard mineral separation procedures including crushing/grinding, water table, magnetic separation, and heavy liquid separation. From each sample, 3–7 inclusion-free apatite grains were selected (except samples 14KRD-356 and 12KRD-149, only two grains were picked from each due to scarcity of suitable grains) with consideration to their shape and size (60–100 μm in width) and packed as single-grain aliquots in platinum tubes. Individual aliquots were degassed at 1020°C for 5 min using a diode laser and the released ^{4}He measured by a quadrupole mass spectrometer. Aliquots were reheated and reextracted to ensure all He was released. After He analysis, the aliquots were spiked with ^{230}Th, ^{235}U, and ^{149}Sm, dissolved in 30% HNO_3, and analyzed by inductively coupled plasma mass spectrometry (ICP-MS) to determine concentrations of ^{238}U, ^{235}U, ^{232}Th, and ^{147}Sm. For quality control purposes, Durango apatites (31.02 ± 0.22 Ma; McDowell et al., 2005) were analyzed as well as procedure standards. The Ft correction was applied to all grains (Cooperdock et al., 2019; Farley et al., 1996; Farley & Stockli, 2002). All reported errors are 6% (2σ) of age, based on lab internal standard reproducibility. In this study, the reported sample ages represent the arithmetic mean of the aliquots with their corresponding standard error. All data were analyzed at the UTChron laboratories at the University of Texas at Austin.

3.2. Sampling Strategy

Samples were collected from key structures to determine the timing of exhumation and growth of the NW Zagros. Where possible, the sampling strategy involved collection of medium- to coarse-grained sandstone samples throughout a stratigraphic succession to detect the level of HePRZ and facilitate the determination of fully reset samples (Ehlers & Farley, 2003; Stockli et al., 2000) (Figures 2 and 4). AHe data for 36 new samples are reported in this study, mainly from the central part of the study area (Erbil transect; Figure 2b), with two samples with <2 single-grain aliquots were excluded from the interpretation (12KRD-151 and 14KRD343). The new data are integrated with previously published AHe results from the Sulaimani area (Figure 2b; Koshnaw et al., 2017). Most samples were collected from synorogenic Neogene foreland basin deposits of the Fatha (Lower Fars), Injana (Upper Fars), Mukdadiya (Lower Bakhtiari), and Bai-Hasan (Upper Bakhtiari) Formations, with samples gathered from the proto-Zagros foreland basin strata of the Tanjero and Kolosh Formations. Additionally, samples were analyzed from the Govanda overlying Merga Red Bed units, and the Naopurdan and Walash Groups (middle Eocene-Oligocene; Al-Banna & Al-Mutwali, 2008; Ali et al., 2013) in the thrust belt interior near the Zagros Suture and Imbricate zones.

Along the Erbil transect (Figure 2), samples were collected from a traverse encompassing the different tectonic provinces of the NW Zagros from above the Main Zagros fault, the Imbricate zone, the High Folded zone near the Kurak anticline, to the Dinarta and Mirawa synclines internal to the Mountain Front Flexure (MFF). Along the MFF, samples were collected along the SW limbs of the Pirat, Piramam, and

10.1029/2019TC005865

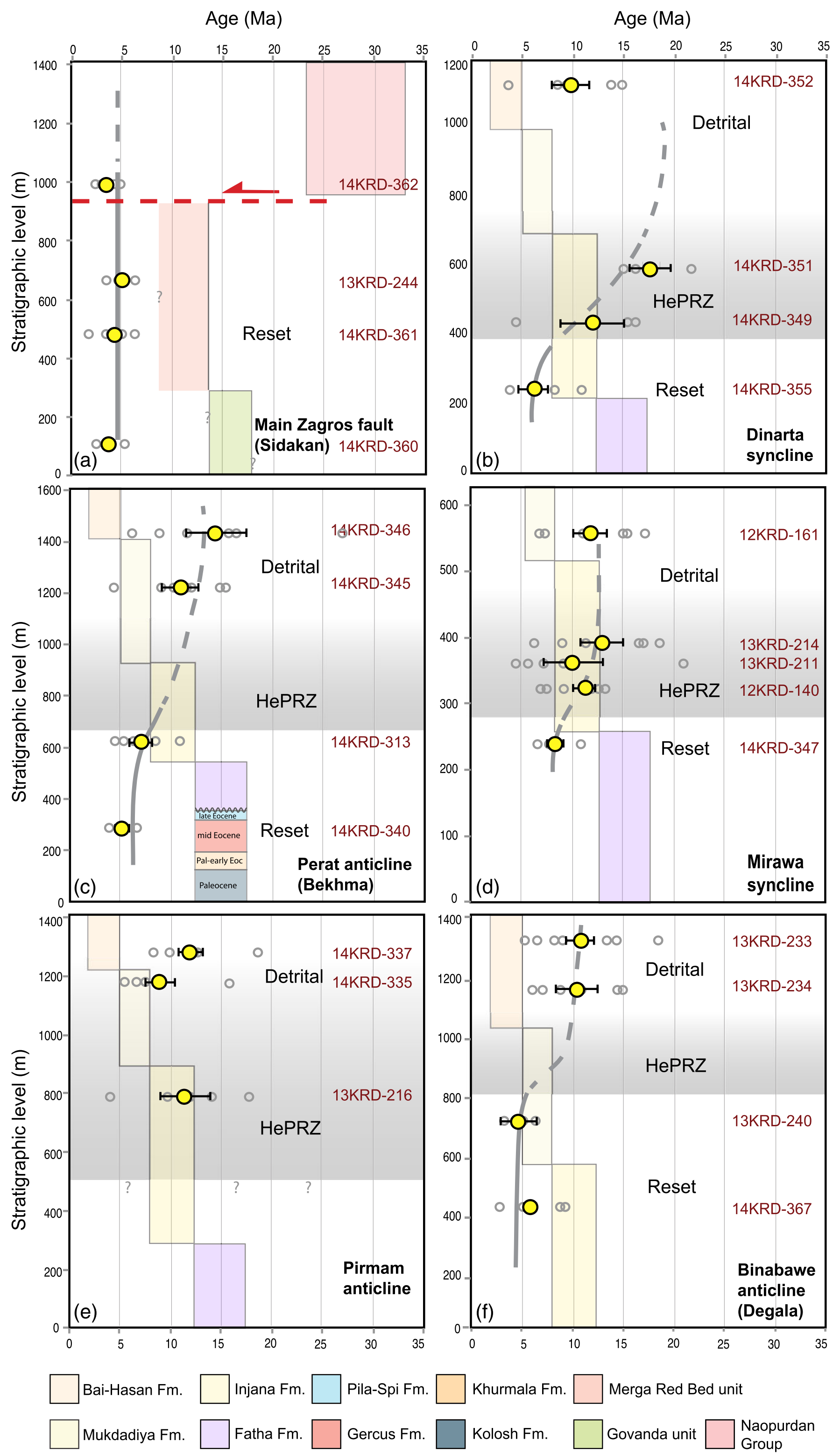

Figure 4. Stratigraphic plot of apatite (U-Th)/He results for sites that have more than two samples. The yellow circles stand for arithmetic mean of the samples with their corresponding standard error, and the gray open circles stand for single-grain aliquots. Colored boxes represent stratigraphic ages.

Binabawe anticlines. From the Low Folded zone, samples were collected on the eastern segment of the Kirkuk fault hanging wall (Khurmala dome) and NE limb of the Qarachugh anticline. Along the Sulaimani traverse, two new samples are presented: from the NE limb of Azmar anticline (12KRD-125) in the Imbricate zone and near the Sangaw anticlines (12KRD-123) in front of the MFF.

3.3. Apatite (U-Th)/He Results and Interpretations

Mean AHe ages for each sample were plotted against stratigraphic levels for each of the structure to identify the inflection points of the individual data arrays. These inflection points were used to determine whether samples were fully thermally reset, partially reset, or not reset (i.e., retaining detrital ages) and hence to pinpointing the timing of rapid cooling and exhumation (Harrison & Zeitler, 2005; Stockli et al., 2000). For example, samples with AHe ages invariant with stratigraphic level and younger than the depositional age were considered to be thermally reset (e.g., Carrapa et al., 2011; Mackaman-Lofland et al., 2020).

3.3.1. Erbil Transect

3.3.1.1. Main Zagros Fault

A sample from the middle Miocene Merga Red Bed unit (13KRD-243) below the NW segment of the Main Zagros fault (MZF) yielded a thermally reset age of 6.0 ± 0.6 Ma ($n = 5$; n: number of grains). This unit rests conformably on limestone beds of the early to middle Miocene (Burdigalian-Langhian; 20.4–13.8 Ma) Govanda Formation (Jassim et al., 2006). Along strike, a sample above the MZF from the Oligocne Naopurdan Group (14KRD-362) gave a reset age of 3.5 ± 0.5 Ma ($n = 5$). At the same locality, three samples (14KRD-360: Govanda Formation; 14KRD-361, 13KRD-244: Merga Red Bed unit) below the fault zone yielded ages of 3.8 ± 0.8 Ma ($n = 3$), 4.4 ± 0.6 Ma ($n = 7$), and 5.1 ± 0.4 Ma ($n = 6$), respectively (Figures 2b, 4a, and 5). These AHe ages are significantly younger than the depositional ages of the rock units, indicating fully reset samples (Figure 4). These results indicate a ~4.5 Ma exhumation age along the MZF at this locality. Another sample above the MZF zone (14KRD-332), from the middle Eocene Walash Group, which is constrained by foraminiferal assemblages as Lutetian (47.8–41.2 Ma) in age (Al-Banna & Al-Mutwali, 2008), exhibited a reset AHe age of 8.3 ± 0.9 Ma ($n = 7$).

3.3.1.2. Imbricate Zone

In the Imbricate zone, a sample (14KRD-356) from the Maastrichtian Tanjero Formation (Abdel-Kireem, 1986) provided an AHe age of 8.2 ± 1.8 Ma ($n = 2$) (Figures 2b and 5). Along the SW limb of Zozik anticline, another Tanjero sample (12KRD-152) (Figures 2b and 5) and yielded an age of 6.7 ± 2.9 Ma ($n = 3$). Both samples are considered reset, as their AHe ages are younger than the depositional age.

3.3.1.3. High Folded Zone

In the High Folded Zone, along the SW limb of Kurak anticline, a sample (12KRD-149) from the Paleocene-lower Eocene Kolosh Formation (Bellen et al., 1959) gave a reset age of 8.5 ± 0.9 Ma ($n = 2$) (Figures 2b and 5). Within the High Folded zone, from the Dinarta syncline behind the Mountain Front Flexure, four samples from Neogene basin fill (Injana Formation: 14KRD-355, 14KRD-349, 14KRD-351; Bai-Hasan Formation: 14KRD-352) gave ages of 6.6 ± 1.0 Ma ($n = 7$), 12.1 ± 3.8 Ma ($n = 3$), 17.7 ± 2.0 Ma ($n = 3$), and 10.0 ± 1.4 ($n = 7$) Ma, respectively (Figures 2b, 4b, and 5). The lowest sample from the Injana Formation (14KRD-355) was considered to be reset, as the AHe age is younger than the depositional age (~12.4–8 Ma; Koshnaw et al., 2020). However, the other two samples from the Injana Formation (14KRD-349 and 14KRD-351) are interpreted as partially reset to nonreset. The highest sample with the Bai-Hasan Formation is considered nonreset (detrital), as the AHe age is older than the depositional age (<5 Ma; Koshnaw et al., 2020). From bottom to top, the AHe ages of these samples show a clear transition from reset to HePRZ to nonreset ages (Figure 4b). From the Mirawa syncline, within the High Folded Zone, five samples were collected (Fatha Formation: 14KRD-347; Injana Formation: 12KRD-140, 13KRD-211, 13KRD-214; Mukdadiya Formation: 12KRD-161). The sample mean AHe ages were 8.1 ± 0.8 Ma ($n = 7$), 9.9 ± 1.1 Ma ($n = 7$), 9.2 ± 2.4 Ma ($n = 7$), 12.8 ± 2.0 Ma ($n = 6$), and 11.7 ± 1.6 Ma ($n = 7$), respectively. We interpret sample 14KRD-347 with an AHe age of 8.1 ± 0.8 Ma from the middle Miocene Fatha Formation (Bellen et al., 1959; Hawramy & Khalaf, 2013) to be reset, but the others are partially reset to nonreset (Figures 2b, 4d, and 5).

3.3.1.4. Mountain Front Flexure

Four samples were collected near the MFF in the Bekhma gorge, along the SW limb of the Perat anticline (Figure 4c). These samples (Gercus Formation: 14KRD-340; Injana Formation 14KRD-313; Mukdadiya Formation: 14KRD-345; Bai-Hasan Formation: 14KRD-346) yielded AHe ages of 5.1 ± 0.8 Ma ($n = 3$),

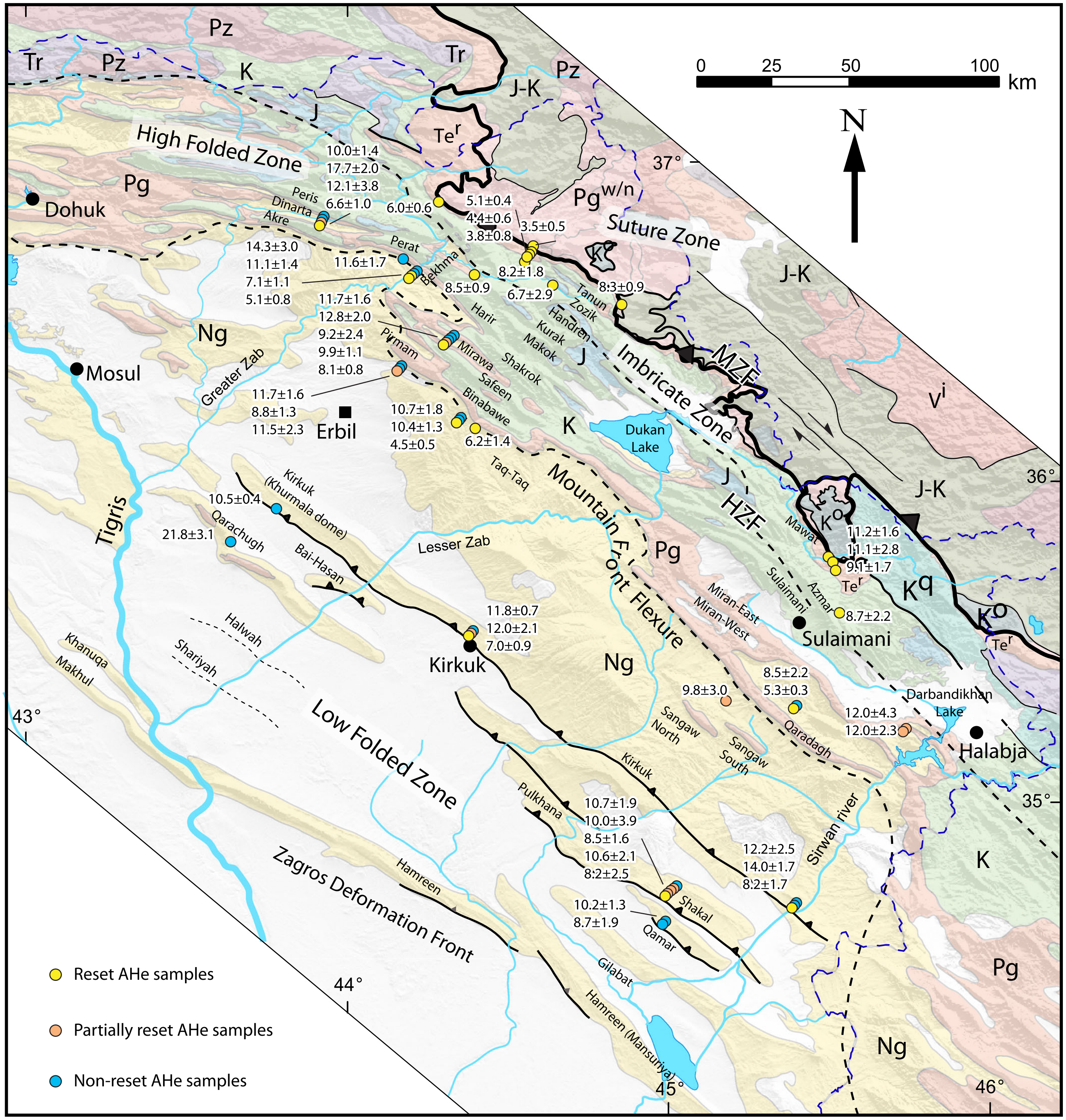

Figure 5. Regional geologic map of the NW Zagros orogenic belt denoting the AHe ages and sample locations. The sample ages represent the arithmetic mean of single-grained aliquots with the corresponding standard error.

7.1 ± 1.1 Ma ($n = 5$), 11.1 ± 1.4 Ma ($n = 7$), and 14.3 ± 3.0 Ma ($n = 6$), respectively. Samples 14KRD-340 (Gercus Formation: middle Eocene; Bellen et al., 1959) and 14KRD-313 (Injana Formation) are interpreted as reset samples, whereas samples 14KRD-345 (Mukdadiya Formation: ~8–5 Ma; Koshnaw et al., 2020) and 14KRD-346 (Bai-Hasan Formation) are nonreset. Along strike, a nonreset sample from the Mukdadiya Formation (12KRD-136) yielded an age of 11.6 ± 1.7 Ma ($n = 5$). From the MFF-related anticline of Pirmam (Figure 2b), samples from the Injana (13KRD-216), Mukdadiya (14KRD-335), and Bai-Hasan (14KRD-337) Formations yielded AHe ages of 11.5 ± 2.3 Ma ($n = 6$), 8.8 ± 1.3 Ma ($n = 6$), and 11.7 ± 1.5 Ma ($n = 6$), respectively (Figures 2b, 4e, and 5). The mean AHe age of sample 13KRD-216 from the Injana Formation is interpreted as partially reset and the others as nonreset, because their AHe ages are older than their host formations. Adjacent to the Pirmam anticline, samples from the SW limb of Binabawe anticline were collected from the Mukdadiya (13KRD-240) and Bai-Hasan (13KRD-233, 13KRD-234) Formations; the resulting AHe ages are 4.5 ± 0.5 Ma ($n = 5$), 10.4 ± 1.3 Ma ($n = 7$), and 10.7 ± 1.8 Ma ($n = 7$), respectively. The Mukdadiya sample (13KRD-240) is interpreted to be reset, whereas the others are nonreset (Figures 2b, 4f, and 5). In close proximity, a sample from the Injana Formation (14KRD-367) gave an AHe age of 6.2 ± 1.4 Ma ($n = 5$). This age is younger than the Injana depositional age, and therefore interpreted as reset.

3.3.1.5. Low Folded Zone

In the Low Folded zone, along the frontal structures, two samples were collected and analyzed from the NW segment of the Kirkuk fault (Khurmala dome) and Qarachugh anticline (Figures 2b and 5). In the Khurmala dome, a sample from the Mukdadiya Formation (13KRD-242) yielded an age of 10.5 ± 0.4 Ma ($n = 5$). In the Qarachugh anticline, a sample from the Injana Formation (13KRD-241) exhibited an age of 21.8 ± 3.1 Ma ($n = 5$). Because these AHe ages are significantly older than the late Miocene depositional ages of the Injana and Mukdadiya Formations, we interpreted them as nonreset samples.

3.3.2. Sulaimani Transect

Along the Sulaimani transect in the SE portion of the study area, two new samples were collected from the Tanjero Formation near the Azmar anticline within the Imbricate zone (12KRD-125) and from the Injana Formation near the Sangaw-North anticline within the Low Folded zone (12KRD-123) (Figures 2b and 5). The Maastrichtian Tanjero sample gave a fully reset AHe age of 8.7 ± 2.2 ($n = 3$), while the Miocene Injana Formation near the Sangaw-North anticline yielded an age of 9.8 ± 3.0 Ma ($n = 4$), which overlaps its stratigraphic age and therefore interpreted as a partially reset sample. Along the Sulaimani transect, previously published AHe age results (Koshnaw et al., 2017) from samples near the MZF, MFF, and frontal structures all showed reset ages of ~11, ~5, and ~8 Ma, respectively.

Collectively, these results from the Erbil and Sulaimani transects show the following: (i) multiple pulses of exhumation along the MZF between ~11 and 4 Ma that appear to become younger toward the NW; (ii) prolonged exhumation in the HFZ and LFZ from ~10 Ma onward; and (iii) a major pulse of exhumation along the MFF between the HFZ and LFZ by ~5 Ma (Figures 5 and 6a). Subdividing AHe ages for the NW Zagros into reset and nonreset ages (excluding the partially reset samples) reveals that exhumation of the reset samples occurred mostly after ~10 Ma, whereas exhumation ages of the mostly nonreset samples are older (Figure 6b).

4. Balanced Cross Sections

4.1. Methods

To investigate the interplay between the timing and style of shortening, two regional line length and area balanced cross sections were constructed across the central (Erbil transect) and southern (Sulaimani transect) sectors of the NW Zagros in the Kurdistan region of Iraq (Figure 7). The sections were based on geologic maps (1:250,000, Sissakian, 1993, 1997; 1:1000,000, Sissakian, 2000; 1:250,000, Sissakian & Fouad, 2014; Omar et al., 2015, Figure 1), published and proprietary seismic profiles where available (Shamaran Petroleum Group, 2009, 2011; Garland et al., 2010, Figure 6; Kent, 2010, Figure 15; Fouad, 2012, Figure 5; Min et al., 2012, Figure 3; Oil Search, 2012; Hayward, 2014; Allouche et al., 2015, Figure 3), and field measurements and observations from this study in combination with bed attitudes calculated from publicly available remote sensing image and digital elevation models (ArcGIS webscene and Google Earth Pro). The length of the restored top Cretaceous is ~280 km for the Erbil cross section and ~232 km for the Sulaimani cross section. Thicknesses of Phanerozoic rock units in the NW Zagros were compiled from Bellen et al. (1959), Janvier et al. (1984), Cater and Tunbridge (1992), Najar (1999) in Al-Hadidy (2007), Frehner et al. (2012), Ghienne et al. (2010), Ahmed et al. (2016), Liu et al. (2017), Lawa (2018), and Koshnaw et al. (2019). Cross sections construction and kinematic forward models were performed using *Move* software (2D). Cross sections were restored and balanced assuming conservation of bed lengths for

10.1029/2019TC005865

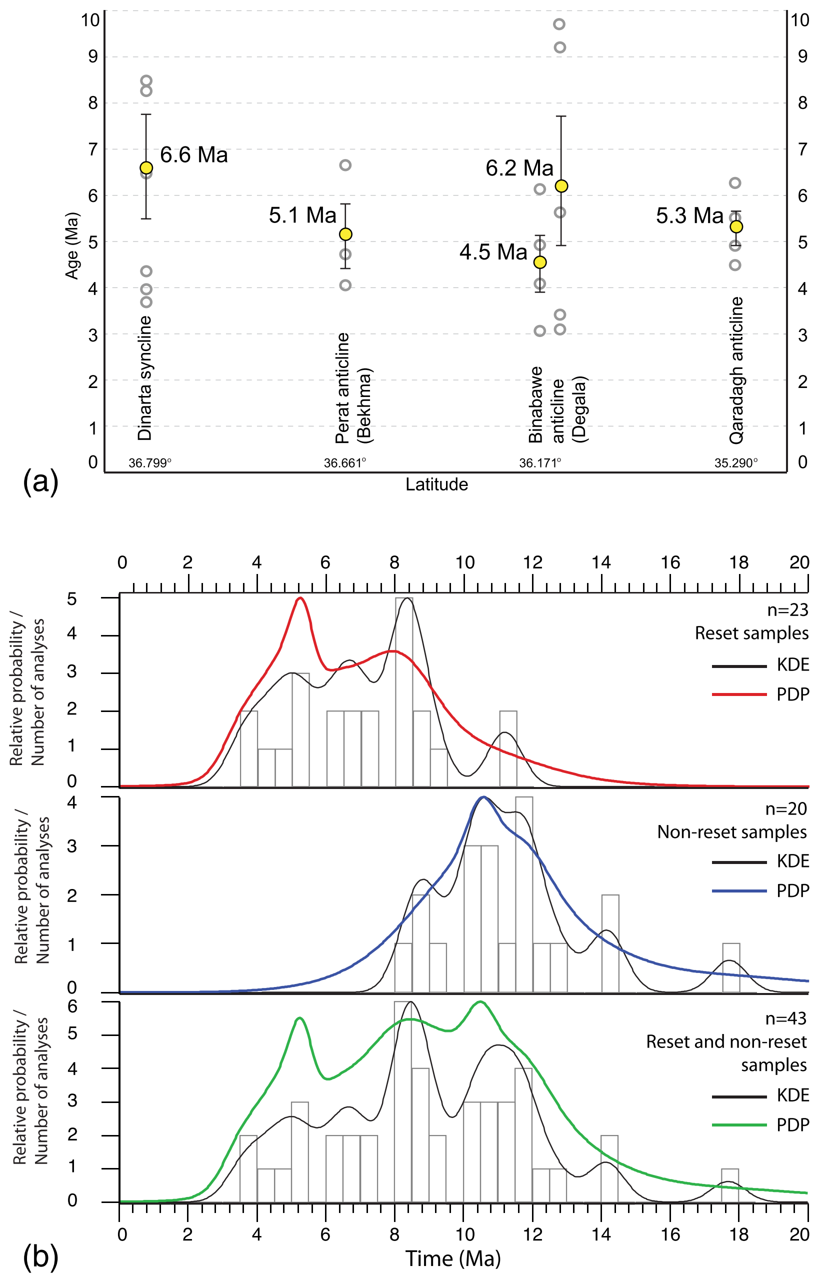

Figure 6. (a) AHe ages versus latitude plot for the reset samples in the vicinity of the mountain front flexure (MFF) along the NW Zagros orogenic belt in the Kurdistan region of Iraq. The yellow circles stand for arithmetic mean of the samples with their corresponding standard error, and the gray open circles stand for single-grain aliquots. Colored boxes represent stratigraphic ages. (b) Probability density plot (PDP; bandwidth = 0.5, bin width = 0.5) and kernel density estimation (KDE; bandwidth = 0.5, bin width = 0.5) (Vermeesch, 2012) of reset AHe samples (red), nonreset AHe samples (blue), and both reset and nonreset AHe samples combined (green), excluding partially reset samples, showing peak exhumation times at ~12, ~8, and ~5 Ma.

the competent units, by employing line length unfolding and fault-bend-fold algorithms, considering the timing and sequence of the shortening structures. The kinematic forward models were constructed by hand drawing with the aid of fault-bend-fold and detachment-fold algorithms. Furthermore, no inherited extensional structures were taken into account given uncertainties in their scale and location as well as their limited effect on balancing a cross section at this scale.

10.1029/2019TC005865

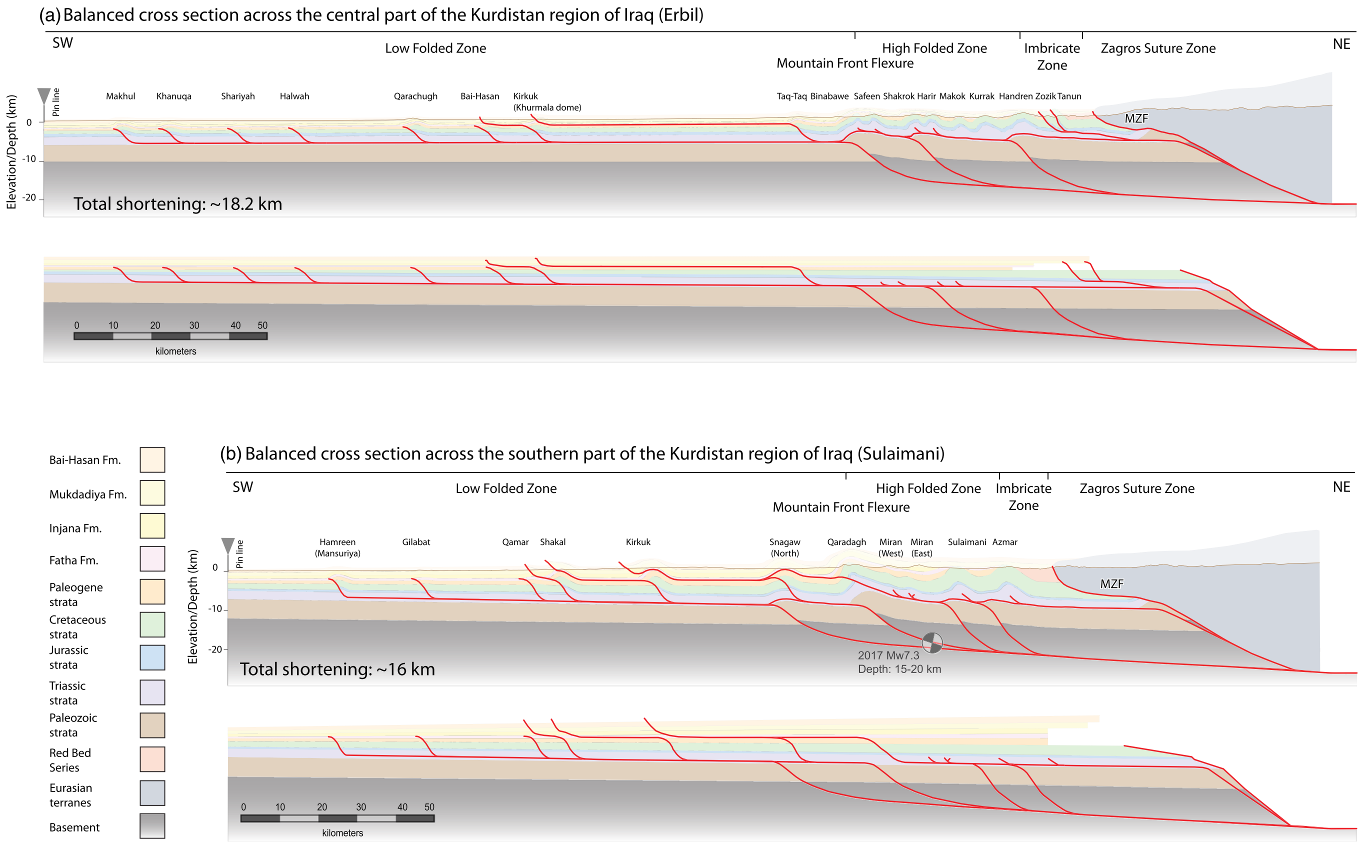

Figure 7. Balanced and restored cross sections across the NW Zagros orogenic belt in the central (a: Erbil) and southern (b: Sulaimani) parts of the Kurdistan region of Iraq. Scale is in kilometers with no vertical exaggeration. The 2017 *Mw*7.3 earthquake low angle thrust fault (dip of ~14°E; Nissen et al., 2019) focal mechanism is projected vertically on the cross section across the southern part due to the proximity of the epicenter. The hypocenter of the earthquake is in agreement with where a deep-rooted basement fault is expected.

4.2. Results and Interpretations

The balanced cross sections show that basement involvement is a required in the NW Zagros to account for the structural elevation of various horizons and the relatively small magnitude of horizontal shortening. Using a top Jurassic marker horizon, restoration of the balanced sections yielded a minimum total shortening of ~18.2 km (6%) along the central Erbil cross section and ~16 km (7%) along the southern Sulaimani cross section (Figure 7).

The overall topography, structural level, and intensity of deformation show stepwise decreases across strike from NE toward SW, from the Zagros hinterland (suture, imbricate, high folded zones) to foreland (low folded zone, Mesopotamian foredeep). These differences in structural levels are well expressed in regional geologic maps, such that Cretaceous rocks are exposed in the internal hinterland, mostly Paleogene rocks in the more external hinterland, and dominantly Neogene rocks toward the foreland (Figure 2b). In addition, Neogene deposits in hinterland synclines are preserved at higher structural levels (higher elevation) compared to their foreland equivalents (Koshnaw et al., 2017; Le Garzic et al., 2019; Tozer et al., 2019). For both the Erbil and Sulaimani cross sections, using the top of the Neogene Fatha Formation and top of the Cretaceous rocks, the estimated structural elevation gain is ~2.5–3 km for a hinterland width of ~40–50 km over a ~200 km length. Such a broad structural high mandates basement involved deformation and duplexing in the internal portions of the fold and thrust belt. A similar magnitude of structural relief (2.6 km) has also been estimated for the NW Zagros fold-thrust belt in the study area based on surface geological data (Zebari et al., 2020).

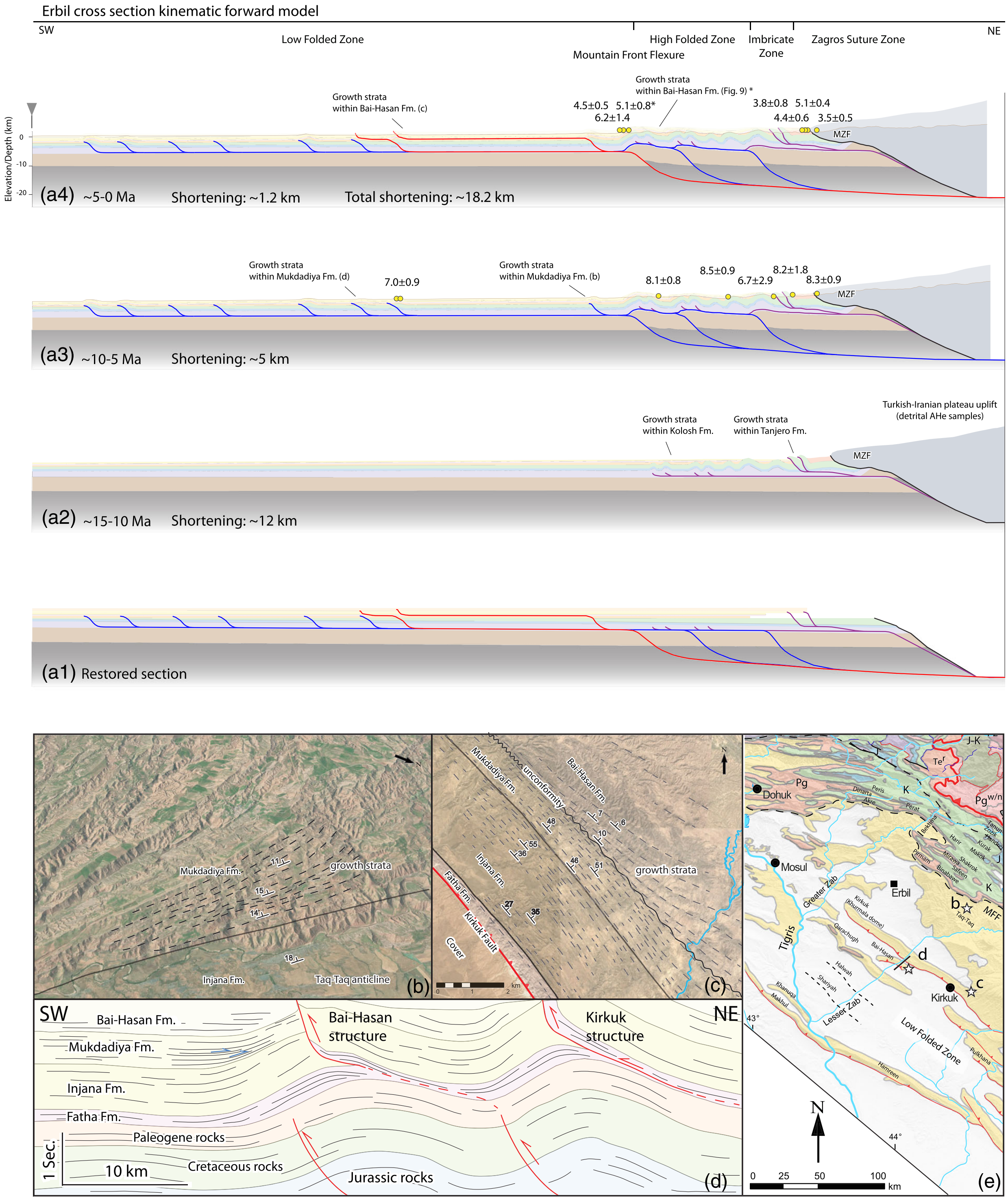

Figure 8. (a) Kinematic evolution diagram showing the structural development of the central cross section (Erbil) by sequentially deforming the restored section. Scale is in kilometers with no vertical exaggeration. The growth strata and AHe sample with asterisk symbol are from along-strike locations. Location of the growth strata within the Tanjero and Kolosh formations are based on Allouche et al. (2015) and Le Garzic et al. (2019). (b) Satellite image view (ArcGIS webscene) of the SW limb of Taq-Taq anticline that shows growth strata within the Mukdadiya formation. (c) Satellite image view (GoogleEarth) of the NW Kirkuk structure that shows growth strata within Bai-Hasan formation. (d) Line tracing and interpretation of a seismic reflection profile across the Kirkuk and Bai-Hasan structures (Fouad, 2012; Figure 5) that shows growth strata within the Mukdadiya formation on the SW limb of the Bai-Hasan structure. (d) Geologic map showing location of the satellite images and the seismic reflection profile.

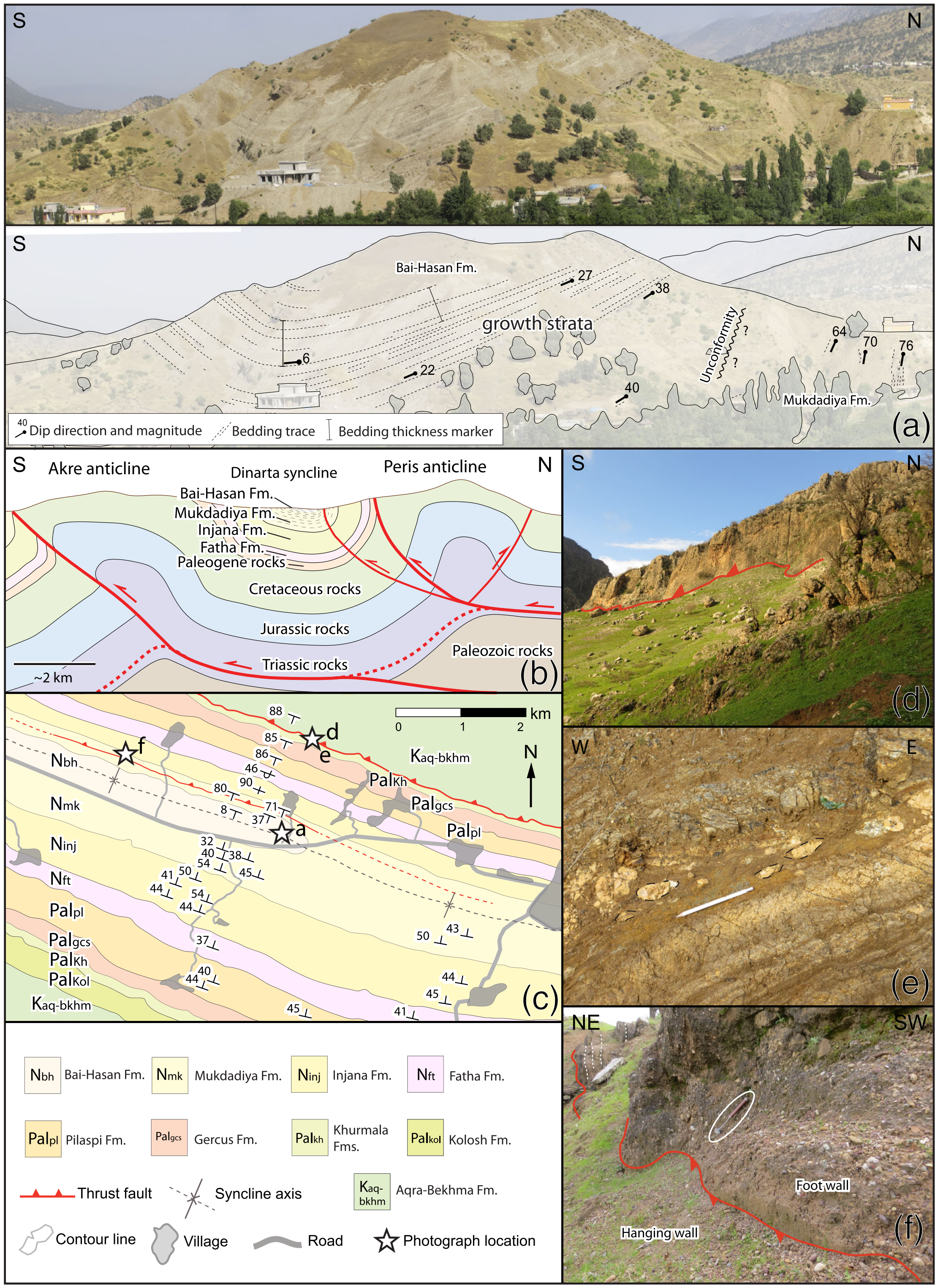

Figure 9. (a) Growth strata preserved within the Bai-Hasan formation that lies unconformably on steep beds of the Mukdadiya formation. (b) Schematic cross section that shows the structural setting of the Dinarta syncline, where the growth strata of the Bai-Hasan formation is preserved. The cross section is based on Zebari and Burberry (2015) and Zebari et al. (2019). (c) Geologic map of the Dinarta syncline that shows a major and a minor reverse fault, and locations of filed photographs. At this locality the Kolosh formation is missing. (d) A large block of carbonate rock (~100 m length X ~ 40 m high) with a semi-flat surface that is interpreted as the hanging-wall of the mapped reverse fault. (e) Sheared carbonate pebbles within the Khurmala formation at the bottom of the major fault. Pencil for scale. (f) Subvertical dipping beds from the footwall of the minor reverse fault within the Mukdadiya formation. Hammer for scale.

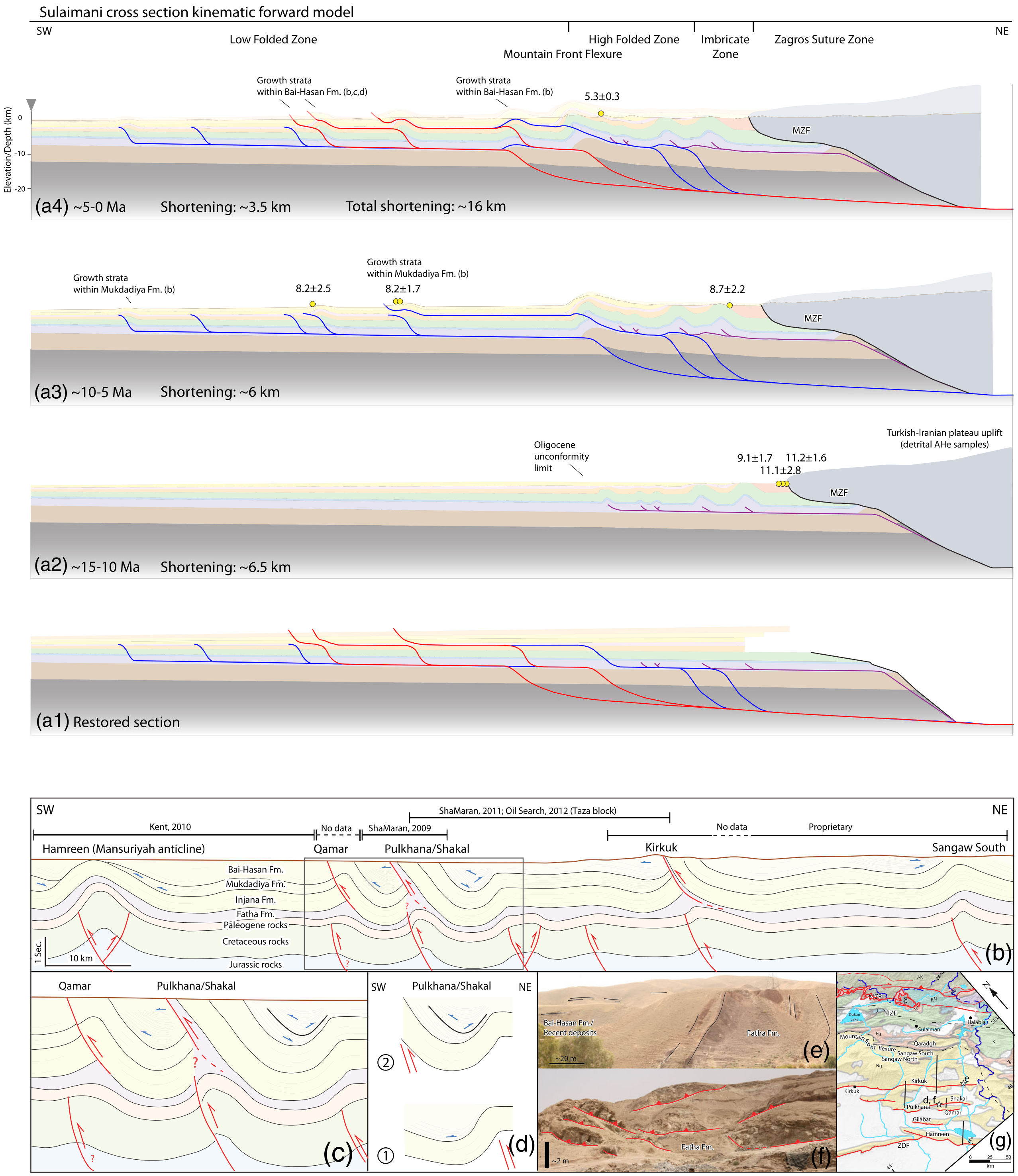

Figure 10. (a) Kinematic evolution diagram showing the structural development of the southern cross section (Sulaimani) by sequentially deforming the restored section. Scale is in kilometers with no vertical exaggeration. (b) Line tracing and interpretation of a composite seismic reflection profile across the low folded zone structures in the southern part of the study area that growth strata within the Mukdadiya and Bai-Hasan formations at different locality, see text for details. (c) Zoomed-in view of Pulkhana/Shakal and Qamar structures that shows growth strata thinning at different directions and at different times, during the deposition of the Bai-Hasan formation. (d) Interpretation of the Pulkhana/Shakal structure illustrating an existing topography at NE (1) prior to faulting at the SW (2). (e) Field example from the front of the Kirkuk fault that shows Fatha formation in sharp contact with subvertical beds of Bai-Hasan and/or Quaternary deposits. (f) Field example of the mechanically weak beds of the Fatha formation at front of the Shakal fault. (g) Geologic map showing location of the field examples and the seismic reflection profiles.

10.1029/2019TC005865

The main décollement levels were considered to be the Lower Triassic Mirga Mir and Beduh Formations and the middle Miocene Fatha Formation layers. The extensive disharmonic deformation of the Fatha Formation and thrusting of strata above it are observable both in the field and seismic profiles (Figures 9d, 10b, 10e, and 10f). The depth of the deeper décollement level is estimated by applying the excess-area of multiple horizons method by Epard and Groshong (1993) to individual structures (e.g., Handren, Shakrok, and Azmar anticlines in the High Folded zone and Hamreen anticline in the Low Folded zone) and yielding a depth of 4–4.5 km below the top of Cretaceous strata, which is in accordance with the depth of the Lower Triassic strata. Hence, the basal décollement is considered to reside in the Mirga Mir and Beduh Formations rather than the younger Kurra Chine and Baluti Formations, as a greater Triassic thickness is required to avoid space problems in anticlinal cores relative to mechanically weak layers above. Whereas local preexisting structures, additional detachment levels, or thickness changes would complicate this depth estimate, the regional significance of the Lower Triassic décollement appears unquestionable. In the Imbricate zone of the Erbil cross section, the Tanun and Zozik structures underwent considerable shortening (~5 km) relative to other hinterland structures. As imbricate fans have a shared lower detachment floor thrust (Mitra, 1986), the tightly spaced Tanun and Zozik structures are likely generating from the same floor thrust. The limited space between the Tanun and Zozik structures requires their floor thrust to be at a higher level than the Lower Triassic strata, but below Jurassic rocks. Therefore, mechanically weak Upper Triassic strata are considered the best candidates for this décollement level. Such a structural template has also been proposed by Le Garzic et al. (2019). Furthermore, the Mitra and Namson (1989) method, which is based on the relation between excess area and amount of shortening of individual horizons according to the area conservation principle of Chamberlain (1910), was also attempted. In contrast to the previous method, in Mitra and Namson (1989) method the resulting depth-to-detachment was 8–8.5 km, which would correspond to lower Paleozoic levels. However, a lower Paleozoic décollement level near the basement-cover interface has been excluded, as no disharmonic deformation is documented along the outcropped weak shales in the Ora Formation (Le Garzic et al., 2019).

In both the Erbil and Sulaimani cross sections, the basal Lower Triassic décollement level was interpreted to transfer displacement from the hinterland to the foreland, leading to the formation of shallow frontal structures that accommodate deeper basement-involved shortening in the hinterland. During later stages of the collision, Neogene foreland basin strata underwent shortening to accommodate further hinterland basement deformation. At this time, the regional décollement climbed from Lower Triassic levels to middle Miocene evaporite deposits near the MFF. The MFF is interpreted as the surface manifestation of a basement-involved, monoclinal fault-bend fold, as it represents the major contrast in structural level between the High Folded and Low Folded zones. The depth of basement faults under the Zagros fold belt was inferred from the 2017 *Mw*7.3 NW Zagros earthquake at a depth of ~15–20 km within the basement of the Arabian plate with a low angle dip of ~14°E (Barnhart et al., 2018; Chen et al., 2018; Nissen et al., 2019; Tavani, Corradetti, et al., 2018; Utkucu, 2017) and a midcrustal brittle-ductile transition zone depth of ~25–30 km in the NW Zagros (Abdulnaby et al., 2014; Engdahl et al., 2006; Karasözen et al., 2019; Nissen et al., 2019).

5. Kinematics of Shortening

Sequential forward modeling was performed to validate the balanced cross sections and their restorations. Due to uncertainties in kinematic histories and subsurface geometries, the surface relationships can be explained by several different solutions (McQuarrie & Ehlers, 2017; Woodward et al., 1989). Therefore, information on structural timing is essential to constrain cross-section kinematics. The new AHe low-temperature thermochronometric ages are combined with field and seismic evidence across both the Erbil and Sulaimani cross sections to determine the sequence of deformation in the NW Zagros.

5.1. Erbil Cross Section Kinematic Forward Model

The kinematic model for the Erbil section is presented in Figure 8. Initial shortening is represented by the proto-Zagros fold-thrust belt and foreland basin that formed during the Maastrichtian-Paleocene ophiolite obduction onto the Arabian passive margin (Figure 8a2). The timing of deformation of the proto-Zagros belt is constrained by growth synclines within the preserved Maastrichtian Tanjero Formation in the hanging wall of Tanun structure and the Paleocene Kolosh Formation between the Shakrok and Safeen anticlines (Allouche et al., 2015, Figure 3; Le Garzic et al., 2019, Figure 7) (Figures 8a2 and 2b). This stage was

10.1029/2019TC005865

followed by collision of Arabia and Eurasia by late Oligocene time (Agard et al., 2005; Fakhari et al., 2008; Homke et al., 2010; Horton et al., 2008; Koshnaw et al., 2019; Pirouz et al., 2017; Zadeh et al., 2017), deposition of the Red Bed Series, thrusting of Walash-Naopurdan arc-related terrains, and emplacement of ophiolitic thrust sheets by out-of-sequence deformation (Agard et al., 2005, 2011; Ali et al., 2012, 2014; Homke et al., 2010; Ismail et al., 2020; Saura et al., 2015). Early Zagros deformation was not restored, as the pre-Neogene tectono-stratigraphic packages are beyond the scope of this research.

After the Arabia-Eurasia collision, deformation of the Zagros suture zone, rapid Neogene growth of the Zagros foreland basin and the relatively quiescent middle Miocene was followed by activation of the MZF in the Suture zone during the late middle Miocene-early late Miocene (~14–10 Ma) (Figure 8a2). This deformation phase is not recorded in the suture zone of the Erbil cross section, but reset AHe samples indicate ~11 Ma cooling along strike of the MZF in the Sulaimani cross section. This deformation phase is also inferred from the ~14–10 Ma time of exhumation recorded by nonreset (detrital) AHe ages with a peak time of ~12–10 Ma (Figures 2b, 5, 6b, and 8a2). The estimated shortening at this stage is ~12 km (~4%).

By the late Miocene (~10–5 Ma), hinterland uplift affected the Suture, Imbricate, and High Folded zones, as evidenced from reset AHe ages near the MZF, Tanun, Handren, and Kurak anticlines, and Mirawa syncline (Figure 8a3). In the Low Folded zone, AHe samples from the NW segment of the Kirkuk (Khurmala dome) and Qarachugh structures are not reset, in contrast to reset samples from the more deeply eroded middle portion of the Kirkuk structure indicative of rapid cooling at 7.0 ± 0.9 Ma. In addition, the SW limb of the Taq-Taq anticline shows a growth strata fan within the latest Miocene Mukdadiya Formation (Figures 8a3 and 8b). Seismic profiles across Kirkuk and Bai-Hasan frontal structures show growth strata in the SW limb of Bai-Hasan structure within the Mukdadiya Formation (Figure 8d) (Fouad, 2012, Figure 5). The onset of deposition of the Mukdadiya Formation is proposed to be ~8 Ma based on magnetostratigraphy (Koshnaw et al., 2020). We interpreted this timing correlation between the hinterland and foreland frontal structures as the result of the commencement of the basement uplift in the hinterland and displacement transfer along the Lower Triassic décollement level. The estimated shortening at this stage is ~5 km (1.6%).

As shortening continued, by early Pliocene time (~5 Ma), the Zagros hinterland experienced a major exhumation event that is clearly evidenced by reset AHe ages from the Suture zone, Dinarta syncline, and SW limb of Perat anticline (Bekhma gorge) in the High Folded zone, and SW limb of Binabawe anticline along the MFF (Figures 2b, 4c, 4f, 5, and 8a4). Additionally, detailed field mapping in the Dinarta syncline revealed relatively minor reverse fault that likely is splaying from a major fault (Figures 9b–9f). Sheared carbonate pebbles at the bottom of a large (~100 m length and ~40 m height) dismembered block of carbonate rock near the bottom of the SW limb of Peris anticline, as well as disappearance of the Paleocene to early Eocene Kolosh Formation beneath the older Cretaceous Aqra-Bekhma Formations suggest presence of a major fault that breaks through the SW limb of the Peris anticline. This major fault has also been required to construct a balanced cross section across the eastern end of the Peris anticline (Zebari & Burberry, 2015). A growth syncline, between the Peris and Perat anticlines preserved conglomeratic deposits of the Bai-Hasan Formation, displays an abrupt change in dip and thickness of beds adjacent to mapped faults (Figure 9a). These Bai-Hasan growth strata rest atop subvertical beds of the Mukdadiya Formation, which suggests presence of syncline with the inclined beds of the Mukdadiya Formation. The lack of growth and conglomerates in the Mukdadiya Formation suggests that local faults and folds were not active until the time of Bai-Hasan Formation deposition. Previously, Mukdadiya and Bai-Hasan Formations had been proposed as Injana (Upper Fars) Formation with growth strata in this location (László et al., 2012); however, detailed field mapping in this study contradict this assertion. Overall, field relationship in the High Folded zone and in the vicinity of MFF point to a major deformation event during and prior to deposition of the Bai-Hasan Formation. This interpretation is in line with the previous estimates of timing for major shortening during late Miocene and suggests development of the MFF between the High Folded and Low Folded zones at ~5 Ma. In the Low Folded zone, field relationship at the NE limb of Kirkuk structure show an unconformity between the Mukdadiya and Bai-Hasan Formations with growth strata within the Bai-Hasan Formation (Figure 8c), similar to the field observations in the Dinarta syncline. Therefore the Kirkuk structure must have been reactivated during the deposition of the Bai-Hasan Formation that likely commenced as a result of the regional hinterland uplift by ~5 Ma (Koshnaw et al., 2020). At this stage (Figure 8a4), transferring displacement from the hinterland to foreland required reactivation of basement faults below the MFF along a fault ramp from

10.1029/2019TC005865

the Lower Triassic décollement level to the middle Miocene Fatha Formation likely through the Taq-Taq anticline. Such a fault is necessary for reactivation of the Kirkuk and Bai-Hasan structures. At this stage the estimated shortening amount is 1.2 km (0.4%).

5.2. Sulaimani Cross Section Kinematic Forward Model

The kinematic forward model steps in the Sulaimani cross section are similar to the Erbil section, with prelate Miocene (~15–10 Ma), late Miocene (~10–5 Ma), and base Pliocene-Present (~5 Ma) steps (Figure 10a). The prelate Miocene initial stage marks the proto-Zagros fold-thrust belt shortening up to the Qaradagh anticline, as evidenced by the Oligocene unconformity at its vicinity, and the later activation of the MZF (Figure 10a2). The exposed mid-Cenozoic margin of the marine basin was located near the MFF and Kirkuk structure, generating a regional Oligocene unconformity in the study area (Abdullah et al., 2019; Ameen, 2009; Bellen et al., 1959; Dunnington, 1958; Karim et al., 2020; Khanqa et al., 2009; Lawa et al., 2013; Lawa & Ghafur, 2015). During the middle to late Miocene transition, the MZF was active, based on reset AHe ages of ~11 Ma (Koshnaw et al., 2017) and a similar dominant detrital age mode (~12–10 Ma), suggestive of a major exhumation phase, likely along the Suture zone. At this stage shortening is estimated to be ~6.5 km (2.9%).

During the late Miocene time (~10–5 Ma), basement shortening initiated and displacement transferred toward the foreland, creating the frontal structures and breaching the SW limb of the Qaradagh anticline (Figures 10a3 and 10b–10g). In the High Folded zone, an AHe sample from the Tanjero Formation near the Azmar anticline (12KRD-125) exhibits a reset age of 8.7 $\pm$ 2.2 Ma, this cooling age likely resulted from exhumation due to basement uplift at this stage (Figures 2, 5, and 10a3). In the Low Folded zone, the AHe samples from the frontal structures record activation at ~8–7 Ma (Koshnaw et al., 2017). In the central sector along the Erbil cross section, samples from the Khurmala dome and Qarachugh frontal structures, from the Mukdadiya and Injana Formations, were not fully reset. These variations in AHe ages between the central and southern sectors suggest a greater overburden to the south, consistent with measured stratigraphic thicknesses (Koshnaw et al., 2020).

Seismic profiles in the SE segment of the Kirkuk fault show clear growth strata in the latest Miocene Mukdadiya Formation but not the younger Bai-Hasan Formation (Koshnaw et al., 2017; Le Garzic et al., 2019), indicating that the Kirkuk fault was active during Mukdadiya deposition (~8 Ma). Moreover, farther toward the foreland, the frontal structures of Shakal/Pulkhana, Qamar, and Hamreen also contain growth strata (Figures 2 and 10b–10d). The Hamreen structure, which represents the Zagros Deformation front (ZDF), preserves growth strata within the Mukdadiya Formation, whereas the overlying Bai-Hasan Formation beds are subhorizontal (Kent, 2010). In the Shakal/Pulkhana structure, the Bai-Hasan Formation contains two separate growth strata packages (Figures 10b–10d) (Oil Search Limited, 2012; Shamaran Petroleum Group, 2009, 2011). At this location the Shakal/Pulkhana structural profile suggests termination of the lowermost reflectors of the Bai-Hasan Formation against a preexisting high in the NE. Subsequently, the SW end of the structure was faulted, leading to the development of a growth syncline farther to the NE during deposition of the Bai-Hasan Formation (Figures 10b–10d). Along the Sulaimani cross section, shortening at this stage is estimated to be ~6 km (2.6%).

By the earliest Pliocene time (~5 Ma), significant uplift along the MFF is recorded by a ~5 Ma reset AHe sample from the NE limb of Qaradagh anticline and Pliocene age ($\leq$ ~5 Ma) growth strata in the Bai-Hasan Formation (Figure 10b NE end of section) adjacent to the Sangaw South anticline (Koshnaw et al., 2017). At the start of this stage (Figure 10a4), we propose that in addition to reactivation of the previously formed basement faults, a new basement fault was formed near the MFF that followed the Lower Triassic décollement and ramped upsection to reach the middle Miocene (Fatha) décollement. Reactivation of the older basement fault and upsection ramping formed the Sangaw structures. Reverse displacement along these hinterland basement faults ultimately emerged in the Kirkuk, Shakal, and Qamar structures (above and below the Fatha décollement) as recorded by growth strata in the Bai-Hasan Formation, (Figures 10a4 and 10b–10d). The estimated shortening amount is ~3.5 km (1.5%) at this stage. This out-of-sequence, basement involved scenario offers as self-consistent explanation for the regional hinterland uplift, continued deformation along the MFF, and additional shortening along the trailing frontal structures, honoring geologic, subsurface seismic, and thermochronometric relationships.

6. Discussion

6.1. Thick-Skinned, Out-of-Sequence Versus Thin-Skinned, In-Sequence Modes of Deformation

In the NW Zagros, the kinematic history of upper crustal shortening is obtained from balanced cross sections and kinematic forward modelings, AHe thermochronometric ages, and structural and stratigraphic relationships. These data sets are consistent with a hybrid thin- and thick-skinned contractional belt characterized by out-of-sequence basement-involved shortening.

The AHe ages show exhumation associated with different contractional structural domains during the middle Miocene and Pliocene, generally trending younger toward NW along the MZF (Figure 11). Shortening by ~8 Ma marks the onset of regional deformation via basement involvement under the Zagros fold belt and development of the foreland frontal structures, and later pronounced growth of the MFF by ~5 Ma. We advocate that this period represents the timing of the shift from a prolonged thin-skinned detachment-fold system to a hybrid thin-skinned and basement-involved fold-thrust system that developed remarkable structural steps and out-of-sequence growth of the MFF by ~5 Ma. As evidenced by the AHe ages and the spatial distribution of growth strata wedges in the Mukdadiya and Bai-Hasan Formations at the deformation front, the early Pliocene (~5 Ma) growth of the MFF represents a phase of out-of-sequence deformation (Figure 11d). For the Erbil cross section, out-of-sequence growth in the Low Folded zone structures is suggested by geomorphic evidence showing development of the ZDF structures of Makhul and Khanuqa before most other structures (Obaid & Allen, 2017). For the Sulaimani cross section, the ZDF structure of Hamreen shows no growth strata within the youngest beds of the Bai-Hasan Formation, whereas trailing structures show clear Bai-Hasan growth strata (Figures 10b, 11c, and 11d) (Kent, 2010, Figure 15). For the tectonic style during the latest Miocene and onward a basement-involved shortening is preferred by taking into account the structural steps variation and the relatively low amount of the sedimentary cover shortening (6–7%). Based on the cross-sectional area of the sedimentary cover, any model with no basement deformation would necessitate greater shortening than can be observed in surface geologic relationships. Most basement-involved hinterland shortening took place after ~8 Ma in both cross sections of Erbil (~6.2 km) and Sulaimani (~9.5 km). This basement shortening was transferred toward the nearest frontal structures via the upper-level middle Miocene Fatha décollement. The Taq-Taq anticline grew at ~8 Ma as documented by Mukdadiya Formation growth strata (Figures 8b and 11c), while the Sangaw anticlines formed at ~5 (or younger) as expressed by the Bai-Hasan Formation growth strata (Figures 10b and 11d). These timing constraints on the evolution of the MFF in the NW Zagros are similar to the age of initiation and growth of the MFF (~8–2.5 Ma) in the Lurestan segment in Iran (Homke et al., 2004). In this study, the early in-sequence deformation is in agreement with previous interpretations of the deformation history during most of the Cenozoic (Lawa et al., 2013; Le Garzic et al., 2019). However, the new thermochronologic data from this study and Koshnaw et al. (2017), as well as the spatial distribution of growth strata of different ages, provide evidences for a major post ~8 Ma out-of-sequence deformation.

In the Lurestan and Fars segments, the sedimentary cover has undergone ~50–70 km of shortening (McQuarrie, 2004; Sherkati et al., 2006), significantly more than the ~15–20 km in the NW Zagros (this study). This contrast in relation to thick- versus thin-skinned deformation between different segments of the Zagros is in line with other fold-thrust belts. Most thick-skinned belts are characterized by limited horizontal shortening, whereas thin-skinned fold-thrust belts typically display significantly higher values (Fuentes et al., 2016; Kley et al., 1999; Lacombe & Bellahsen, 2016; Mescua et al., 2016; Mouthereau et al., 2013). For example, the thick-skinned Marche sector of northern Apennines shows ~8.5 km of shortening (Butler et al., 2004), whereas the thin-skinned North American Cordillera is characterized by shortening in excess of ~100–150 km (DeCelles & Coogan, 2006; Fuentes et al., 2012). In the Fars segment of the Zagros, depending on crosscutting relationships and relative timing of deformation of major faults (e.g., Lardogarm thrust near the MZF, Molinaro, Leturmy, et al., 2005) a similar thin-skinned fold-thrust belt followed by an out-of-sequence thick-skinned deformation has also been suggested (Molinaro, Leturmy, et al., 2005). Others have proposed thick-skinned deformation to account for high-magnitude surface uplift, but not necessarily in an out-of-sequence pattern (Mouthereau, Tensi, et al., 2007; Sherkati & Letouzey, 2004). Based on earthquake slip vector scatter and crosscutting folds in the outer eastern Fars segment, a recent study (Edey et al., 2020) suggests that potentially both thin-skinned and thick-skinned deformation have been taking place since an early stage with no necessity for switching from a thin-skinned to a thick-skinned style.

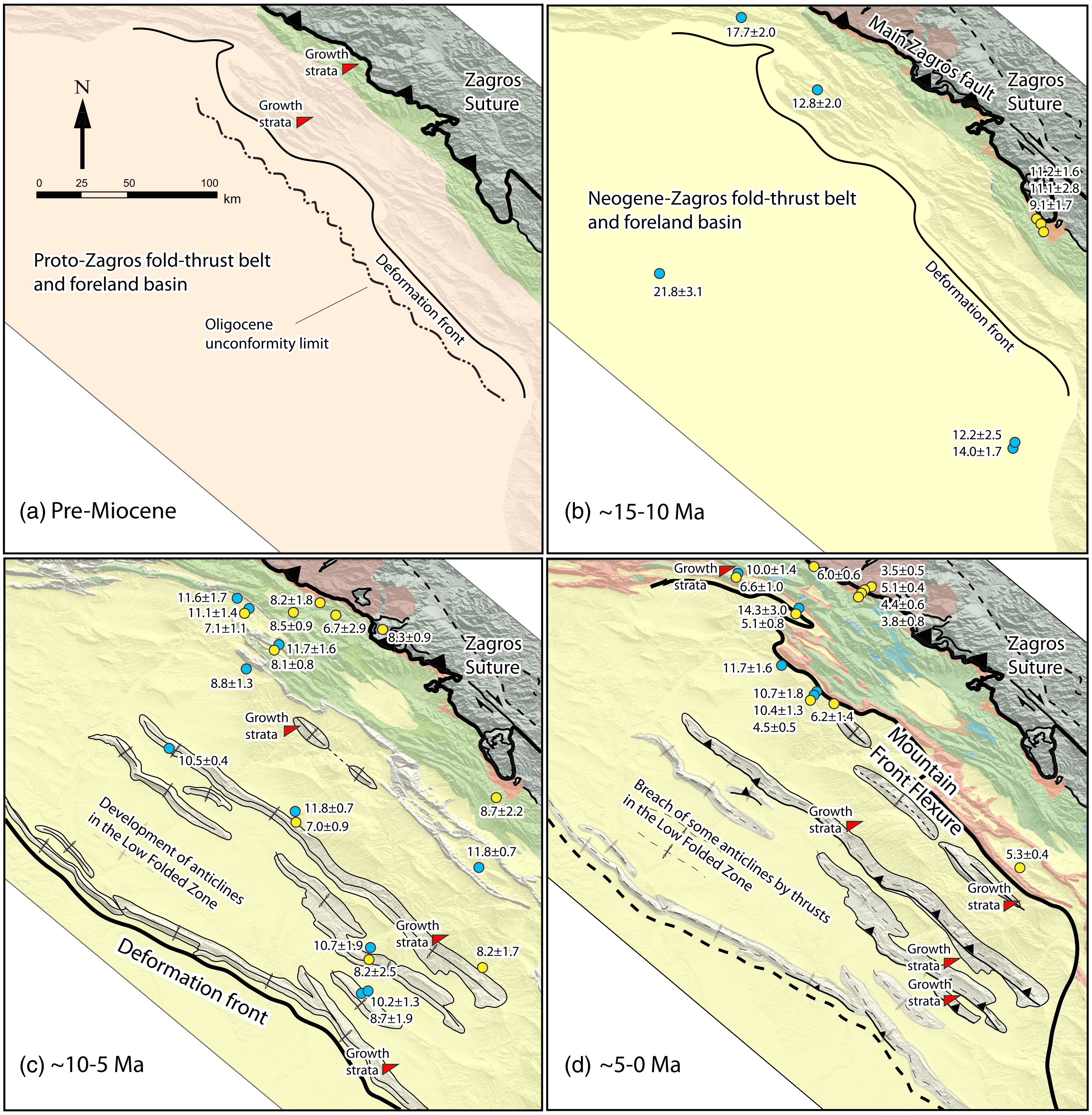

Figure 11. Schematic map view structural reconstruction of the pre-Miocene to present history of the NW Zagros in the Kurdistan region of Iraq. (a) Pre-Miocene structural framework showing documented growth strata in the proto-Zagoros fold-thrust belt (Allouche et al., 2015, Figure 3; Le Garzic et al., 2019, Figure 7), inferred deformation front, and possible Oligocene marine basin margin (see text for references). (b) Late middle Miocene to early late Miocene time showing early stage of the Neogene-Zagros fold-thrust belt and foreland basin during deposition of the Fatha and Injana formations with thermally reset (yellow) and nonreset (blue) samples, uplift of the Zagros sure zone and reactivation of the Main Zagros fault as well as initiation of the right-lateral strike-slip component (Main Zagros recent fault). (c) Late Miocene time depicting deformation front advance into the foreland during deposition of the Mukdadiya formation and location of the associated growth strata, as well as thermally reset and nonreset samples. (d) Pliocene to present structural configuration showing deformation retreat toward the hinterland and manifestation of the mountain front flexure (MFF) during deposition of the Bai-Hasan formation and location of the associated growth strata, as well as thermally reset and nonreset samples.

In the study area, within the NW Zagros inner belt, the MFF appears to be composed of different segments with variable degrees of foreland propagation, as observed NW of the Erbil cross section, where deformation was less advanced, resembling fault segment linkage patterns via tip propagation (Figure 2b). This structural limit of the MFF also corresponds to the geographic distribution of the Tanjero Formation, which shows a rapid reduction in thickness from ~2,000 to 500 m across the hinterland, with the greater thicknesses SE of the study area (Ahmed et al., 2016; Bellen et al., 1959; Lawa, 2018). The similarity of spatial distribution of the proto-Zagros foreland basin and the location of the curvilinear MFF feature might be controlled by structures associated with the early Mesozoic Arabian rift margin. Later after inversion, these structures possibly influenced the spatial configuration of the latest Oligocene marine basin margin, the basement-involved out-of-sequence structures, and the present-day MFF position. Inherited structural weakness zones have been shown to influence the timing, location, and style of later deformation (e.g., Bosworth et al., 2008; Kley et al., 2005; Nemčok et al., 2013; Perez et al., 2016, 2019). Therefore, the geometry of the proposed deeply rooted basement faults in the cross sections of this study is plausibly linked to inversion of normal faults (Jackson, 1980), similar to shortcut faults in the Lurestan area of Iran (Tavani, Corradetti, et al., 2018; Tavani et al., 2020; Tavani, Parente, et al., 2018). Based on surface geologic relationships, including structural dimensions and vergence direction, inversion of passive margin normal faults in the NW Zagros has been proposed by other researchers (Ameen, 1991b; Numan & Azzawi, 1993), and outcrop-scale normal fault inversion have been documented in the vicinity of the MFF (Al-Khatony et al., 2019; Al-Kubaisi & Barno, 2015). However, detailed regional thickness and facies maps based on surface and subsurface data are needed to further test this hypothesis.

In the Low Folded zone of the foreland area, published seismic lines and interpretations show the shallow structures and faults extend below Jurassic levels (Fouad, 2012, Figure 5; Grabowski, 2014, Figure 56; Kent, 2010, Figure 15; Koshnaw et al., 2017, Figure 7; Le Garzic et al., 2019, Figure 8; Marouf & Al-Kubaisi, 2005, Figures 3, 5, and 9; Oil Search Limited, 2012; Shamaran Petroleum Group, 2009, 2011). In most seismic profiles, Late Cretaceous grabens, filled with deposits of the Campanian Shiranish Formation, can be identified below the Fatha Formation décollement level, similar to the Taq-Taq anticline near the MFF (Garland et al., 2010, Figure 6). The inversion of grabens, the paired occurrence of contractional structures, as well as the geometry of frontal structures have been portrayed as evidence for major NE dipping listric rift-related normal faults with a depth-to-detachment of at ~20 km (Kent, 2010; Marouf, 1999 in Marouf & Al-Kubaisi, 2005; Obaid & Allen, 2017). However, the lack of high-quality seismic reflection profiles below the Triassic rock levels in the Low Folded zone inhibits direct observation to determine whether steep faults below the Triassic level generates from basement or not. Alternatively, the frontal structures can be interpreted as ramp in the shallower Triassic décollement level as suggested by a thrust fault drilled in in the Makhul frontal structure (Grabowski, 2014; Kent, 2010). In the cross sections of this study, the Triassic strata are chosen as the main décollement level for structures in the Low Folded zone, responsible for the formation of pre-Pliocene anticlines related to either the proto-Zagros fold-thrust belt development or the hinterland growth during the late Miocene as indicated by the Mukdadiya Formation growth strata. The Triassic strata are preferred as the main décollement level because major reversals of a basement-rooted listric fault system would have resulted in basement uplifts within the present-day Low Folded zone similar to those in the High Folded and Imbricate zones. However, inherited basement weakness zones might have influenced the spatial distribution of the late Miocene and Pliocene structures (Kent, 2010). Additionally, 3-D numerical modeling simulation successfully reproduced the Kirkuk (Khurmala dome) and Qarachugh anticlines as typical detachment folds (Grasemann & Schmalholz, 2012). In their numerical model, the initial thickness ratio of competent to incompetent layers is 2. Considering the depth to the Triassic décollement based on the published well QT-1 in the nearby area (Min et al., 2012), the thickness ratio of 2 translates into an estimated thickness of ~4 km for the competent stratigraphic layers above ~2 km of the incompetent Triassic and Jurassic strata. Furthermore, in the Dezful reentrant, which resembles the Kirkuk embayment, seismic profiles show strikingly similar frontal structures that detached on the Triassic Dashtak décollement level with possible influence of deeper deformation (Alipoor et al., 2019; Asgari et al., 2019; Derikvand et al., 2019; Ghanadian et al., 2017; Sherkati et al., 2006), although more resent research argued for décollement at the basement cover interface (Vatandoust et al., 2020).

Lastly, we speculate that the potential Arabian margin normal faults reactivated selectively and in an out-of-sequence manner as a function of the favorability of inherited normal fault orientations during N-S directioned collision as has been observed along the entire northern margin of Arabia and NE Africa (e.g., Bosworth et al., 2008), and/or due to variation in the throw of the earlier normal fault (Reilly et al., 2015). Differential reactivation is likely further promoted by a shift in the Arabian plate trajectory from NE-SW to N-S ~15–10 Ma ago (ArRajehi et al., 2010; McQuarrie et al., 2003; Molnar et al., 2017; Navabpour et al., 2008).

10.1029/2019TC005865

While a kinematic model that includes basement involvement and an out-of-sequence mode of deformation is the most plausible, further subsurface data are needed to confirm this inferred style and directly image basement faults and their displacement transfers into the sedimentary cover. However, on the basis of our new geologic and thermochronometric data, a nonsequential hybrid thin- and thick-skinned fold-thrust system best describes the tectonic style and evolution of the NW Zagros in the Kurdistan region of Iraq (Figures 6, 7, and 3).

6.2. Driving Mechanism of NW Zagros Uplift and Geodynamic Implications

The pattern of exhumation tracked by AHe thermochronometric ages in the study area outlines an evolution of the NW Zagros belt in response to broader regional tectonic events. This study shows major contractional deformation and exhumation from ~14 Ma onward (Figures 6b, 8, and 10), affecting the area along the Main Zagros fault (MZF) and across the entire fold-thrust belt (Figures 5 and 11). In Iran, in the Lurestan segment, the AHe ages record progressive exhumation from the fold-thrust belt toward the foreland between ~9 to ~6 Ma; similar to the Dezful segment, farther south, where samples from the High Zagros fault recorded rapid exhumation from ~10 to 7 Ma (Barber et al., 2018; Gavillot et al., 2010). Magnetostratigraphic results from the Push-e Kush arc in Lurestan suggest an onset of deformation in the MFF at ~8 Ma that continued to ~5–2 Ma (Homke et al., 2004). The regional similarity in timing of deformation along the MZF, uplift of the internal Zagros fold and thrust belt, and the MFF implies a genetic linkage and a large-scale geodynamic driving mechanism.

The ~2 km high Turkish-Iranian plateau, which dominates the modern topographic expression of most of southeastern Turkey (East Anatolian Plateau, EAP) and northwestern Iran (Figure 1), experienced uplift during Serravallian times (~12 Ma) and onward based on the transition from marine to nonmarine basin deposits (Dewey et al., 1986; Gelati, 1975; Yilmaz & Yilmaz, 2019). This is supported by apatite fission track (AFT) along the Bitlis suture with Arabia recording exhumation between 18–13 Ma (Okay et al., 2010). Temporally, this timing also coincides with inception of motion along North Anatolian Fault (NAF) at ~12 Ma (Authemayou et al., 2006; Şengör et al., 2005). Considering the potential linkage of the Main Zagros Recent Fault (MZRF) with the NAF and the Anatolia extrusion as well as accelerated convergence of Arabia in response to the opening of the Red Sea, a ~12–10 Ma is postulated for the Turkish-Iranian plateau uplift (McQuarrie et al., 2003; Mouthereau et al., 2012; Stockli & Bosworth, 2020). In NW Iran, the orogenic hinterland experienced initial uplift in the Burdigalian as evidenced by end of marine Qom Formation and beginning of clastic Upper Red Bed Formation deposition. This depositional facies transition also appears to temporally coincide with a change in the tectonic regime from transtention to transpression (Ballato et al., 2011; Harzhauser et al., 2007; Morley et al., 2009; Schuster & Wielandt, 1999). Apatite and zircon fission track ages of ~11 Ma (Reichenbacher et al., 2011) suggest a major phase of exhumation of the central Iranian plateau in the middle Miocene. In the study area, this major episode of plateau uplift is also documented by introduction of nonmarine clastic foreland deposits of the Injana Formation (~12.4 Ma) that are characterized by detrital zircon U-Pb signatures recording sediment provenance mostly from SE Turkey (Koshnaw et al., 2020). In Lurestan, the Aghajari Formation (Injana Formation equivalent) also recorded outward migration of deformation at ~14–12 Ma (Homke et al., 2004; Vergés et al., 2019), while AHe data from the internal hinterland portion recorded exhumation in the Sanandaj-Sirjan zone at ~15 Ma and the High Zagros by ~9 Ma (Barber et al., 2018). Additionally, in the Alborz Mountains in northern Iran exhumation has also been recorded at ~12 Ma and interpreted as the onset of denudation (Guest et al., 2006). These lines of evidence for a regionally synchronous onset of the Turkish-Iranian plateau uplift hint at larger-scale geodynamic processes that led to uplift, exhumation, and plateau expansion. The orogenic plateau uplift potentially could be due to crustal thickening as in the Tibetan plateau (Tapponnier et al., 2001) or due to lithospheric mantle removal (Garzione et al., 2006). The regional uplift of the Turkish-Iranian plateau due to crustal thickening is undesirable because of inconsistent timing between the late-middle Miocene uplift of the plateau and the post middle Miocene basement involvement and crustal thickening that potentially impeded Arabia-Eurasia convergence (Austermann & Iaffaldano, 2013; Emami et al., 2010; Homke et al., 2004; Koshnaw et al., 2017). Evidence from the interior of the plateau is necessary to assert whether a large-scale crustal thickening took place or not at an earlier time. Alternatively, asthenospheric upwelling and dynamic uplift are preferred to explain the NW Zagros kinematics. Geological, geochemical, and geophysical data as well as numerical and analog

10.1029/2019TC005865

modeling, have been used to suggest a potential slab breakoff (Davies & von Blanckenburg, 1995) and/or lithospheric mantle delamination (Bird, 1979) as the principal driver triggering the regional uplift event (Agard et al., 2011; Barazangi et al., 2006; Bottrill et al., 2012; Faccenna et al., 2006; Göğüş & Pysklywec, 2008; Hafkenscheid et al., 2006; Jahangiri, 2007; Keskin, 2003, 2007; Memiş et al., 2020; Omrani et al., 2008; Şengör et al., 2003, 2008; van Hunen & Allen, 2011). Tomographic data appear to show relatively slow seismic wave velocities indicative of hot mantle material beneath the Turkish-Iranian plateau that are distinct from faster velocities (Alinaghi et al., 2007; Amini et al., 2012; Bavali et al., 2016; Chang et al., 2010; Hafkenscheid et al., 2006; Kaban et al., 2018; Koulakov et al., 2012; Lei & Zhao, 2007; Rahmani et al., 2019; Sandvol et al., 2001; Tunini et al., 2014; Vergés, Goodarzi, et al., 2011; Zhao & Xie, 2016; Zor, 2008). Depending on 48,000 Pn arrival times, a high lateral resolution velocity image of the upper mantle shows a distinct transition along the MZF in the NW Zagros from a high-velocity zone beneath Arabia to a low-velocity zone beneath Eurasia (Amini et al., 2012, Figure 7). Additionally, a deep (~1,000 km) regional vertical tomographic profile across the Turkish-Iranian plateau and the surrounding areas shows a high-angle downgoing high-velocity material beneath Arabia in the study area and ascending low-velocity material beneath Eurasia in NW Iran, with an abrupt velocity anomaly transition along the MZF in the uppermost part (Koulakov et al., 2012, Figure 5, section 3). Furthermore, this tomography profile displays potentially a fragmented downgoing Arabia slab and a thinned crust beneath Eurasia. The disconnected high-velocity domains are suggestive of slab breakoff of the downgoing Neotethys slab, whereas presence of the low-velocity material at shallow depths is indicative of arising asthenosphere and possible delamination beneath Eurasia in NW Iran (Kaviani et al., 2018; Koulakov et al., 2012; Rahmani et al., 2019).

As the hot asthenospheric material ascends, the lower lithosphere thermally thins and weakens, reducing the elastic thickness and rock strength (Burov & Diament, 1995; Hyndman et al., 2009; Jammes & Huismans, 2012). This rheological change might also lead to a possible partial decoupling of the brittle upper crust and the ductile lower crust (Hyndman et al., 2009). According to natural examples (Bellahsen et al., 2012, 2014; Butler et al., 2006; Lacombe & Bellahsen, 2016) and thermomechanical numerical model of orogens with inherited extensional structures (Jammes & Huismans, 2012), weak crust can promote crustal-scale thick-skinned deformation. A thermomechanical numerical model (Nilfouroushan et al., 2013) that highlighted the role of Moho temperature on the degree of basement involvement in the deformation indicated localization of thick-skinned deformation in the hinterland at relatively cold Moho (400°C at 36 km depth), whereas relatively hot Moho temperatures (600°C at 36 km depth) lead to involvement of basement in the foreland portions. Basilici et al. (2019) calculated thermal structure of the Lurestan segment of Zagros and suggested later gradient in heat flow from the hinterland (>500°C at 30 km depth) to the foreland (~400°C at 30 km depth). Such lateral thermal gradient would be conducive to basement-involved deformation and shortening in the hinterland and the limited or no basement deformation in the foreland as predicted by thermomechanical numerical models. This is in line with the global census of orogenic belts that shows relatively young orogens have high geothermal gradients, weak lithospheric mantle, and moderate amount of deformation that involves deeply rooted basement ramps (Mouthereau et al., 2013). This model of a brittle upper crust over a ductile lower crust has been applied in the Fars segment of the Zagros to explain surface topography and assuming that detached deformation above the Hormuz salt prevents buildup of critical taper topography (Ford, 2004; Mouthereau et al., 2006). In the NW Zagros, the regional orogenic deformation behavior can be explained in the context of critical taper as well (e.g., Dahlen & Suppe, 1988; DeCelles & Mitra, 1995). The orogenic wedge build up by involving the basement during ~8–5 Ma could be an attempt to increase taper to reach the critical state, marking an adjustment from a subcritical state. After a possible lithospheric mantle delamination and slab breakoff by ~12 Ma, the wider orogenic wedge uplifted and exhumed, reducing the wedge taper. To rebuild the wedge taper and increase the β angle, the basement involved in the deformation processes during ~8–5 Ma and amplified along the MFF by ~5 Ma (Figures 8a4 and 10a4), similar to a suggested model for the Fars segment of Zagros (Molinaro et al., 2005). Taken together, these syntheses of data suggest that the hinterland of the NW Zagros may be thermally weakened due to potential lithospheric mantle delamination and slab breakoff, leading to basement involvement in the deformation process (Figure 12).

At the same time of the ongoing deformation along the northeastern margin of the Arabian plate during Miocene and Pliocene, the western and southern margins of Arabia also experienced major plate tectonic changes, affecting the plate kinematics of the plate. Following initial rifting in the Red Sea starting at

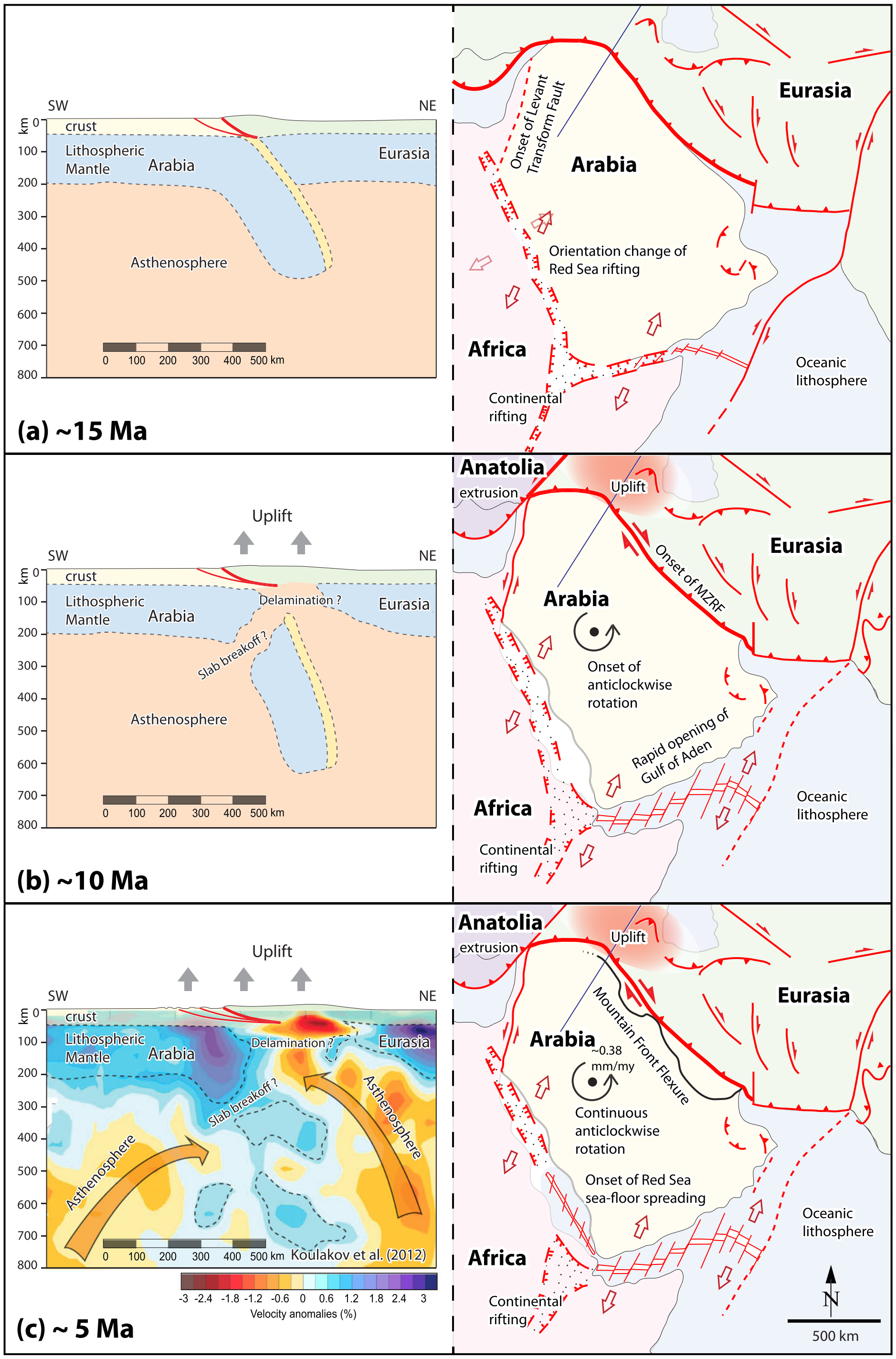

Figure 12. Schematic diagrams that show plate tectonic kinematics of the Middle East. (a) Suturing of the Arabia-Eurasia and change in the direction of the Red Sea rifting as well as commencement of the Levant transform fault prior to potential slab breakoff. (b) Turkish-Iranian plateau uplift due to potential slab breakoff and lithospheric mantle delamination that likely started to modify the lower crust rheological behavior, initiation of the right-lateral strike-slip component of the Main Zagros fault (Main Zagros recent fault, MZRF) coeval with extrusion of the Anatolia, Gulf of Aden rapid opening, and onset of the Arabian plate anticlockwise rotation. (c) Expansion of Turkish-Iranian plateau and rapid uplift along its margin in the NW Zagros orogenic belt as manifested by the growth of the MFF and basement involvement in the deformation process, likely due to the lower crust thermal weakening. This phase of tectonic deformation is also coeval with the onset of the Red Sea seafloor spreading and enhanced anticlockwise rotation of the Arabian plate. Diagrams are based on Hempton (1987), Bosworth et al. (2005), Molinaro, Zeyen, and Laurencin (2005), Hansman et al. (2017), Barber et al. (2018), and Burg (2018). Crustal thickness is estimated based on Paul et al. (2010) and Motaghi et al. (2017). The tomographic profile (c, left) is from Koulakov et al. (2012, Figure 5, section 3). Present-day Arabian plate rotation velocity is adopted for 5 Ma phase from ArRajehi et al. (2010).

~23 Ma (Stockli & Bosworth, 2020), the onset of motion along the Aqaba transform fault at ~14 Ma, marked an acceleration of Red Sea opening and a transition from ENE-WSW oriented orthogonal to NNE–SSW oriented oblique extension. The Aqaba transform fault also directly linked the northern Red Sea with the Zagros-Bitlis suture zone (Bosworth et al., 2005; Stockli & Bosworth, 2020). By ~10 Ma, the Gulf of Aden opened abruptly and probably accounts for the anticlockwise rotation of the Arabian plate (ArRajehi et al., 2010; Bosworth et al., 2005; Molnar et al., 2017). Later by ~5 Ma, seafloor spreading and genesis of the oceanic lithosphere in the Red Sea commenced (Bosworth, 2015; Bosworth & Stockli, 2016; Cochran & Karner, 2007; Stockli & Bosworth, 2020; Szymanski et al., 2016). Comparable timing of uplift and exhumation in Alborz, northern Iran has also been reported and linked to a likely choking of the Neotethyan subduction zone due to arrival of the buoyant Arabian lithosphere (Axen et al., 2001). However, more recent studies point at the early Miocene for such subduction zone locking (Ballato et al., 2011; Madanipour et al., 2017). Moreover, Arabia-Eurasia convergence accommodation by further shortening in the northern Middle East potentially due to suturing of the Afghan block with the western margin of the Indian plate during Pliocene could be an additional mechanism for the enhanced deformation in NW Zagros (Allen et al., 2011). In general, such similarities in the timing of major tectonic deformations around the Arabian plate boundary suggest that several geodynamic events influenced the present-day ~2,000 km long Zagros orogenic belt. Kinematic organization of the Red Sea (~14 Ma), opening of the Gulf of Aden (~10 Ma) and the Red Sea seafloor spreading (~5 Ma) are likely important contributors to the Zagros orogenic kinematics on a plate tectonic scale, influencing the development of the right-lateral strike-slip fault of MZRF and MFF (Figure 12).

In summary, we argue that the key drivers for the basement-involved deformation and hinterland uplift are combination of slab breakoff, lithospheric mantle delamination, and the consequent thermomechanical behavior change of the crust, as well as plate tectonic boundary condition changes associated with Red Sea rifting.

7. Conclusions

During the late Miocene (~8–5 Ma), the NW Zagros in the Kurdistan region of Iraq shifted from a thin-skinned, basement-detached fold-thrust belt to a hybrid thin- and thick-skinned orogenic system. This fundamental change in the tectonic style coincided with a hindward retreat in the locus deformation and associated exhumation that was promoted by the presence of inherited basement weaknesses and potentially driven by the thermomechanical effects of slab breakoff. Basement-involved deformation likely initiated by ~8 Ma and intensified at ~5 Ma, leading to growth of the MFF in an out-of-sequence manner. Horizontal shortening across the NW Zagros was estimated to be ~18.2 km (6%) in the central sector and ~16 km (7%) in the southern sector of the Kurdistan region of Iraq as deduced from balanced cross sections. The results from this study constrain the timing of key crustal structures in the NW Zagros orogenic belt and highlight the role of basement discontinuities combined with mechanical stratigraphy in the development of fold-thrust belts. Additionally, we conclude that the late Miocene shift in tectonic style, which led to enhanced basement involvement and orogenic wedge buildup, may represent a response to both breakoff of the subducting Arabian plate and mantle delamination under the Turkish-Iran plateau, as well as plate tectonic changes associated with Red Sea rifting, resulting in activation of regional strike-slip deformation along the boundaries of northern Arabia.

Data Availability Statement

The data discussed in this article are provided in the supporting information (Data Sets S1–S2) and are available at this site (http://www.geochron.org/viewfile.php?pkey=15509).

Acknowledgments

This research was supported by an industry research grant awarded to PI Brian K. Horton and Co-PI Daniel F. Stockli, and Geological Society of America Graduate Student Research Grants, the Jackson School of Geosciences Ronald K. DeFord Field Scholarship, and the American Ph.D. scholarship from the Iraq Scholars and Leaders Program awarded to Renas I. Koshnaw. We thank Mjahid M. Zebari, Bahroz G. Abdullah, Halo A. Fateh, Hajar R. Abdul Qadr, Mahdi K. Aswad, Bawar S. Ahmed, Rebwar A. Farman, and Rojgar H. Ali for providing logistical support and field assistance. We express gratitude to George A. Yacu at the Ministry of Natural Resources, Kurdistan Regional Government, Iraq, for facilitating the subsurface data sharing agreement. The Structural Geology group at the University of Bern, Switzerland, and the Structural Geology and Geodynamic group at the University of Göttingen enabled use of Move software through academic licenses provided by Midland Valley-Petex. We also thank Desmond B. Patterson, Lisa G. Stockli, Yomayra Roman, Michael G. Prior, and Spencer Seman for analytical assistance in the laboratory, and Jonas Kley and Martin R. Correa for scientific discussions. We extend gratitude to Nadine McQuarrie, Mark Allen, Jamshid Hassanzadeh, and the Editor Laurent Jolivet for their constructive criticism on an earlier version of the manuscript.

References

Abdel-Kireem, M. R. (1986). Planktonic foraminifera and stratigraphy of the Tanjero formation (Maastrichtian), northeastern Iraq. *Micropaleontology*, *32*(3), 215–231. https://doi.org/10.2307/1485618

Abdullah, H. G., Collier, R. E. L., & Mountney, N. P. (2019). The palaeoshoreline of Early Miocene formations (Euphrates and Jeribe) at the periphery of the Zagros Foreland Basin, Sulaimani governorate, Kurdistan region, NE Iraq. *Arabian Journal of Geosciences*, *12*(18), 574. https://doi.org/10.1007/s12517-019-4716-2

Abdulnaby, W., Mahdi, H., Numan, N. M., & Al-Shukri, H. (2014). Seismotectonics of the Bitlis–Zagros fold and thrust belt in northern Iraq and surrounding regions from moment tensor analysis. *Pure and Applied Geophysics*, *171*(7), 1237–1250. https://doi.org/10.1007/s00024-013-0688-4

Agard, P., Omrani, J., Jolivet, L., & Mouthereau, F. (2005). Convergence history across Zagros (Iran): Constraints from collisional and earlier deformation. *International Journal of Earth Sciences*, *94*(3), 401–419. https://doi.org/10.1007/s00531-005-0481-4

Agard, P., Omrani, J., Jolivet, L., Whitechurch, H., Vrielynck, B., Spakman, W., et al. (2011). Zagros orogeny: A subduction-dominated process. *Geological Magazine*, *148*(5–6), 692–725. https://doi.org/10.1017/S001675681100046X

Ahmadhadi, F., Daniel, J. M., Azzizadeh, M., & Lacombe, O. (2008). Evidence for pre-folding vein development in the Oligo-Miocene Asmari formation in the central Zagros Fold Belt, Iran. *Tectonics*, *27*, TC1016. https://doi.org/10.1029/2006TC001978

Ahmadhadi, F., Lacombe, O., & Daniel, J. M. (2007). Early reactivation of basement faults in Central Zagros (SW Iran): Evidence from pre-folding fracture populations in Asmari formation and lower tertiary paleogeography. In *Thrust Belts and Foreland Basins* (pp. 205–228). Berlin, Heidelberg: Springer. https://doi.org/10.1007/978-3-540-69426-7_11

Ahmed, S. H., Barrier, É., & Müller, C. (2016). Basin evolution model during Cretaceous in the northeastern of Arabian plate in Kurdistan region. *Arabian Journal of Geosciences*, *9*(14), 645. https://doi.org/10.1007/s12517-016-2677-2

Alavi, M. (1991). *Tectonic map of the Middle East, Ministry of Industries and Mines, scale, 1, 5,000,000*. Tehran, Iran: Ministry of Industries & Mines.

Alavi, M. (1994). Tectonics of the Zagros orogenic belt of Iran: New data and interpretations. *Tectonophysics*, *229*(3–4), 211–238. https://doi.org/10.1016/0040-1951(94)90030-2

Alavi, M. (2007). Structures of the Zagros fold-thrust belt in Iran. *American Journal of Science*, *307*(9), 1064–1095. https://doi.org/10.2475/09.2007.02

Al-Banna, N. Y., & Al-Mutwali, M. M. (2008). Microfacies and age determination of the sedimentary sequences within Walash volcano-sedimentary group, Mawat complex, Northeast Iraq. *Tikrit Journal of Pure Science*, *13*(3), 46–52.

Al-Bassam, K. S. (2010). Petrology, geochemistry and depositional environment of the Khabour formation in Ora and Khabour localities, Northern Iraq. *Iraqi Bulletin of Geology and Mining*, *6*(2), 71–94.

Al-Hadidy, A. H. (2007). Paleozoic stratigraphic lexicon and hydrocarbon habitat of Iraq. *GeoArabia*, *12*(1), 63–130.

Ali, S. A., Buckman, S., Aswad, K. J., Jones, B. G., Ismail, S. A., & Nutman, A. P. (2012). Recognition of late cretaceous Hasanbag ophiolite-arc rocks in the Kurdistan region of the Iraqi Zagros suture zone: A missing link in the paleogeography of the closing Neotethys Ocean. *Lithosphere*, *4*(5), 395–410. https://doi.org/10.1130/L207.1

Ali, S. A., Buckman, S., Aswad, K. J., Jones, B. G., Ismail, S. A., & Nutman, A. P. (2013). The tectonic evolution of a Neo-Tethyan (Eocene–Oligocene) island-arc (Walash and Naopurdan groups) in the Kurdistan region of the Northeast Iraqi Zagros suture zone. *Island Arc*, *22*(1), 104–125. https://doi.org/10.1111/iar.12007

Ali, S. A., Mohajjel, M., Aswad, K., Ismail, S., Buckman, S., & Jones, B. (2014). Tectono-stratigraphy and structure of the northwestern Zagros collision zone across the Iraq-Iran border.

Ali, S. A., & Mohmmad, E. M. (2018). Geochemistry and provenance of sandstone unit in Tanjero formation in Sulimania area, NE-Iraq. *Kirkuk University Journal for Scientific Studies*, *13*(4), 113–126. https://doi.org/10.32894/kujss.2018.13.4.9

Alinaghi, A., Koulakov, I., & Thybo, H. (2007). Seismic tomographic imaging of *P*- and *S*-waves velocity perturbations in the upper mantle beneath Iran. *Geophysical Journal International*, *169*(3), 1089–1102. https://doi.org/10.1111/j.1365-246X.2007.03317.x

Alipoor, R., Alavi, S. A., Fard, I. A., Ghassemi, M. R., Mohseni, H., Mokhtari, M., & Golalzadeh, A. (2019). Structural analysis of the Aghajari and Pazanan anticlines, Dezful embayment, SW Iran. *Journal of Petroleum Science and Engineering*, *176*, 27–42. https://doi.org/10.1016/j.petrol.2019.01.033

Al-Khatony, S. E., Al-Azzawi, N. K., & Lawa, F. A. (2019). Structural and tectonic study of Qara Sard anticline and Choplagh syncline, from Sulaimaniya area, Kurdistan region, Northeastern Iraq. *Iraqi National Journal of Earth Science*, *19*(1), 39–58.

Al-Kubaisi, M. S., & Barno, J. M. (2015). Fold geometry and kinematics of inversion tectonics for Kosrat anticline, northeastern Iraq. *Arabian Journal of Geosciences*, *8*(11), 3.

Allen, M. B., Kheirkhah, M., Emami, M. H., & Jones, S. J. (2011). Right-lateral shear across Iran and kinematic change in the Arabia–Eurasia collision zone. *Geophysical Journal International*, *184*(2), 555–574. https://doi.org/10.1111/j.1365-246X.2010.04874.x

Allen, M. B., Saville, C., Blanc, E. P., Talebian, M., & Nissen, E. (2013). Orogenic plateau growth: Expansion of the Turkish-Iranian plateau across the Zagros fold-and-thrust belt. *Tectonics*, *32*, 171–190. https://doi.org/10.1002/tect.20025

Allouche, H., Sapin, F., Chevallier, B., Cheriyan, T., & Brosille, E. (2015). Seismic imaging in western Zagros and impact on hydrocarbon exploration: A case study from Kurdistan Region of Iraq. In *Abu Dhabi International Petroleum Exhibition and Conference*. Richardson, TX: Society of Petroleum Engineers. Retrieved from https://www.onepetro.org/conference-paper/SPE-177526-MS, https://search.spe.org/i2kweb/SPE/search?filters=taxnodes%3ACountry%7CAsia%7CMiddle+East%7CIraq%7CKurdistan+Region&sort=score+desc&q=SPE-177526-MS

Alsharhan, A. S., & Nairn, A. E. M. (1997). *Sedimentary basins and petroleum geology of the Middle East*. New York: Elsevier.

Ameen, B. M. (2009). Lthological indicators for the Oligocene unconformity, NE Iraq. *Iraqi Bulletin of Geology and Mining*, *5*(1), 25–34.

Ameen, M. S. (1991a). Alpine geowarpings in the Zagros-Taurus range: Influence on hydrocarbon generation, migration and accumulation. *Journal of Petroleum Geology*, *14*(4), 417–428. https://doi.org/10.1111/j.1747-5457.1991.tb01034.x

Ameen, M. S. (1991b). Possible forced folding in the Taurus–Zagros belt of northern Iraq. *Geological Magazine*, *128*(6), 561–584. https://doi.org/10.1017/S0016756800019695

Ameen, M. S. (1992). Effect of basement tectonics on hydrocarbon generation, migration, and accumulation in northern Iraq (1). *AAPG Bulletin*, *76*(3), 356–370.

Amini, S., Shomali, Z. H., Koyi, H., & Roberts, R. G. (2012). Tomographic upper-mantle velocity structure beneath the Iranian plateau. *Tectonophysics*, *554*, 42–49.

Anderson, R. B., Long, S. P., Horton, B. K., Thomson, S. N., Calle, A. Z., & Stockli, D. F. (2018). Orogenic wedge evolution of the Central Andes, Bolivia (21°S): Implications for cordilleran cyclicity. *Tectonics*, *37*, 3577–3609. https://doi.org/10.1029/2018TC005132

Aqrawi, A. A. M., Goff, J. C., Horbury, A. D., & Sadooni, F. N. (2010). *The petroleum geology of Iraq*. Beaconsfield, UK: Scientific Press.

ArRajehi, A., McClusky, S., Reilinger, R., Daoud, M., Alchalbi, A., Ergintav, S., et al. (2010). Geodetic constraints on present-day motion of the Arabian plate: Implications for Red Sea and Gulf of Aden rifting. *Tectonics*, *29*, TC3011. https://doi.org/10.1029/2009TC002482

Asgari, G. R., Ghaemi, F., Soleimany, B., Rahimi, B., & Shekarian, Y. (2019). Role of incompetent strata and geometry of faults on the folding mechanism, a case study: The Karun oil field in the Dezful embayment, Iran. *Modeling Earth Systems and Environment*, *5*(4), 1781–1800. https://doi.org/10.1007/s40808-019-00636-5

ASTER Global Digital Elevation Map (GDEM) v.2 (2011). ASTER GDEM is a product of *NASA and METI*, accessed July 10, 2015, https://asterweb.jpl.nasa.gov/gdem.asp
Austermann, J., & Iaffaldano, G. (2013). The role of the Zagros orogeny in slowing down Arabia-Eurasia convergence since~ 5 Ma. *Tectonics*, *32*, 351–363. https://doi.org/10.1002/tect.20027
Authemayou, C., Chardon, D., Bellier, O., Malekzadeh, Z., Shabanian, E., & Abbassi, M. R. (2006). Late Cenozoic partitioning of oblique plate convergence in the Zagros fold-and-thrust belt (Iran). *Tectonics*, *25*, TC3002. https://doi.org/10.1029/2005TC001860
Awdal, A. H., Braathen, A., Wennberg, O. P., & Sherwani, G. H. (2013). The characteristics of fracture networks in the Shiranish formation of the Bina Bawi anticline; comparison with the Taq Taq field, zagros, Kurdistan, NE Iraq. *Petroleum Geoscience*, *19*(2), 139–155. https://doi.org/10.1144/petgeo2012-036
Axen, G. J., Lam, P. S., Grove, M., Stockli, D. F., & Hassanzadeh, J. (2001). Exhumation of the west-central Alborz Mountains, Iran, Caspian subsidence, and collision-related tectonics. *Geology*, *29*(6), 559–562. https://doi.org/10.1130/0091-7613(2001)029<0559:EOTWCA>2.0.CO;2
Bahroudi, A., & Koyi, H. A. (2003). Effect of spatial distribution of Hormuz salt on deformation style in the Zagros fold and thrust belt: An analogue modelling approach. *Journal of the Geological Society of London*, *160*(5), 719–733. https://doi.org/10.1144/0016-764902-135
Bahroudi, A., & Koyi, H. A. (2004). Tectono-sedimentary framework of the Gachsaran formation in the Zagros foreland basin. *Marine and Petroleum Geology*, *21*(10), 1295–1310. https://doi.org/10.1016/j.marpetgeo.2004.09.001
Bahroudi, A., & Talbot, C. J. (2003). The configuration of the basement beneath the Zagros Basin. *Journal of Petroleum Geology*, *26*(3), 257–282. https://doi.org/10.1111/j.1747-5457.2003.tb00030.x
Balaki, H. G. K., & Omar, A. A. (2019). Structural assessment of the Bradost and Berat structures in imbricate and high folded zones—Iraqi Kurdistan Zagros belt. *Arabian Journal of Geosciences*, *12*(4), 106. https://doi.org/10.1007/s12517-019-4251-1
Ballato, P., Uba, C. E., Landgraf, A., Strecker, M. R., Sudo, M., Stockli, D. F., et al. (2011). Arabia-Eurasia continental collision: Insights from late tertiary foreland-basin evolution in the Alborz Mountains, northern Iran. *Bulletin*, *123*(1–2), 106–131.
Barazangi, M., Sandvol, E., & Seber, D. (2006). Structure and tectonic evolution of the Anatolian plateau in eastern Turkey. In Y. Dilek & S. Pavlides (Eds.), *Postcollisional tectonics and magmatism in the Mediterranean Region and Asia*, *Special Paper* (Vol. 409, pp. 463–473). Boulder, CO: Geological Society of America. Retrieved from https://pubs.geoscienceworld.org/books/book/583/Postcollisional-Tectonics-and-Magmatism-in-the; https://www.geosociety.org/GSA/Publications/Books/GSA/Pubs/Books/home.aspx?hkey=b14a4633-f629-43b7-9a79-9fe4d633767a
Barber, D. E., Stockli, D. F., & Galster, F. (2019). The proto-Zagros Foreland basin in Lorestan, Western Iran: Insights from multimineral detrital geothermochronometric and trace elemental provenance analysis. *Geochemistry, Geophysics, Geosystems*, *20*, 2657–2680. https://doi.org/10.1029/2019GC008185
Barber, D. E., Stockli, D. F., Horton, B. K., & Koshnaw, R. I. (2018). Cenozoic exhumation and foreland basin evolution of the Zagros orogen during the Arabia-Eurasia collision, western Iran. *Tectonics*, *37*, 4396–4420. https://doi.org/10.1029/2018TC005328
Barnhart, W. D., Brengman, C. M., Li, S., & Peterson, K. E. (2018). Ramp-flat basement structures of the Zagros Mountains inferred from co-seismic slip and afterslip of the 2017 *Mw*7. 3 Darbandikhan, Iran/Iraq earthquake. *Earth and Planetary Science Letters*, *496*, 96–107. https://doi.org/10.1016/j.epsl.2018.05.036
Basilici, M., Mazzoli, S., Megna, A., Santini, S., & Tavani, S. (2019). Geothermal model of the shallow crustal structure across the "mountain front fault" in Western Lurestan, Zagros Thrust Belt, Iran. *Geosciences*, *9*, 301. https://doi.org/10.3390/geosciences9070301
Bavali, K., Motaghi, K., Sobouti, F., Ghods, A., Abbasi, M., Priestley, K., et al. (2016). Lithospheric structure beneath NW Iran using regional and teleseismic travel-time tomography. *Physics of the Earth and Planetary Interiors*, *253*, 97–107. https://doi.org/10.1016/j.pepi.2016.02.006
Bellahsen, N., Jolivet, L., Lacombe, O., Bellanger, M., Boutoux, A., Garcia, S., et al. (2012). Mechanisms of margin inversion in the external Western Alps: Implications for crustal rheology. *Tectonophysics*, *560*, 62–83.
Bellahsen, N., Mouthereau, F., Boutoux, A., Bellanger, M., Lacombe, O., Jolivet, L., & Rolland, Y. (2014). Collision kinematics in the western external Alps. *Tectonics*, *33*, 1055–1088. https://doi.org/10.1002/2013TC003453
Bellen, V. R. C., Dunnington, H. V., Wetzel, R., & Morton, D. M. (1959). Lexique Stratigraphique International. 3. Asie, fasc. 10a, Iraq. CNRS (Cent. Natl. Rech. Sci.), Paris.
Berberian, M. (1995). Master "blind" thrust faults hidden under the Zagros folds: Active basement tectonics and surface morphotectonics. *Tectonophysics*, *241*(3–4), 193–224. https://doi.org/10.1016/0040-1951(94)00185-C
Berberian, M., & King, G. C. P. (1981). Towards a paleogeography and tectonic evolution of Iran. *Canadian Journal of Earth Sciences*, *18*(2), 210–265. https://doi.org/10.1139/e81-019
Beydoun, Z. R. (1993). Evolution of the northeastern Arabian plate margin and shelf: Hydrocarbon habitat and conceptual future potential. *Revue de l'Institut Français du Pétrole*, *48*(4), 311–345. https://doi.org/10.2516/ogst:1993021
Bird, P. (1979). Continental delamination and the Colorado plateau. *Journal of Geophysical Research*, *84*(B13), 7561–7571. https://doi.org/10.1029/JB084iB13p07561
Blanc, E. P., Allen, M. B., Inger, S., & Hassani, H. (2003). Structural styles in the Zagros simple folded zone, Iran. *Journal of the Geological Society*, *160*(3), 401–412. https://doi.org/10.1144/0016-764902-110
Bosworth, W. (2015). Geological evolution of the Red Sea: Historical background, review, and synthesis. In *The Red Sea* (pp. 45–78). Berlin, Heidelberg: Springer.
Bosworth, W., El-Hawat, A. S., Helgeson, D. E., & Burke, K. (2008). Cyrenaican "shock absorber" and associated inversion strain shadow in the collision zone of Northeast Africa. *Geology*, *36*(9), 695–698. https://doi.org/10.1130/G24909A.1
Bosworth, W., Guiraud, R., & Kessler, L. G. (1999). Late Cretaceous (ca. 84 Ma) compressive deformation of the stable platform of northeast Africa (Egypt): Far-field stress effects of the "Santonian event" and origin of the Syrian arc deformation belt. *Geology*, *27*(7), 633–636. https://doi.org/10.1130/0091-7613(1999)027<0633:LCCMCD>2.3.CO;2
Bosworth, W., Huchon, P., & McClay, K. (2005). The Red Sea and Gulf of Aden basins. *Journal of African Earth Sciences*, *43*(1–3), 334–378. https://doi.org/10.1016/j.jafrearsci.2005.07.020
Bosworth, W., & Stockli, D. F. (2016). Early magmatism in the greater Red Sea rift: Timing and significance. *Canadian Journal of Earth Sciences*, *53*(11), 1158–1176. https://doi.org/10.1139/cjes-2016-0019
Bottrill, A. D., van Hunen, J., & Allen, M. B. (2012). Insight into collision zone dynamics from topography: Numerical modelling results and observations. *Solid Earth.*, *3*(2), 387–399. https://doi.org/10.5194/se-3-387-2012
Brew, G., Barazangi, M., Al-Maleh, A. K., & Sawaf, T. (2001). Tectonic and geologic evolution of Syria. *GeoArabia*, *6*(4), 573–616.
Brew, G., Best, J., Barazangi, M., & Sawaf, T. (2003). Tectonic evolution of the NE Palmyride mountain belt, Syria: The Bishri crustal block. *Journal of the Geological Society*, *160*(5), 677–685. https://doi.org/10.1144/0016-764902-161

10.1029/2019TC005865

Burberry, C. M. (2015). The effect of basement fault reactivation on the Triassic—recent geology of Kurdistan, north Iraq. *Journal of Petroleum Geology*, *38*(1), 37–58. https://doi.org/10.1111/jpg.12597

Burg, J. (2018). Oman: An obduction orogen, lecture notes, ETH Zürich and Universität Zürich http://www.files.ethz.ch/structuralgeology/JPB/files/English/Omaneng.pdf

Burov, E. B., & Diament, M. (1995). The effective elastic thickness (Te) of continental lithosphere: What does it really mean? *Journal of Geophysical Research*, *100*(B3), 3905–3927. https://doi.org/10.1029/94JB02770

Butler, R. W. H., Holdsworth, R. E., & Matthews, S. J. (2006). *Styles of basement involvement in the Moine thrust belt, NW Scotland*, *Special Papers* (Vol. 414, pp. 133–151). Boulder, CO: Geological Society of America.

Butler, R. W. H., Mazzoli, S., Corrado, S., De Donatis, M., Di Bucci, D., Gambini, R., et al. (2004). Applying thick-skinned tectonic models to the Apennine thrust belt of Italy—Limitations and implications. In K. R. McClay (Ed.), *Thrust tectonics and hydrocarbon systems*, *AAPG Memoir* (Vol. 82, pp. 647–667). Tulsa, OK: American Association of Petroleum Geologists.

Butler, R. W. H., & McCaffrey, W. D. (2004). Nature of thrust zones in deep water sand-shale sequences: Outcrop examples from the Champsaur sandstones of SE France. *Marine and Petroleum Geology*, *21*(7), 911–921. https://doi.org/10.1016/j.marpetgeo.2003.07.005

Carrapa, B., Trimble, J. D., & Stockli, D. F. (2011). Patterns and timing of exhumation and deformation in the Eastern Cordillera of NW Argentina revealed by (U-Th)/H thermochronology. *Tectonics*, *30*, TC3003. https://doi.org/10.1029/2010TC002707

Casciello, E., Vergés, J., Saura, E., Casini, G., Fernández, N., Blanc, E., et al. (2009). Fold patterns and multilayer rheology of the Lurestan Province, Zagros simply folded belt (Iran). *Journal of the Geological Society*, *166*(5), 947–959. https://doi.org/10.1144/0016-76492008-138

Cater, J. M. L., & Tunbridge, I. P. (1992). Palaeozoic tectonic history of SE Turkey. *Journal of Petroleum Geology*, *15*(1), 35–50. https://doi.org/10.1111/j.1747-5457.1992.tb00864.x

Cawood, A. J., & Bond, C. E. (2018). 3D mechanical stratigraphy of a deformed multi-layer: Linking sedimentary architecture and strain partitioning. *Journal of Structural Geology*, *106*, 54–69. https://doi.org/10.1016/j.jsg.2017.11.011

Çelik, H., & Salih, T. M. H. (2018). Provenance investigation from sedimentary petrography of the upper cretaceous deep marine low density turbidites of the Tanjero formation around Arbat, northeastern Iraq. *Turkish Journal of Earth Sciences*, *27*(6), 432–459. https://doi.org/10.3906/yer-1712-29

Chaimov, T. A., Barazangi, M., Al-Saad, D., Sawaf, T., & Gebran, A. L. I. (1992). Mesozoic and Cenozoic deformation inferred from seismic stratigraphy in the southwestern intracontinental Palmyride fold-thrust belt, Syria. *Geological Society of America Bulletin*, *104*(6), 704–715. https://doi.org/10.1130/0016-7606(1992)104<0704:MACDIF>2.3.CO;2

Chamberlain, R. T. (1910). The Appalachian folds of Central Pennsylvania. *Journal of Geology*, *I*, 228–251.

Chang, S. J., van der Lee, S., Flanagan, M. P., Bedle, H., Marone, F., Matzel, E. M., et al. (2010). Joint inversion for three-dimensional S velocity mantle structure along the Tethyan margin. *Journal of Geophysical Research*, *115*, B08309. https://doi.org/10.1029/2009JB007204

Chapple, W. M. (1978). Mechanics of thin-skinned fold-and-thrust belts. *Geological Society of America Bulletin*, *89*(8), 1189–1198. https://doi.org/10.1130/0016-7606(1978)89<1189:MOTFB>2.0.CO;2

Chen, K., Xu, W., Mai, P. M., Gao, H., Zhang, L., & Ding, X. (2018). The 2017 *Mw* 7.3 Sarpol Zahāb earthquake, Iran: A compact blind shallow-dipping thrust event in the mountain front fault basement. *Tectonophysics*, *747*, 108–114.

Cochran, J. R., & Karner, G. D. (2007). *Constraints on the deformation and rupturing of continental lithosphere of the Red Sea: The transition from rifting to drifting*, *Special Publications* (Vol. 282, pp. 265–289). London: Geological Society. https://doi.org/10.1144/SP282.13

Cooper, M., & Warren, M. J. (2010). *The geometric characteristics, genesis and petroleum significance of inversion structures*, *Special Publications* (Vol. 335, pp. 827–846). London: Geological Society. https://doi.org/10.1144/SP335.33

Cooperdock, E. H., Ketcham, R. A., & Stockli, D. F. (2019). Resolving the effects of 2-D versus 3-D grain measurements on apatite (U–Th)/He age data and reproducibility. *Geochronology*, *1*(1), 17–41. https://doi.org/10.5194/gchron-1-17-2019

Cotton, J. T., & Koyi, H. A. (2000). Modeling of thrust fronts above ductile and frictional detachments: Application to structures in the salt range and Potwar plateau, Pakistan. *Geological Society of America Bulletin*, *112*(3), 351–363. https://doi.org/10.1130/0016-7606(2000)112<351:MOTFAD>2.0.CO;2

Coward, M. P. (1983). Thrust tectonics, thin skinned or thick skinned, and the continuation of thrusts to deep in the crust. *Journal of Structural Geology*, *5*(2), 113–123. https://doi.org/10.1016/0191-8141(83)90037-8

Dahlen, F. A., & Suppe, J. (1988). Mechanics, growth, and erosion of mountain belts. In S. P. Clark, Jr., B. C. Burchfiel, & J. Suppe (Eds.), *Processes in continental lithospheric deformation*, *Special Paper* (Vol. 218, pp. 161–178). America: Geological Society of America. https://doi.org/10.1130/SPE218-p161

Dahlstrom, C. D. A. (1969). Balanced cross sections. *Canadian Journal of Earth Sciences*, *6*(4), 743–757. https://doi.org/10.1139/e69-069

Davies, J. H., & von Blanckenburg, F. (1995). Slab breakoff: A model of lithosphere detachment and its test in the magmatism and deformation of collisional orogens. *Earth and Planetary Science Letters*, *129*(1–4), 85–102. https://doi.org/10.1016/0012-821X(94)00237-S

de Lamotte, D. F., Raulin, C., Mouchot, N., Wrobel-Daveau, J. C., Blanpied, C., & Ringenbach, J. C. (2011). The southernmost margin of the Tethys realm during the Mesozoic and Cenozoic: Initial geometry and timing of the inversion processes. *Tectonics*, *30*, TC3002. https://doi.org/10.1029/2010TC002691

de Vera, J., Gines, J., Oehlers, M., McClay, K., & Doski, J. (2009). Structure of the Zagros fold and thrust belt in the Kurdistan region, northern Iraq. *Trabajos de Geologia*, *29*(29), 213–217.

DeCelles, P. G. (2004). Late Jurassic to Eocene evolution of the cordilleran thrust belt and foreland basin system, western U.S.a. *American Journal of Science*, *304*(2), 105–168. https://doi.org/10.2475/ajs.304.2.105

DeCelles, P. G., & Coogan, J. C. (2006). Regional structure and kinematic history of the Sevier fold-and-thrust belt, Central Utah. *Geological Society of America Bulletin*, *118*(7–8), 841–864. https://doi.org/10.1130/B25759.1

DeCelles, P. G., & Giles, K. A. (1996). Foreland basin systems. *Basin Research*, *8*(2), 105–123. https://doi.org/10.1046/j.1365-2117.1996.01491.x

DeCelles, P. G., & Mitra, G. (1995). History of the Sevier orogenic wedge in terms of critical taper models, northeast Utah and southwest Wyoming. *Geological Society of America Bulletin*, *107*(4), 454–462. https://doi.org/10.1130/0016-7606(1995)107<0454:HOTSOW>2.3.CO;2

Dercourt, J., Zonenshain, L. P., Ricou, L. E., Kazmin, V. G., Le Pichon, X., Knipper, A. L., et al. (1986). Geological evolution of the Tethys belt from the Atlantic to the Pamirs since the Lias. *Tectonophysics*, *123*(1–4), 241–315. https://doi.org/10.1016/0040-1951(86)90199-X

Derikvand, B., Alavi, S. A., Fard, I. A., & Jalali, L. (2019). Changing in fold geometry from faulted detachment fold to fault-bend fold, a case study: The Zeloi anticline in the Dezful embayment, southwest of Iran. *Journal of Petroleum Science and Engineering*, *173*, 381–401. https://doi.org/10.1016/j.petrol.2018.10.033

Dewey, J. F., Hempton, M. R., Kidd, W. S. F., Saroglu, F. A. M. C., & Şengör, A. M. C. (1986). *Shortening of continental lithosphere: The neotectonics of eastern Anatolia—A young collision zone*, *Special Publications* (Vol. 19, pp. 1–36). London: Geological Society. https://doi.org/10.1144/GSL.SP.1986.019.01.01

Dickinson, W. R. (2004). Evolution of the North American Cordillera. *Annual Review of Earth and Planetary Sciences*, *32*(1), 13–45. https://doi.org/10.1146/annurev.earth.32.101802.120257

Dunnington, H. V. (1958). Generation, migration, accumulation and dissipation of oil in northern Iraq. In L. G. Weeks (Ed.), *Habitat of oil, a symposium* (pp. 1149–1251). Tulsa: American Association of Petroleum Geologists.

Dunnington, H. V. (1968). *Salt-tectonic features of northern Iraq*, *Special Papers* (Vol. 88, pp. 183–228). Boulder, CO: Geological Society of America. https://doi.org/10.1130/SPE88-p183

Edey, A., Allen, M. B., & Nilfouroushan, F. (2020). Kinematic variation within the Fars Arc, eastern Zagros, and the development of fold-and-thrust belt curvature. *Tectonics*, *39*, e2019TC005941. https://doi.org/10.1029/2019TC005941

Edgell, H. S. (1996). *Salt tectonism in the Persian Gulf basin*, *Special Publications* (Vol. 100, pp. 129–151). London: Geological Society. https://doi.org/10.1144/GSL.SP.1996.100.01.10

Ehlers, T. A., & Farley, K. A. (2003). Apatite (U–Th)/He thermochronometry: Methods and applications to problems in tectonic and surface processes. *Earth and Planetary Science Letters*, *206*(1–2), 1–14. https://doi.org/10.1016/S0012-821X(02)01069-5

Emami, H., Vergés, J., Nalpas, T., Gillespie, P., Sharp, I., Karpuz, R., et al. (2010). *Structure of the mountain front flexure along the Anaran anticline in the Pusht-e Kuh Arc (NW Zagros, Iran): Insights from sand box models*, *Special Publications* (Vol. 330, pp. 155–178). London: Geological Society. https://doi.org/10.1144/SP330.9

Engdahl, E. R., Jackson, J. A., Myers, S. C., Bergman, E. A., & Priestley, K. (2006). Relocation and assessment of seismicity in the Iran region. *Geophysical Journal International*, *167*(2), 761–778. https://doi.org/10.1111/j.1365-246X.2006.03127.x

English, J. M., Lunn, G. A., Ferreira, L., & Yacu, G. (2015). Geologic evolution of the Iraqi Zagros, and its influence on the distribution of hydrocarbons in the Kurdistan region. *AAPG Bulletin*, *99*(02), 231–272. https://doi.org/10.1306/06271413205

Epard, J. L., & Groshong, R. H. Jr. (1993). Excess area and depth to detachment. *AAPG Bulletin*, *77*(8), 1291–1302.

Faccenna, C., Bellier, O., Martinod, J., Piromallo, C., & Regard, V. (2006). Slab detachment beneath eastern Anatolia: A possible cause for the formation of the North Anatolian fault. *Earth and Planetary Science Letters*, *242*(1–2), 85–97. https://doi.org/10.1016/j.epsl.2005.11.046

Fakhari, M. D., Axen, G. J., Horton, B. K., Hassanzadeh, J., & Amini, A. (2008). Revised age of proximal deposits in the Zagros foreland basin and implications for Cenozoic evolution of the high Zagros. *Tectonophysics*, *451*(1–4), 170–185. https://doi.org/10.1016/j.tecto.2007.11.064

Falcon, N. L. (1961). Major earth-flexuring in the Zagros Mountains of south-west Iran. *Quarterly Journal of the Geological Society*, *117*(1–4), 367–376. https://doi.org/10.1144/gsjgs.117.1.0367

Farahpour, M. M., & Hessami, K. (2012). Cretaceous sequence of deformation in the SE Zagros fold–thrust belt. *Journal of the Geological Society*, *169*(6), 733–743. https://doi.org/10.1144/jgs2012-042

Farley, K. A. (2000). Helium diffusion from apatite: General behavior as illustrated by Durango fluorapatite. *Journal of Geophysical Research*, *105*(B2), 2903–2914. https://doi.org/10.1029/1999JB900348

Farley, K. A. (2002). (U-Th)/He dating: Techniques, calibrations, and applications. *Reviews in Mineralogy and Geochemistry*, *47*(1), 819–844. https://doi.org/10.2138/rmg.2002.47.18

Farley, K. A., & Stockli, D. F. (2002). (U-Th)/He dating of phosphates: Apatite, monazite, and xenotime. *Reviews in Mineralogy and Geochemistry*, *48*(1), 559–577. https://doi.org/10.2138/rmg.2002.48.15

Farley, K. A., Wolf, R. A., & Silver, L. T. (1996). The effects of long alpha-stopping distances on (U-Th)/He ages. *Geochimica et Cosmochimica Acta*, *60*(21), 4223–4229. https://doi.org/10.1016/S0016-7037(96)00193-7

Farzipour-Saein, A., Yassaghi, A., Sherkati, S., & Koyi, H. (2009). Mechanical stratigraphy and folding style of the Lurestan region in the Zagros fold–Thrust Belt, Iran. *Journal of the Geological Society*, *166*(6), 1101–1115. https://doi.org/10.1144/0016-76492008-162

Flowers, R. M., Ketcham, R. A., Shuster, D. L., & Farley, K. A. (2009). Apatite (U–Th)/He thermochronometry using a radiation damage accumulation and annealing model. *Geochimica et Cosmochimica Acta*, *73*(8), 2347–2365. https://doi.org/10.1016/j.gca.2009.01.015

Ford, M. (2004). Depositional wedge tops: Interaction between low basal friction external orogenic wedges and flexural foreland basins. *Basin Research*, *16*(3), 361–375. https://doi.org/10.1111/j.1365-2117.2004.00236.x

Fosdick, J. C., Carrapa, B., & Ortíz, G. (2015). Faulting and erosion in the Argentine Precordillera during changes in subduction regime: Reconciling bedrock cooling and detrital records. *Earth and Planetary Science Letters*, *432*, 73–83. https://doi.org/10.1016/j.epsl.2015.09.041

Fouad, S. F. (2007). Tectonic and structural evolution. *Iraqi Bulletin of Geology and Mining*, *1*, 29–50.

Fouad, S. F. (2012). Western Zagros fold–thrust belt, part I: The low folded zone. *Iraqi Bulletin of Geology and Mining*, *5*, 39–62.

Fouad, S. F. (2014). Western Zagros fold–thrust belt, part II: The high folded zone. *Iraqi Bulletin of Geology and Mining*, *6*, 53–71.

Fouad, S. F. (2015). Tectonic map of Iraq, scale 1: 1000 000, 2012. *Iraqi Bulletin of Geology and Mining*, *11*(1), 1–7.

Fouad, S. F., & Nasir, W. A. A. (2009). Tectonic and structural evolution of Al-Jazira area. *Iraqi Bulletin of Geology and Mining*, *3*, 33–48.

Frehner, M., Reif, D., & Grasemann, B. (2012). Mechanical versus kinematical shortening reconstructions of the Zagros high folded zone (Kurdistan region of Iraq). *Tectonics*, *31*, TC3002. https://doi.org/10.1029/2011TC003010

Fuentes, F., DeCelles, P. G., & Constenius, K. N. (2012). Regional structure and kinematic history of the Cordilleran fold-thrust belt in northwestern Montana, USA. *Geosphere*, *8*(5), 1104–1128. https://doi.org/10.1130/GES00773.1

Fuentes, F., Horton, B. K., Starck, D., & Boll, A. (2016). Structure and tectonic evolution of hybrid thick-and thin-skinned systems in the Malargüe fold–thrust belt, Neuquén basin, Argentina. *Geological Magazine*, *153*(5–6), 1066–1084. https://doi.org/10.1017/S0016756816000583

Garland, C. R., Abalioglu, I., Akca, L., Cassidy, A., Chiffoleau, Y., Godail, L., et al. (2010, January). *Appraisal and development of the Taq Taq field, Kurdistan region, Iraq*, *Petroleum Geology Conference Series* (Vol. 7, pp. 801–810). London: Geological Society of London.

Garzione, C. N., Molnar, P., Libarkin, J. C., & MacFadden, B. J. (2006). Rapid late Miocene rise of the Bolivian Altiplano: Evidence for removal of mantle lithosphere. *Earth and Planetary Science Letters*, *241*(3–4), 543–556. https://doi.org/10.1016/j.epsl.2005.11.026

Gavillot, Y., Axen, G. J., Stockli, D. F., Horton, B. K., & Fakhari, M. D. (2010). Timing of thrust activity in the high Zagros fold-thrust belt, Iran, from (U-Th)/He thermochronometry. *Tectonics*, *29*, TC4025. https://doi.org/10.1029/2009TC002484

Gelati, R. (1975). Miocene marine sequence from Lake Van, eastern Turkey. *Rivista Italiana di Paleontologia e Stratigrafia*, *81*, 477–490.

Ghanadian, M., Faghih, A., Fard, I. A., Kusky, T., & Maleki, M. (2017). On the role of incompetent strata in the structural evolution of the Zagros fold-thrust belt, Dezful embayment, Iran. *Marine and Petroleum Geology*, *81*, 320–333. https://doi.org/10.1016/j.marpetgeo.2017.01.010

Ghienne, J. F., Monod, O., Kozlu, H., & Dean, W. T. (2010). Cambrian–Ordovician depositional sequences in the Middle East: A perspective from Turkey. *Earth-Science Reviews*, *101*(3–4), 101–146. https://doi.org/10.1016/j.earscirev.2010.04.004

Göğüş, O. H., & Pysklywec, R. N. (2008). Mantle lithosphere delamination driving plateau uplift and synconvergent extension in eastern Anatolia. *Geology*, *36*(9), 723–726. https://doi.org/10.1130/G24982A.1

Grabowski, G. J., Jr. (2014). Iraq. In L. Marlow, C. Kendall, & L. Yose (Eds.), *Petroleum systems of the Tethyan region*, *AAPG Memoir* (Vol. 106, pp. 379–467). Tulsa, OK: American Association of Petroleum Geologists. https://doi.org/10.1306/13431863M1063618

Grasemann, B., & Schmalholz, S. M. (2012). Lateral fold growth and fold linkage. *Geology*, *40*(11), 1039–1042. https://doi.org/10.1130/G33613.1

Guest, B., Stockli, D. F., Grove, M., Axen, G. J., Lam, P. S., & Hassanzadeh, J. (2006). Thermal histories from the central Alborz Mountains, northern Iran: Implications for the spatial and temporal distribution of deformation in northern Iran. *Geological Society of America Bulletin*, *118*(11–12), 1507–1521. https://doi.org/10.1130/B25819.1

Gunay, Y., & Senel, M. (2002). *Geological map of Turkey-Cizre, general directorate of mineral research and exploration, Ankara, Turkey, Scale 1:500,000*. Ankara, Turkey: General Directorate of Mineral Research and Exploration.

Hafkenscheid, E., Wortel, M. J. R., & Spakman, W. (2006). Subduction history of the Tethyan region derived from seismic tomography and tectonic reconstructions. *Journal of Geophysical Research*, *111*, B08401. https://doi.org/10.1029/2005JB003791

Haghipour, A. (2009). *International geological map of the Middle East. Subcommission for the Middle East, scale 1:5,000,000* (2nd ed.). Paris, France: Commission for the Geological Map of the World.

Haghipour, A., & Aghanabati, A. (1989). *Geological Map of Iran, scale 1:2,500,000* (2nd ed.). Tehran, Iran: Ministry of Mines and Metals, Geological Survey of Iran.

Hansman, R. J., Ring, U., Thomson, S. N., den Brok, B., & Stübner, K. (2017). Late Eocene uplift of the Al Hajar Mountains, Oman, supported by stratigraphy and low-temperature thermochronology. *Tectonics*, *36*, 3081–3109. https://doi.org/10.1002/2017TC004672

Harrison, T. M., & Zeitler, P. K. (2005). Fundamentals of noble gas thermochronometry. *Reviews in Mineralogy and Geochemistry*, *58*(1), 123–149. https://doi.org/10.2138/rmg.2005.58.5

Harzhauser, M., Kroh, A., Mandic, O., Piller, W. E., Göhlich, U., Reuter, M., & Berning, B. (2007). Biogeographic responses to geodynamics: A key study all around the Oligo–Miocene Tethyan seaway. *Zoologischer Anzeiger-A Journal of Comparative Zoology*, *246*(4), 241–256. https://doi.org/10.1016/j.jcz.2007.05.001

Hawramy, O. A., & Khalaf, S. K. (2013). Ostracoda of Fat'ha formation (middle Miocene) from (Darbandikhan and Aghjalar) sections, Sulaimani-Kurdistan region/Northeastern Iraq. *Journal of Zankoy Sulaimani-Part A (JZS-A)*, *15*(3), 3.

Hayward, T. (2014). The opening of the Kurdistan oil and gas province: the making of a nation. In AAPG Search and Discovery Article 10688.

Hempton, M. R. (1987). Constraints on Arabian plate motion and extensional history of the Red Sea. *Tectonics*, *6*(6), 687–705. https://doi.org/10.1029/TC006i006p00687

Hessami, K., Koyi, H. A., & Talbot, C. J. (2001). The significance of strike-slip faulting in the basement of the Zagros fold and thrust belt. *Journal of Petroleum Geology*, *24*(1), 5–28. https://doi.org/10.1111/j.1747-5457.2001.tb00659.x

Hinsch, R., & Bretis, B. (2015). A semi-balanced section in the northwestern Zagros region: Constraining the structural architecture of the mountain front flexure in the Kirkuk embayment, Iraq. *GeoArabia*, *20*(4), 41–62.

Homke, S., Vergés, J., Garcés, M., Emami, H., & Karpuz, R. (2004). Magnetostratigraphy of Miocene–Pliocene Zagros foreland deposits in the front of the push-e Kush arc (Lurestan Province, Iran). *Earth and Planetary Science Letters*, *225*(3–4), 397–410. https://doi.org/10.1016/j.epsl.2004.07.002

Homke, S., Vergés, J., Serra-Kiel, J., Bernaola, G., Sharp, I., Garcés, M., et al. (2009). Late Cretaceous–Paleocene formation of the proto–Zagros foreland basin, Lurestan Province, SW Iran. *Geological Society of America Bulletin*, *121*(7–8), 963–978. https://doi.org/10.1130/B26035.1

Homke, S., Vergés, J., van der Beek, P., Fernàndez, M., Saura, E., Barbero, L., et al. (2010). Insights in the exhumation history of the NW Zagros from bedrock and detrital apatite fission-track analysis: Evidence for a long-lived orogeny. *Basin Research*, *22*(5), 659–680. https://doi.org/10.1111/j.1365-2117.2009.00431.x

Horton, B. K. (2018a). Sedimentary record of Andean mountain building. *Earth Science Reviews*, *178*, 279–309. https://doi.org/10.1016/j.earscirev.2017.11.025

Horton, B. K. (2018b). Tectonic regimes of the central and southern Andes: Responses to variations in plate coupling during subduction. *Tectonics*, *37*, 402–429. https://doi.org/10.1002/2017TC004624

Horton, B. K., Hassanzadeh, J., Stockli, D. F., Axen, G. J., Gillis, R. J., Guest, B., et al. (2008). Detrital zircon provenance of Neoproterozoic to Cenozoic deposits in Iran: Implications for chronostratigraphy and collisional tectonics. *Tectonophysics*, *451*(1–4), 97–122. https://doi.org/10.1016/j.tecto.2007.11.063

Hyndman, R. D., Currie, C. A., Mazzotti, S., & Frederiksen, A. (2009). Temperature control of continental lithosphere elastic thickness, Te vs. *Earth and Planetary Science Letters*, *277*(3–4), 539–548. https://doi.org/10.1016/j.epsl.2008.11.023

Ismail, S. A., Koshnaw, R. I., Barber, D. E., Al Humadi, H., & Stockli, D. F. (2020). Generation and exhumation of granitoid intrusions in the Penjween ophiolite complex, NW Zagros of the Kurdistan region of Iraq: Implications for the geodynamic evolution of the Arabia-Eurasia collision zone. *Lithos*, *376-377*, 105714. https://doi.org/10.1016/j.lithos.2020.105714

Jackson, J. A. (1980). Reactivation of basement faults and crustal shortening in orogenic belts. *Nature*, *283*(5745), 343–346. https://doi.org/10.1038/283343a0

Jahangiri, A. (2007). Post-collisional Miocene adakitic volcanism in NW Iran: Geochemical and geodynamic implications. *Journal of Asian Earth Sciences*, *30*(3–4), 433–447. https://doi.org/10.1016/j.jseaes.2006.11.008

Jammes, S., & Huismans, R. S. (2012). Structural styles of mountain building: Controls of lithospheric rheologic stratification and extensional inheritance. *Journal of Geophysical Research*, *117*, B10403. https://doi.org/10.1029/2012JB009376

Janvier, P., Lethiers, F., Monod, O., & Balkaş, Ö. (1984). Discovery of a vertebrate fauna at the Devonian-Carboniferous boundary in SE Turkey (Hakkari Province). *Journal of Petroleum Geology*, *7*(2), 147–168. https://doi.org/10.1111/j.1747-5457.1984.tb00172.x

Jassim, S. Z., & Buday, T. (2006). Tectonic framework. In S. Z. Jassim, & J. C. Goff (Eds.), *Geology of Iraq* (pp. 35–52). Prague and Brno, Czech Republic: Dolin and Moravian Museum.

Jassim, S. Z., Buday, T., Cicha, I., & Opletal, M. (2006). Tectonostratigraphy of the Zagros Sutre. In S. Z. Jassim, & J. C. Goff (Eds.), *Geology of Iraq* (pp. 276–297). Prague and Brno, Czech Republic: Dolin and Moravian Museum.

Kaban, M. K., Petrunin, A. G., El Khrepy, S., & Al-Arifi, N. (2018). Diverse continental subduction scenarios along the Arabia-Eurasia collision zone. *Geophysical Research Letters*, *45*, 6898–6906. https://doi.org/10.1029/2018GL078074

Karasözen, E., Nissen, E., Bergman, E. A., & Ghods, A. (2019). Seismotectonics of the Zagros (Iran) from Orogen-wide, calibrated earthquake relocations. *Journal of Geophysical Research: Solid Earth*, *124*, 9109–9129. https://doi.org/10.1029/2019JB017336

Karim, K. H., Khanaqa, P. A., Kharajiani, S. O., Taha, Z. A., & Baziany, M. M. (2020). Depositional and erosional features of Oligocene paleokarsts in the Kirkuk Group, Kurdistan region, Northeast Iraq. *Arabian Journal of Geosciences*, *13*(6), 1–12.

Karim, K. H., & Surdashy, A. M. (2005a). Paleocurrent analysis of Upper Cretaceous Zagros foreland basin: A case study for Tanjero formation in Sulaimaniya area NE-Iraq. *Iraqi National Journal of Earth Sciences*, *5*(1), 30–44.

Karim, K. H., & Surdashy, A. M. (2005b). Tectonic and depositional history of Upper Cretaceous Tanjero formation in Sulaimaniya area NE-Iraq. *Journal of Sulaimaniya University (JZS)*, *8*, 1–20.

Kaviani, A., Sandvol, E., Moradi, A., Rümpker, G., Tang, Z., & Mai, P. M. (2018). Mantle transition zone thickness beneath the Middle East: Evidence for segmented Tethyan slabs, delaminated lithosphere, and lower mantle upwelling. *Journal of Geophysical Research: Solid Earth*, *123*, 4886–4905. https://doi.org/10.1029/2018JB015627

Kendall, J., Vergés, J., Koshnaw, R., & Louterbach, M. (2019). *Petroleum tectonic comparison of fold-thrust belts: The Sevier of the western US, the Pyrenees of Spain, the Zagros of Iraq and Iran, and the Beni sub Andean of Bolivia*, *Special Publications* (Vol. 490, pp. 79–103). London: Geological Society. https://doi.org/10.1144/SP490-2018-102

Kent, P. E. (1979). The emergent Hormuz salt plugs of southern Iran. *Journal of Petroleum Geology*, *2*(2), 117–144. https://doi.org/10.1111/j.1747-5457.1979.tb00698.x

Kent, W. N. (2010). Structures of the Kirkuk embayment, northern Iraq: Foreland structures or Zagros fold belt structures? *GeoArabia*, *15*(4), 147–188.

Keskin, M. (2003). Magma generation by slab steepening and breakoff beneath a subduction-accretion complex: An alternative model for collision-related volcanism in eastern Anatolia, Turkey. *Geophysical Research Letters*, *30*(24), 8046. https://doi.org/10.1029/2003GL018019

Keskin, M. (2007). *Eastern Anatolia: A hotspot in a collision zone without a mantle plume*, *Special Papers* (Vol. 430, pp. 693–722). Boulder, CO: Geological Society of America.

Khanqa, P. A., Karim, S. A., Sissakian, V. K., & Kareem, K. H. (2009). Lithostratigraphic study of a late Oligocene–Early Miocene succession, south of Sulaimaniyah, NE Iraq. *Iraqi Bulletin of Geology and mining*, *5*(2), 41–57.

Kley, J. (1996). Transition from basement-involved to thin-skinned thrusting in the Cordillera Oriental of southern Bolivia. *Tectonics*, *15*(4), 763–775. https://doi.org/10.1029/95TC03868

Kley, J., Monaldi, C. R., & Salfity, J. A. (1999). Along-strike segmentation of the Andean foreland: Causes and consequences. *Tectonophysics*, *301*(1–2), 75–94. https://doi.org/10.1016/S0040-1951(98)90223-2

Kley, J., Rossello, E. A., Monaldi, C. R., & Habighorst, B. (2005). Seismic and field evidence for selective inversion of cretaceous normal faults, Salta rift, Northwest Argentina. *Tectonophysics*, *399*(1–4), 155–172. https://doi.org/10.1016/j.tecto.2004.12.020

Konert, G., Afifi, A. M., Al-Hajri, S. I. A., & Droste, H. J. (2001). Paleozoic stratigraphy and hydrocarbon habitat of the Arabian plate. *GeoArabia*, *6*(3), 407–442.

Koop, W. J., & Stoneley, R. (1982). Subsidence history of the Middle East Zagros basin, Permian to recent. *Philosophical Transactions of the Royal Society of London. Series A, Mathematical and Physical Sciences*, *305*(1489), 149–168.

Koshnaw, R. I., Horton, B. K., Stockli, D. F., Barber, D. E., & Tamar-Agha, M. Y. (2020). Sediment routing in the Zagros foreland basin: Drainage reorganization and a shift from axial to transverse sediment dispersal in the Kurdistan region of Iraq. *Basin Research*, *32*(4), 688–715. https://doi.org/10.1111/bre.12391

Koshnaw, R. I., Horton, B. K., Stockli, D. F., Barber, D. E., Tamar-Agha, M. Y., & Kendall, J. J. (2017). Neogene shortening and exhumation of the Zagros fold-thrust belt and foreland basin in the Kurdistan region of northern Iraq. *Tectonophysics*, *694*, 332–355. https://doi.org/10.1016/j.tecto.2016.11.016

Koshnaw, R. I., Stockli, D. F., & Schlunegger, F. (2019). Timing of the Arabia-Eurasia continental collision—Evidence from detrital zircon U-Pb geochronology of the red bed series strata of the northwest Zagros hinterland, Kurdistan region of Iraq. *Geology*, *47*(1), 47–50. https://doi.org/10.1130/G45499.1

Koulakov, I., Zabelina, I., Amanatashvili, I., & Meskhia, V. (2012). Nature of orogenesis and volcanism in the Caucasus region based on results of regional tomography. *Solid Earth*, *3*(2), 327–337. https://doi.org/10.5194/se-3-327-2012

Lacombe, O., & Bellahsen, N. (2016). Thick-skinned tectonics and basement-involved fold–thrust belts: Insights from selected Cenozoic orogens. *Geological Magazine*, *153*(5–6), 763–810. https://doi.org/10.1017/S0016756816000078

Lacombe, O., & Mouthereau, F. (2002). Basement-involved shortening and deep detachment tectonics in forelands of orogens: Insights from recent collision belts (Taiwan, Western Alps, Pyrenees). *Tectonics*, *21*(4), 1030. https://doi.org/10.1029/2001TC901018

Lacombe, O., Ruh, J., Brown, D., & Nilfouroushan, F. (2016). Introduction: Tectonic evolution and mechanics of basement-involved fold-and-thrust belts. *Geological Magazine*, *153*(5–6), 759–762. https://doi.org/10.1017/S0016756816000650

László, C., Ágoston, S., Tamás, P., László, K., Salae, A. T., & Athar, A. (2012). Structural evolution of the northwestern Zagros, Kurdistan region, Iraq: Implications on oil migration. *GeoArabia*, *17*(2), 81–116.

Lawa, F. A., Koyi, H., & Ibrahim, A. (2013). Tectono-stratigraphic evolution of the NW segment OF the Zagros fold-thrust belt, Kurdistan, NE Iraq. *Journal of Petroleum Geology*, *36*(1), 75–96. https://doi.org/10.1111/jpg.12543

Lawa, F. A. A. (2018). Late Campanian–Maastrichtian sequence stratigraphy from Kurdistan foreland basin, NE/Iraq. *Journal of Petroleum Exploration and Production Technology*, *8*(3), 713–732. https://doi.org/10.1007/s13202-017-0424-1

Lawa, F. A. A., & Ghafur, A. A. (2015). Sequence stratigraphy and biostratigraphy of the prolific late Eocene, Oligocene and early Miocene carbonates from Zagros fold-thrust belt in Kurdistan region. *Arabian Journal of Geosciences*, *8*(10), 8143–8174. https://doi.org/10.1007/s12517-015-1817-4

Le Garzic, E., Vergés, J., Sapin, F., Saura, E., Meresse, F., & Ringenbach, J. C. (2019). Evolution of the NW Zagros fold-and-thrust belt in Kurdistan region of Iraq from balanced and restored crustal-scale sections and forward modeling. *Journal of Structural Geology*, *124*, 51–69. https://doi.org/10.1016/j.jsg.2019.04.006

Lee, H., Jang, Y., Kwon, S., Park, M. H., & Mitra, G. (2018). The role of mechanical stratigraphy in the lateral variations of thrust development along the Central Alberta foothills, Canada. *Geoscience Frontiers*, *9*(5), 1451–1464. https://doi.org/10.1016/j.gsf.2018.03.006

Lei, J., & Zhao, D. (2007). Teleseismic evidence for a break-off subducting slab under eastern Turkey. *Earth and Planetary Science Letters*, *257*(1–2), 14–28. https://doi.org/10.1016/j.epsl.2007.02.011

Leturmy, P., Molinaro, M., & de Lamotte, D. F. (2010). *Structure, timing and morphological signature of hidden reverse basement faults in the Fars arc of the Zagros (Iran)*, *Special Publications* (Vol. 330, pp. 121–138). London: Geological Society. https://doi.org/10.1144/SP330.7

Levina, M., Horton, B. K., Fuentes, F., & Stockli, D. F. (2014). Cenozoic sedimentation and exhumation of the foreland basin system preserved in the Precordillera thrust belt (31–32 S), southern Central Andes, Argentina. *Tectonics*, *33*, 1659–1680. https://doi.org/10.1002/2013TC003424

Liu, C., Alway, R., Moreton, D. J., Samara, A., & Hmasalih, F. (2017). Recommendation for a practical log-based stratigraphic framework for the Kurdistan Region of Iraq. In AAPG Search and Discovery Article 30487.

Lock, J., & Willett, S. (2008). Low-temperature thermochronometric ages in fold-and-thrust belts. *Tectonophysics*, *456*(3–4), 147–162. https://doi.org/10.1016/j.tecto.2008.03.007

Lovelock, P. E. R. (1984). A review of the tectonics of the northern Middle East region. *Geological Magazine*, *121*(6), 577–587. https://doi.org/10.1017/S0016756800030727

Ma'ala, K. A. (2008). *Geological map of the Sulaimaniyah Quadrangle, sheet NJ-38-3, Scale 1:250000*. Baghdad, Iraq: State Company of Geological Survey and Mining.

Mackaman-Lofland, C., Horton, B. K., Fuentes, F., Constenius, K. N., Ketcham, R. A., Capaldi, T. N., et al. (2020). Andean mountain building and foreland basin evolution during thin-and thick-skinned Neogene deformation (32−33°S). *Tectonics*, *39*, e2019TC005838. https://doi.org/10.1029/2019TC005838

Madanipour, S., Ehlers, T. A., Yassaghi, A., & Enkelmann, E. (2017). Accelerated middle Miocene exhumation of the Talesh Mountains constrained by U-Th/he thermochronometry: Evidence for the Arabia-Eurasia collision in the NW Iranian plateau. *Tectonics*, *36*, 1538–1561. https://doi.org/10.1002/2016TC004291

Madritsch, H., Schmid, S. M., & Fabbri, O. (2008). Interactions between thin-and thick-skinned tectonics at the northwestern front of the Jura fold-and-thrust belt (eastern France). *Tectonics*, *27*, TC5005. https://doi.org/10.1029/2008TC002282

Marouf, N. Z., & Al-Kubaisi, M. S. A. (2005). Inversion and folding of the southern un-elevated folded belt in North Iraq. *The Iraqi Geological Journal*, 1–36.

McDowell, F. W., McIntosh, W. C., & Farley, K. A. (2005). A precise ^{40}Ar-^{39}Ar reference age for the Durango apatite (U-Th)/He and fission-track dating standard. *Chemical Geology*, *214*(3–4), 249–263. https://doi.org/10.1016/j.chemgeo.2004.10.002

McQuarrie, N. (2004). Crustal scale geometry of the Zagros fold–thrust belt, Iran. *Journal of Structural Geology*, *26*(3), 519–535. https://doi.org/10.1016/j.jsg.2003.08.009

McQuarrie, N., & Ehlers, T. A. (2017). Techniques for understanding fold-thrust belt kinematics and thermal evolution. In *Linkages and Feedbacks in Orogenic Process: A volume in Honor of Robert D Hatcher Jr.*, *Memoirs* (Vol. 213, pp. 25–54). Boulder, CO, USA: Geological Society of America.

McQuarrie, N., Stock, J. M., Verdel, C., & Wernicke, B. P. (2003). Cenozoic evolution of Neotethys and implications for the causes of plate motions. *Geophysical Research Letters*, *30*(20), 2036. https://doi.org/10.1029/2003GL017992

Memiş, C., Göğüş, O. H., Uluocak, E. Ş., Pysklywec, R., Keskin, M., Şengör, A. C., & Topuz, G. (2020). Long wavelength progressive plateau uplift in eastern Anatolia since 20 Ma: Implications for the role of slab peel-back and break-off. *Geochemistry, Geophysics, Geosystems*, *21*, e2019GC008726. https://doi.org/10.1029/2019GC008726

Mescua, J. F., Giambiagi, L., Barrionuevo, M., Tassara, A., Mardonez, D., Mazzitelli, M., & Lossada, A. (2016). Basement composition and basin geometry controls on upper-crustal deformation in the southern Central Andes (30–36°S). *Geological Magazine*, *153*(5–6), 945–961. https://doi.org/10.1017/S0016756816000364

Min, T., Yi, J., Oh, H., Chun, Y., Bae, J., Jang, G., & Lee, S. (2012). Technical review of the drilling operation of QT-1 in block Qush tappa, Iraq. *Journal of the Korean Earth System Engineering Society*, *49*(1), 80–90.

Mitra, S. (1986). Duplex structures and imbricate thrust systems: Geometry, structural position, and hydrocarbon potential. *AAPG Bulletin*, *70*(9), 1087–1112. https://doi.org/10.1306/94886a7e-1704-11d7-8645000102c1865d

Mitra, S., & Namson, J. S. (1989). Equal-area balancing. *American Journal of Science*, *289*(5), 563–599. https://doi.org/10.2475/ajs.289.5.563

Mohammed, S. A. (2006). Megaseismic section across the northeastern slope of the Arabian plate, Iraq. *GeoArabia*, *11*(4), 77–90.

Molinaro, M., Leturmy, P., Guezou, J. C., Frizon de Lamotte, D., & Eshraghi, S. A. (2005). The structure and kinematics of the southeastern Zagros fold-thrust belt, Iran: From thin-skinned to thick-skinned tectonics. *Tectonics*, *24*, TC3007. https://doi.org/10.1029/2004TC001633

Molinaro, M., Zeyen, H., & Laurencin, X. (2005). Lithospheric structure beneath the south-eastern Zagros Mountains, Iran: Recent slab break-off? *Terra Nova*, *17*(1), 1–6. https://doi.org/10.1111/j.1365-3121.2004.00575.x

Molnar, N. E., Cruden, A. R., & Betts, P. G. (2017). Interactions between propagating rotational rifts and linear rheological heterogeneities: Insights from three-dimensional laboratory experiments. *Tectonics*, *36*, 420–443. https://doi.org/10.1002/2016TC004447

Mora, A., Horton, B. K., Mesa, A., Rubiano, J., Ketcham, R. A., Parra, M., et al. (2010). Migration of Cenozoic deformation in the Eastern Cordillera of Colombia interpreted from fission track results and structural relationships: Implications for petroleum systems. *AAPG Bulletin*, *94*(10), 1543–1580. https://doi.org/10.1306/01051009111

Morley, C. K. (1988). Out-of-sequence thrusts. *Tectonics*, *7*(3), 539–561. https://doi.org/10.1029/TC007i003p00539

Morley, C. K., Kongwung, B., Julapour, A. A., Abdolghafourian, M., Hajian, M., Waples, D., et al. (2009). Structural development of a major late Cenozoic basin and transpressional belt in Central Iran: The Central Basin in the Qom-Saveh area. *Geosphere*, *5*(4), 325–362. https://doi.org/10.1130/GES00223.1

Motaghi, K., Shabanian, E., & Kalvandi, F. (2017). Underplating along the northern portion of the Zagros suture zone, Iran. *Geophysical Journal International*, *210*(1), 375–389. https://doi.org/10.1093/gji/ggx168

Mouthereau, F., Lacombe, O., & Meyer, B. (2006). The Zagros folded belt (Fars, Iran): Constraints from topography and critical wedge modelling. *Geophysical Journal International*, *165*(1), 336–356. https://doi.org/10.1111/j.1365-246X.2006.02855.x

Mouthereau, F., Lacombe, O., Tensi, J., Bellahsen, N., Kargar, S., & Amrouch, K. (2007). Mechanical constraints on the development of the Zagros Folded Belt (Fars). In *Thrust belts and foreland basins* (pp. 247–266). Berlin, Heidelberg: Springer. https://doi.org/10.1007/978-3-540-69426-7_13

Mouthereau, F., Lacombe, O., & Vergés, J. (2012). Building the Zagros collisional orogen: Timing, strain distribution and the dynamics of Arabia/Eurasia plate convergence. *Tectonophysics*, *532*, 27–60.

Mouthereau, F., Tensi, J., Bellahsen, N., Lacombe, O., de Boisgrollier, T., & Kargar, S. (2007). Tertiary sequence of deformation in a thin-skinned/thick-skinned collision belt: The Zagros folded belt (Fars, Iran). *Tectonics*, *26*, TC5006. https://doi.org/10.1029/2007TC002098

Mouthereau, F., Watts, A. B., & Burov, E. (2013). Structure of orogenic belts controlled by lithosphere age. *Nature Geoscience*, *6*(9), 785–789. https://doi.org/10.1038/ngeo1902

Najar, I. M. (1999). Geophysical evidence for Mesozoic and Paleozoic sedimentary basins in the northernpart of the western desert of Iraq. Ph. D Thesis, University of Mosul, p. 217.

Navabpour, P., Angelier, J., & Barrier, E. (2008). Stress state reconstruction of oblique collision and evolution of deformation partitioning in W-Zagros (Iran, Kermanshah). *Geophysical Journal International*, *175*(2), 755–782. https://doi.org/10.1111/j.1365-246X.2008.03916.x

Nemčok, M., Mora, A., & Cosgrove, J. (2013). *Thick-skin-dominated orogens; from initial inversion to full accretion: An introduction*, *Special Publications* (Vol. 377, pp. 1–17). London: Geological Society. https://doi.org/10.1144/SP377.17

Nilfouroushan, F., Pysklywec, R., Cruden, A., & Koyi, H. (2013). Thermal-mechanical modeling of salt-based mountain belts with pre-existing basement faults: Application to the Zagros fold and thrust belt, Southwest Iran. *Tectonics*, *32*, 1212–1226. https://doi.org/10.1002/tect.20075

Nissen, E., Ghods, A., Karasözen, E., Elliott, J. R., Barnhart, W. D., Bergman, E. A., et al. (2019). The 12 November 2017 *Mw* 7.3 Ezgeleh-Sarpolzahab (Iran) earthquake and active tectonics of the Lurestan arc. *Journal of Geophysical Research: Solid Earth*, *124*, 2124–2152. https://doi.org/10.1029/2018JB016221

Numan, N., & Azzawi, N. (1993). Structural and geotectonic interpretation of vergence directions of anticlines in the foreland folds of Iraq. Abhath Al Yarmouk, *Pure Science and Engineering Series*, *2*(2), 57–73.

Obaid, A. K., & Allen, M. B. (2017). Landscape maturity, fold growth sequence and structural style in the Kirkuk embayment of the Zagros, northern Iraq. *Tectonophysics*, *717*, 27–40. https://doi.org/10.1016/j.tecto.2017.07.006

O'Brien, C. A. E. (1957). Salt diapirism in South Persia. *Geologie en Mijnbouw*, *19*(9), 357–376.

Oil Search Limited (2012). Oil search 2012 annual meeting. Accessed January 2016.

Okay, A. I., Zattin, M., & Cavazza, W. (2010). Apatite fission-track data for the Miocene Arabia-Eurasia collision. *Geology*, *38*(1), 35–38. https://doi.org/10.1130/G30234.1

Omar, A. A., Lawa, F. A., & Sulaiman, S. H. (2015). Tectonostratigraphic and structural imprints from balanced sections across the north-western Zagros fold-thrust belt, Kurdistan region, NE Iraq. *Arabian Journal of Geosciences*, *8*(10), 8107–8129. https://doi.org/10.1007/s12517-014-1682-6

Omar, A. A., & Othman, A. T. (2018). Morpho-structural study of the Korek anticline, Zagros fold-thrust belt, Kurdistan of Iraq. *Geotectonics*, *52*(3), 382–400. https://doi.org/10.1134/S0016852118030068

Omar, A. A., & Syan, S. H. (2016). Construction of a structural model for Harir anticline within Zagros fold-thrust belt, Kurdistan of Iraq. *ZANCO Journal of Pure and Applied Sciences*, *28*(6), 90–105.

Omrani, J., Agard, P., Whitechurch, H., Benoit, M., Prouteau, G., & Jolivet, L. (2008). Arc-magmatism and subduction history beneath the Zagros Mountains, Iran: A new report of adakites and geodynamic consequences. *Lithos*, *106*(3–4), 380–398. https://doi.org/10.1016/j.lithos.2008.09.008

Oveisi, B., Lavé, J., van der Beek, P., Carcaillet, J., Benedetti, L., & Aubourg, C. (2009). Thick-and thin-skinned deformation rates in the central Zagros simple folded zone (Iran) indicated by displacement of geomorphic surfaces. *Geophysical Journal International*, *176*(2), 627–654. https://doi.org/10.1111/j.1365-246X.2008.04002.x

Paul, A., Hatzfeld, D., Kaviani, A., Tatar, M., & Péquegnat, C. (2010). *Seismic imaging of the lithospheric structure of the Zagros mountain belt (Iran)*, *Special Publications* (Vol. 330, pp. 5–18). London: Geological Society. https://doi.org/10.1144/SP330.2

Perez, N. D., Horton, B. K., & Carlotto, V. (2016). Structural inheritance and selective reactivation in the Central Andes: Cenozoic deformation guided by pre-Andean structures in southern Peru. *Tectonophysics*, *671*, 264–280. https://doi.org/10.1016/j.tecto.2015.12.031

Perez, N. D., Teixell, A., Gómez-Gras, D., & Stockli, D. F. (2019). Reconstructing extensional basin architecture and provenance in the Marrakech High Atlas of Morocco: Implications for rift basins and inversion tectonics. *Tectonics*, *38*, 1584–1608. https://doi.org/10.1029/2018TC005413

Peterson, J. A., & Wilson, J. (1986). Petroelum stratigraphy of the Northeast Africa-Middle East region. In *Hydrocarbon Potential of Intense Thrust Zones. Proceedings of OAPEC Seminar, December 1986, Abu Dhabi* (Vol. II, pp. 227–230). Kuwait, State of Kuwait: Organization of Arab Petroleum Exporting Countries.

Pfiffner, O. A. (2006). *Thick-skinned and thin-skinned styles of continental contraction*, *Special Papers* (Vol. 414, pp. 153–177). Boulder, CO, USA: Geological Society of America.

Pfiffner, O. A. (2016). Basement-involved thin-skinned and thick-skinned tectonics in the Alps. *Geological Magazine*, *153*(5–6), 1085–1109. https://doi.org/10.1017/S0016756815001090

Pfiffner, O. A. (2017). Thick-skinned and thin-skinned tectonics: A global perspective. *Geosciences*, *7*(3), 71. https://doi.org/10.3390/geosciences7030071

Pirouz, M., Avouac, J. P., Hassanzadeh, J., Kirschvink, J. L., & Bahroudi, A. (2017). Early Neogene foreland of the Zagros, implications for the initial closure of the neo-Tethys and kinematics of crustal shortening. *Earth and Planetary Science Letters*, *477*, 168–182. https://doi.org/10.1016/j.epsl.2017.07.046

Rahmani, M., Motaghi, K., Ghods, A., Sobouti, F., Talebian, M., Ai, Y., & Chen, L. (2019). Deep velocity image of the north Zagros collision zone (Iran) from regional and teleseismic tomography. *Geophysical Journal International*, *219*(3), 1729–1740. https://doi.org/10.1093/gji/ggz393

Ramos, V. A., Zapata, T., Cristallini, E., & Introcaso, A. (2004). The Andean thrust system—Latitudinal variations in structural styles and orogenic shortening. In K. R. McClay (Ed.), *Thrust tectonics and hydrocarbon systems*, *AAPG Memoir* (Vol. 82, pp. 30–50). Tulsa, OK: American Association of Petroleum Geologists.

Reichenbacher, B., Alimohammadian, H., Sabouri, J., Haghfarshi, E., Faridi, M., Abbasi, S., et al. (2011). Late miocene stratigraphy, palaeoecology and palaeogeography of the Tabriz basin (NW Iran, eastern Paratethys). *Palaeogeography, Palaeoclimatology, Palaeoecology*, *311*(1–2), 1–18. https://doi.org/10.1016/j.palaeo.2011.07.009

Reif, D., Decker, K., Grasemann, B., & Peresson, H. (2012). Fracture patterns in the Zagros fold-and-thrust belt, Kurdistan region of Iraq. *Tectonophysics*, *576*, 46–62.

Reif, D., Grasemann, B., & Faber, R. H. (2011). Quantitative structural analysis using remote sensing data: Kurdistan, Northeast Iraq. *AAPG Bulletin*, *95*(6), 941–956. https://doi.org/10.1306/11151010112

Reilly, C., Nicol, A., Walsh, J. J., & Seebeck, H. (2015). Evolution of faulting and plate boundary deformation in the southern Taranaki Basin, New Zealand. *Tectonophysics*, *651*, 1–18.

Reiners, P. W., & Brandon, M. T. (2006). Using thermochronology to understand orogenic erosion. *Annual Review of Earth and Planetary Sciences*, *34*(1), 419–466. https://doi.org/10.1146/annurev.earth.34.031405.125202

Sandvol, E., Al-Damegh, K. H. A. L. E. D., Calvert, A., Seber, D., Barazangi, M., Mohamad, R., et al. (2001). Tomographic imaging of Lg and Sn propagation in the Middle East. *Pure and Applied Geophysics*, *158*(7), 1121–1163. https://doi.org/10.1007/PL00001218

Sapin, F., Allouche, H., Sterbecq, G., Chevallier, B., & Eriksen, B. (2017). Fast-track 2D seismic processing while drilling to ameliorate foothills exploration and optimize well trajectory: An example from the Central Kurdistan region of Iraq. In *Lithosphere Dynamics and Sedimentary Basins of the Arabian Plate and Surrounding Areas* (pp. 187–202). Cham: Springer. https://doi.org/10.1007/978-3-319-44726-1_9

Saura, E., Garcia-Castellanos, D., Casciello, E., Parravano, V., Urruela, A., & Vergés, J. (2015). Modeling the flexural evolution of the Amiran and Mesopotamian foreland basins of NW Zagros (Iran-Iraq). *Tectonics*, *34*, 377–395. https://doi.org/10.1002/2014TC003660

Saura, E., Vergés, J., Homke, S., Blanc, E., Serra-Kiel, J., Bernaola, G., et al. (2011). Basin architecture and growth folding of the NW Zagros early foreland basin during the late Cretaceous and early Tertiary. *Journal of the Geological Society*, *168*(1), 235–250. https://doi.org/10.1144/0016-76492010-092

Schuster, F., & Wielandt, U. (1999). Oligocene and Early Miocene coral faunas from Iran: Palaeoecology and palaeobiogeography. *International Journal of Earth Sciences*, *88*(3), 571–581. https://doi.org/10.1007/s005310050285

Şengör, A. C., Oezeren, M. S., Keskin, M., Sakınç, M., Özbakır, A. D., & Kayan, I. (2008). Eastern Turkish high plateau as a small Turkic-type orogen: Implications for post-collisional crust-forming processes in Turkic-type orogens. *Earth-Science Reviews*, *90*(1–2), 1–48. https://doi.org/10.1016/j.earscirev.2008.05.002

Şengör, A. M. C., Özeren, S., Genç, T., & Zor, E. (2003). East Anatolian high plateau as a mantle-supported, north-south shortened domal structure. *Geophysical Research Letters*, *30*(24), 8045. https://doi.org/10.1029/2003GL017858

Şengör, A. M. C., Tüysüz, O., Imren, C., Sakınç, M., Eyidoğan, H., Görür, N., et al. (2005). The North Anatolian fault: A new look. *Annual Review of Earth and Planetary Sciences*, *33*(1), 37–112. https://doi.org/10.1146/annurev.earth.32.101802.120415

Sepehr, M., Cosgrove, J., & Moieni, M. (2006). The impact of cover rock rheology on the style of folding in the Zagros fold-thrust belt. *Tectonophysics*, *427*(1–4), 265–281. https://doi.org/10.1016/j.tecto.2006.05.021

Sepehr, M., & Cosgrove, J. W. (2005). Role of the Kazerun fault zone in the formation and deformation of the Zagros fold-Thrust Belt, Iran. *Tectonics*, *24*, TC5005. https://doi.org/10.1029/2004TC001725

Shamaran petroleum group (2009). Iraqi-Kurdistan focused oil development and exploration. Accessed January 2013

Shamaran petroleum group (2011). Exploration and development in Kurdistan. Accessed December 2011

Sharland, P. R., Archer, R., Casey, D. M., Davies, R. B., Hall, S. H., Heward, A. P., et al. (2001). *Arabian plate sequence stratigraphy*, *Geo Arabia, Special Publication* (p. 2). Bahrain: PetroLink.

Shawkat, M. G., & Tucker, M. E. (1978). Stromatolites and sabkha cycles from the lower Fars formation (Miocene) of Iraq. *Geological Review*, *67*(1), 1–14.

Sherkati, S., & Letouzey, J. (2004). Variation of structural style and basin evolution in the central Zagros (Izeh zone and Dezful embayment), Iran. *Marine and Petroleum Geology*, *21*(5), 535–554. https://doi.org/10.1016/j.marpetgeo.2004.01.007

Sherkati, S., Letouzey, J., & Frizon de Lamotte, D. (2006). Central Zagros fold-thrust belt (Iran): New insights from seismic data, field observation, and sandbox modeling. *Tectonics*, *25*, TC4007. https://doi.org/10.1029/2004TC001766

Shuster, D. L., Flowers, R. M., & Farley, K. A. (2006). The influence of natural radiation damage on helium diffusion kinetics in apatite. *Earth and Planetary Science Letters*, *249*(3–4), 148–161. https://doi.org/10.1016/j.epsl.2006.07.028

Sissakian, V. K. (1993). *Geological map of Kirkuk quadrangle, sheet NI-38-2, Geological Survey and Mining, Baghdad, Iraq, Scale 1:250,000*. Baghdad, Iraq: State Establishment of Geological Survey and Mining.

Sissakian, V. K. (1997). *Geological map of Arbeel and Mahabad quadrangles sheets NJ-38-14 and NJ-38-15, scale 1:250,000*. Baghdad, Iraq: State Establishment of Geological Survey and Mining.

Sissakian, V. K. (2000). *Geological map of Iraq, scale, 1:1,000,000*. Baghdad, Iraq: State Company of Geological Survey and Mining.

Sissakian, V. K., & Fouad, S. F. (2014). Geological map of Sulaimaniyah quadrangle, sheet NI-38-3, Iraq Geological Survey, scale 1:250,000. Baghdad, Iraq: Ministry of Industry and Minerals.

Stampfli, G. M., & Borel, G. D. (2002). A plate tectonic model for the Paleozoic and Mesozoic constrained by dynamic plate boundaries and restored synthetic oceanic isochrons. *Earth and Planetary Science Letters*, *196*(1–2), 17–33. https://doi.org/10.1016/S0012-821X(01)00588-X

Stampfli, G. M., Hochard, C., Vérard, C., & Wilhem, C. (2013). The formation of Pangea. *Tectonophysics*, *593*, 1–19. https://doi.org/10.1016/j.tecto.2013.02.037

Stern, R. J., & Johnson, P. (2010). Continental lithosphere of the Arabian plate: A geologic, petrologic, and geophysical synthesis. *Earth-Science Reviews*, *101*(1–2), 29–67. https://doi.org/10.1016/j.earscirev.2010.01.002

Stewart, S. A. (2018). Hormuz salt distribution and influence on structural style in NE Saudi Arabia. *Petroleum Geoscience*, *24*(2), 143–158. https://doi.org/10.1144/petgeo2017-011

Stockli, D. F., & Bosworth, W. (2020). Timing of extensional faulting along the magma-poor central and northern Red Sea Rift margin—Transition from regional extension to necking along a hyperextended rifted margin. In *Geological Setting, Palaeoenvironment and Archaeology of the Red Sea* (pp. 81–111). Cham: Springer.

Stockli, D. F., Farley, K. A., & Dumitru, T. A. (2000). Calibration of the apatite (U-Th)/he thermochronometer on an exhumed fault block, White Mountains, California. *Geology*, *28*(11), 983–986. https://doi.org/10.1130/0091-7613(2000)28<983:COTAHT>2.0.CO;2

Stuart, C. J., Nemčok, M., Vangelov, D., Higgins, E. R., Welker, C., & Meaux, D. P. (2011). Structural and depositional evolution of the East Balkan thrust belt, Bulgaria. *AAPG Bulletin*, *95*(4), 649–673. https://doi.org/10.1306/08181008061

Szymanski, E., Stockli, D. F., Johnson, P. R., & Hager, C. (2016). Thermochronometric evidence for diffuse extension and two-phase rifting within the central Arabian margin of the Red Sea Rift. *Tectonics*, *35*, 2863–2895. https://doi.org/10.1002/2016TC004336

Talbot, C. J., & Alavi, M. (1996). *The past of a future syntaxis across the Zagros*, *Special Publications* (Vol. 100, pp. 89–109). London: Geological Society. https://doi.org/10.1144/GSL.SP.1996.100.01.08

Talebian, M., & Jackson, J. (2004). A reappraisal of earthquake focal mechanisms and active shortening in the Zagros mountains of Iran. *Geophysical Journal International*, *156*(3), 506–526. https://doi.org/10.1111/j.1365-246X.2004.02092.x

Tapponnier, P., Zhiqin, X., Roger, F., Meyer, B., Arnaud, N., Wittlinger, G., & Jingsui, Y. (2001). Oblique stepwise rise and growth of the Tibet plateau. *Science*, *294*(5547), 1671–1677. https://doi.org/10.1126/science.105978

Tavani, S., Corradetti, A., Sabbatino, M., Morsalnejad, D., & Mazzoli, S. (2018). The Meso-Cenozoic fracture pattern of the Lurestan region, Iran: The role of rifting, convergence, and differential compaction in the development of pre-orogenic oblique fractures in the Zagros Belt. *Tectonophysics*, *749*, 104–119. https://doi.org/10.1016/j.tecto.2018.10.031

Tavani, S., Giovanni, C., Michele, N., Marco, S., Alessandra, A., Ettore, V., et al. (2020). The mountain front flexure in the Lurestan region of the Zagros belt: Crustal architecture and role of structural inheritances. *Journal of Structural Geology*, *135*, 104022. https://doi.org/10.1016/j.jsg.2020.104022

Tavani, S., Parente, M., Puzone, F., Corradetti, A., Gharabeigli, G., Valinejad, M., et al. (2018). The seismogenic fault system of the 2017 *Mw* 7.3 Iran–Iraq earthquake: Constraints from surface and subsurface data, cross-section balancing, and restoration. *Solid Earth*, *9*(3), 821–831. https://doi.org/10.5194/se-9-821-2018

Tozer, R., Hertle, M., Petersen, H. I., & Zinck-Joergensen, K. (2019). *Quantifying vertical movements in fold and thrust belts: Subsidence uplift and erosion in Kurdistan northern Iraq*, *Special Publications* (Vol. 490, pp. 397–415). London: Geological Society.

Tunini, L., Jiménez-Munt, I., Fernandez, M., Vergés, J., & Villasenor, A. (2014). Lithospheric mantle heterogeneities beneath the Zagros Mountains and the Iranian plateau: A petrological-geophysical study. *Geophysical Journal International*, *200*(1), 596–614. https://doi.org/10.1093/gji/ggu418

Utkucu, M. (2017). Preliminary seismological report on the November 12, 2017 Northern Iran/Western Iraq earthquake, Sakarya University, https://doi.org/10.13140/RG.2.2.17781.27364

van Hunen, J., & Allen, M. B. (2011). Continental collision and slab break-off: A comparison of 3-D numerical models with observations. *Earth and Planetary Science Letters*, *302*(1–2), 27–37. https://doi.org/10.1016/j.epsl.2010.11.035

Vatandoust, M., Faghih, A., Burberry, C. M., & Shafiei, G. (2020). Structural style and kinematic analysis of folding in the southern Dezful embayment oilfields, SW Iran. *Journal of Structural Geology*, *134*, 103989. https://doi.org/10.1016/j.jsg.2020.103989

Vergés, J., Emami, H., Garcés, M., Beamud, E., Homke, S., & Skott, P. (2019). Zagros foreland fold belt timing across Lurestan to constrain Arabia–Iran collision. In *Developments in Structural Geology and Tectonics* (Vol. 3, pp. 29–52). New York: Elsevier.

Vergés, J., Goodarzi, M. G. H., Emami, H., Karpuz, R., Efstathiou, J., & Gillespie, P. (2011). *Multiple detachment folding in Pusht-e Kuh arc*. Zagros: Role of mechanical stratigraphy.

Vergés, J., Ramos, V. A., Meigs, A., Cristallini, E., Bettini, F. H., & Cortes, J. M. (2007). Crustal wedging triggering recent deformation in the Andean thrust front between 31°S and 33°S: Sierras Pampeanas-Precordillera interaction. *Journal of Geophysical Research*, *112*, B03S15. https://doi.org/10.1029/2006JB004287

Vergés, J., Saura, E., Casciello, E., Fernandez, M., Villaseñor, A., Jimenez-Munt, I., & García-Castellanos, D. (2011). Crustal-scale cross-sections across the NW Zagros belt: Implications for the Arabian margin reconstruction. *Geological Magazine*, *148*(5–6), 739–761. https://doi.org/10.1017/S0016756811000331

Vermeesch, P. (2012). On the visualisation of detrital age distributions. *Chemical Geology*, *312*, 190–194.

Wolf, R. A., Farley, K. A., & Silver, L. T. (1996). Helium diffusion and low-temperature thermochronometry of apatite. *Geochimica et Cosmochimica Acta*, *60*(21), 4231–4240. https://doi.org/10.1016/S0016-7037(96)00192-5

Woodward, N. B., Boyer, S. E., & Suppe, J. (1989). *Balanced geological cross-sections: An essential Technique in Geological Research and Exploration* (Vol. 6, p. 132). Washington, DC: American Geophysical Union. https://doi.org/10.1029/SC006

Wrobel-Daveau, J. C., Ringenbach, J. C., Tavakoli, S., Ruiz, G. M., Masse, P., & de Lamotte, D. F. (2010). Evidence for mantle exhumation along the Arabian margin in the Zagros (Kermanshah area, Iran). *Arabian Journal of Geosciences*, *3*(4), 499–513. https://doi.org/10.1007/s12517-010-0209-z

Yamato, P., Kaus, B. J., Mouthereau, F., & Castelltort, S. (2011). Dynamic constraints on the crustal-scale rheology of the Zagros fold belt, Iran. *Geology*, *39*(9), 815–818. https://doi.org/10.1130/G32136.1

Yilmaz, A., & Yilmaz, H. (2019). Structural evolution of the eastern Anatolian basins: An example from collisional to postcollisional tectonic processes, Turkey. *Turkish Journal of Earth Sciences*, *28*(3), 329–350. https://doi.org/10.3906/yer-1805-20

Yonkee, W. A., & Weil, A. B. (2015). Tectonic evolution of the Sevier and Laramide belts within the North American cordillera orogenic system. *Earth-Science Reviews*, *150*, 531–593. https://doi.org/10.1016/j.earscirev.2015.08.001

Zadeh, P. G., Adabi, M. H., Hisada, K. I., Hosseini-Barzi, M., Sadeghi, A., & Ghassemi, M. R. (2017). Revised version of the Cenozoic collision along the Zagros Orogen, insights from Cr-spinel and sandstone modal analyses. *Scientific Reports*, *7*, 10828.

Zebari, M., Balling, P., Grützner, C., Navabpour, P., Witte, J., & Ustaszewski, K. (2020). Structural style of the NW Zagros Mountains and the role of basement thrusting for its mountain front flexure, Kurdistan region of Iraq. *Journal of Structural Geology*, *141*, 104206. https://doi.org/10.1016/j.jsg.2020.104206

Zebari, M., Grützner, C., Navabpour, P., & Ustaszewski, K. (2019). Relative timing of uplift along the Zagros Mountain front flexure (Kurdistan region of Iraq): Constrained by geomorphic indices and landscape evolution modeling. *Solid Earth*, *10*(3), 663–682. https://doi.org/10.5194/se-10-663-2019

Zebari, M. M., & Burberry, C. M. (2015). 4-D evolution of anticlines and implications for hydrocarbon exploration within the Zagros fold-thrust belt, Kurdistan region, Iraq. *GeoArabia*, *20*(1), 161–188.

Zhao, L. F., & Xie, X. B. (2016). Strong Lg-wave attenuation in the Middle East continental collision orogenic belt. *Tectonophysics*, *674*, 135–146. https://doi.org/10.1016/j.tecto.2016.02.025

Ziegler, M. A. (2001). Late Permian to Holocene paleofacies evolution of the Arabian plate and its hydrocarbon occurrences. *Geoarabia-Manama*, *6*, 445–504.

Zor, E. (2008). Tomographic evidence of slab detachment beneath eastern Turkey and the Caucasus. *Geophysical Journal International*, *175*(3), 1273–1282. https://doi.org/10.1111/j.1365-246X.2008.03946.x